Vestibulo-ocular responses in man to gravito-inertial forces

J.T. Marcus

Vestibulo-ocular responses in man to gravito-inertial forces

Vestibulo-oculaire responsies bij de mens
geïnduceerd door traagheidskrachten en de zwaartekracht
(met een samenvatting in het Nederlands)

Proefschrift

ter verkrijging van de graad van doctor aan
de Rijksuniversiteit te Utrecht, op gezag van
de rector magnificus prof.dr. J.A. van Ginkel,
ingevolge het besluit van het college van dekanen
in het openbaar te verdedigen op donderdag
26 november 1992 des namiddags te 2.30 uur

door

Johannes Timotheus Marcus

geboren op 10 september 1954 te Amsterdam

Faculteit der Geneeskunde

Promotor:	prof.dr. G.F. Smoorenburg
Co-promotor:	dr. W. Bles

This research was performed in the Department of Work Environment, Equilibrium & Orientation programme, TNO Institute for Perception, Soesterberg, The Netherlands. Additional financial support was provided by the Space Research Organization in The Netherlands.

aan mijn vader en moeder

CIP-DATA KONINKLIJKE BIBLIOTHEEK, DEN HAAG

Marcus, Johannes Timotheus

Vestibulo-ocular responses in man to gravito-inertial forces /
Johannes Timotheus Marcus.
- Utrecht : Universiteit Utrecht, Faculteit Geneeskunde
Thesis Rijksuniversiteit Utrecht. - With ref. - With summary in Dutch.
ISBN 90-393-0254-5
Subject headings: gravito-inertial forces / microgravity / vestibulo-ocular responses.

VOORWOORD

Het onderzoek dat in dit proefschrift wordt beschreven is uitgevoerd op het Instituut voor Zintuigfysiologie TNO, bij de afdeling Werkomgeving. Het werk maakte deel uit van het onderzoeksprogramma Evenwicht en Oriëntatie. Hiermee is al aangegeven dat velen hebben bijgedragen aan het tot stand komen van dit proefschrift. Mijn erkentelijkheid wil ik hier tot uiting brengen.

Mijn promotor Guido Smoorenburg dank ik voor de inspirerende en stimulerende discussies, die hebben bijgedragen aan de uitwerking van de meetresultaten en de modelvorming. Mijn co-promotor Wim Bles heeft mij geholpen met zijn actieve en kritische begeleiding. De overige leden van de promotiecommissie dank ik voor het beoordelen van het manuscript: prof.dr. H. Collewijn, prof.dr. C.J. Erkelens, prof.dr. A.C. Van Huffelen, prof.dr. W.J. Oosterveld en prof.dr.ir. M.A. Viergever. Waardevolle suggesties ter verbetering werden gegeven door dr. H. Gallé.

Cor Van Holten heeft een belangrijke bijdrage geleverd aan de realisatie van het centrifuge-experiment en de interpretatie van de resultaten. André Kuipers heeft met mij het experiment in paraboolvlucht opgebouwd en uitgevoerd. Het Nationaal Lucht- en Ruimtevaart-Geneeskundig Centrum bood ondersteuning bij de experimenten in de centrifuge en in paraboolvlucht. Jelte Bos en Nico Kistemaker (Medische Fysica, Vrije Universiteit) schreven computerprogramma's waarmee een deel van de data-analyse is uitgevoerd.

De directie van het IZF-TNO ben ik erkentelijk voor de ruimte die mij is geboden om dit proefschrift te voltooien. Binnen het IZF heb ik onmisbare hulp genoten van vele collega's. Met Bernd de Graaf, Lex Wertheim en Kees Wientjes mocht ik vruchtbare inhoudelijke discussies voeren. Leny van der Boon heeft op professionele wijze de tekstverwerking verzorgd en, met veel geduld, de correcties verwerkt. Koos Wolff en Walter van Dijk leverden vakwerk bij de verzorging van de figuren. De technische ondersteuning van Reinier Vunderink, Lex Viersen en Evert Agterhuis was onontbeerlijk bij de opbouw van de experimenten. Arno Krul was steeds paraat voor statistische analyses. Els van Amerongen was altijd behulpzaam als afdelings-secretaresse.

Tenslotte wil ik mijn familie bedanken voor het bieden van een thuisbasis. Daarbij heeft mijn broer Paul mij geholpen bij de modelberekeningen.

Vestibulo-ocular responses in man to gravito-inertial forces

CONTENTS

Page

1 Vestibulo-ocular responses to gravito-inertial forces: current models

2 Methods and experimental conditions

Page

3 Vestibulo-ocular responses in man to $+G_z$ hypergravity

Abstract

4 Otolith responses in man during parabolic flight

Abstract

5 Eye movements in man induced by sinusoidal acceleration on a linear track

Abstract

Chapter 1

Vestibulo-ocular responses to gravito-inertial forces: current models

1.1 Introduction

The origin of the present study is the observation in man of a sustained vertical nystagmus with a downward slow component, in response to hypergravity evoked in a centrifuge (Marcus and Van Holten, 1990). "Hypergravity" is a short notation for the vector resultant of gravity and inertial ("centrifugal") force, which was generated in the free swing gondola of a human centrifuge with 4m radius.

The existence of this vestibulo-ocular response has potential practical importance in high performance aircraft, which are generating even larger hypergravity forces with high onset rates. The aim of this study is therefore to investigate the vestibulo-ocular responses to gravito-inertial forces.

Man has been designed to live on the surface of the earth, exposed to the earth's gravity only. It is not evident that our vestibular system should respond at all to sustained hypergravity. This introductory chapter starts from current models of otolith physiology. Next, data on the frequency response and the force-response characteristics are presented, in order to explore in what force-ranges otolith responses are to be expected. Finally, models of vestibulo-ocular responses are introduced, which will have relevance to the design of our experiments.

1.2 Models of otolith physiology

1.2.1 Anatomy and physiology

The organization of the membranous labyrinth is shown in Fig. 1.1. The otolith organs are located in the utricle and the saccule. Approximately the utricular sensory base is oriented in a plane that is tilted 30 deg backward with respect to the horizontal plane (Fluur, 1970). In the lower part of Fig. 1.1 the sensory bases of the utricle and the saccule are shown as seen from aside. This disposition means that the plane of the utricular base is horizontal when the subject's head is 30 deg tilted forward, which is the natural position of the head during walking.

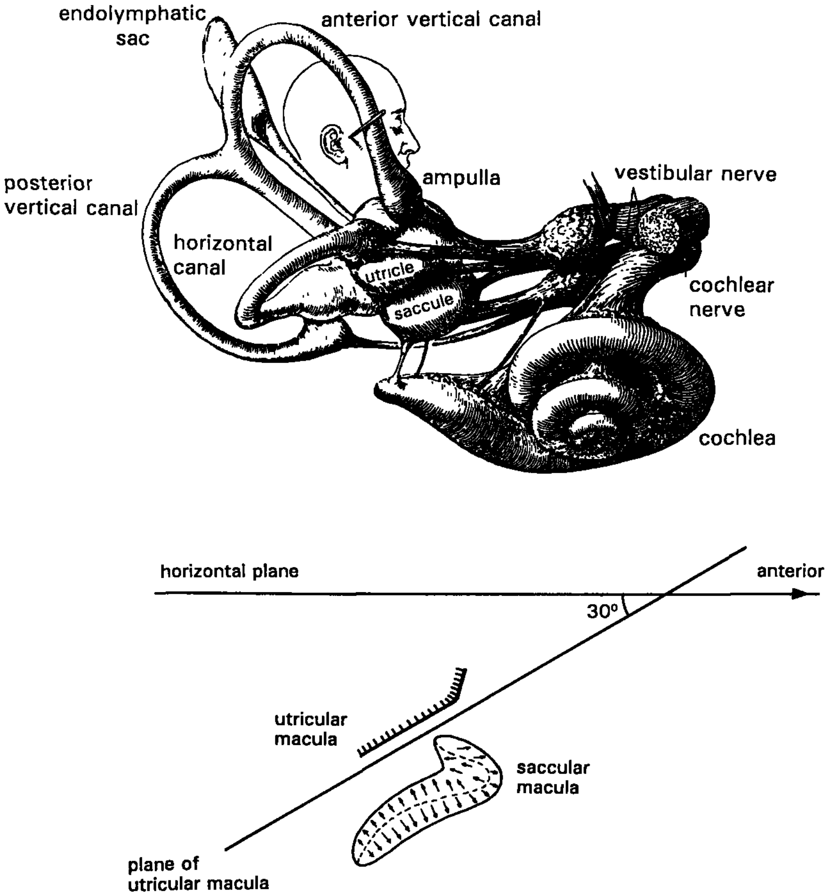

Fig. 1.1 Organization of the membranous labyrinth. The vestibular portion consists of the utricle and the saccule, and the three semicircular ducts which are in mutually orthogonal planes (from Hardy, 1934).

The otolithic membrane is composed of the upper otoconial layer and the lower gelatinous layer. The upper surface is in contact with the endolymph, which supplies viscous damping. The gelatinous layer is attached to the sensory cell base, the macula. With any specific force acting on the head, the denser otoconial layer tends to lag behind this base, inducing a deformation in the gel layer between the otoconial layer and the sensory cell base. The sensory cells detect this shearing deformation by means of small hairs extending into the gel layer, and transduce this deformation into a receptor potential (Guedry, 1974; Clemens and Gallé, 1976; Kelly, 1981; Grant and Best, 1987). The hair cells show a *morphological* polarization: at one side of the cell there is a relatively large hair cell called the "kinocilium", which is an active part of the cell. The other hairs are the "stereocilia". This morphological polarization is coinciding with a *functional* polarization: when the hairs are bended in the direction of the kinocilium, the cell depolarizes; bending in the opposite direction results in hyperpolarization; bending orthogonally to the symmetry axis results in no response. Thus, each hair cell of the macula is maximally excited if the force is acting in the direction of the kinocilium. These functional axes of polarization are shown for the utricle and the saccule in Fig. 1.2. The cells are not polarized in one parallel pattern, which implies that the otolith organs respond to specific forces in a wide range of directions (Fluur, 1970; Kelly, 1981).

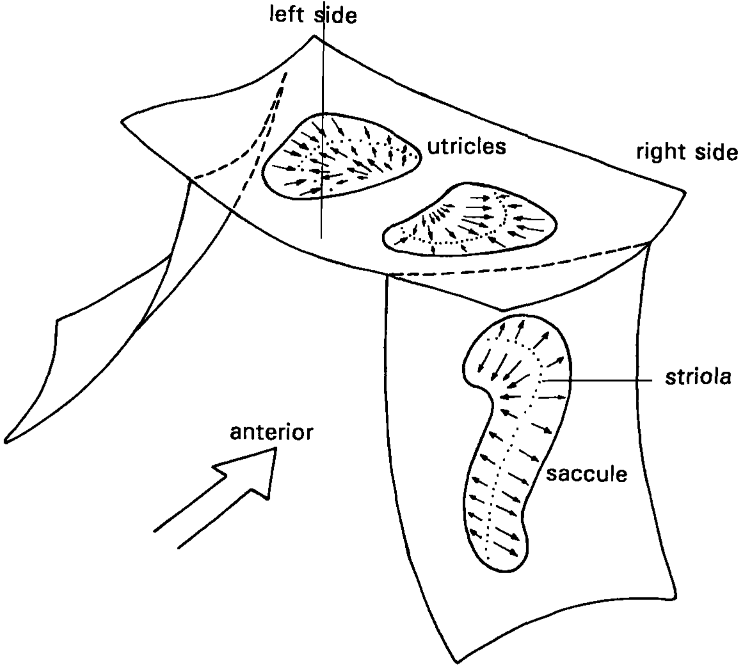

Fig. 1.2 Dispositions of the sensory epithelia, or maculae, in the otolith organs on the two sides of the head. The arrows represent the polarization maps of the sensory hair cells lying within the macular surfaces. The arrows point in that direction of shear that produces depolarization of the hair cells in each region. A shear force applied in the opposite direction produces hyperpolarization. The striola is the boundary between regions of opposite polarity (from Malcolm and Melvill Jones, 1970).

For the utricle the axes of polarization point toward a single curving landmark called the striola, while for the saccule the axes are pointing away from the striola. Fig. 1.1 shows that the major part of the saccular striola is tilted backward 30 deg (like the utricular plane). This means that the saccule is maximally sensitive to vertical accelerations, when the head is tilted forward by 30 deg.

Histologically, the hair cells can be categorized in flask-shaped (type I), and cylindrically shaped (type II) cells. The afferent nerve fibres from these hair cells can be physiologically discriminated by their pattern of action potential discharges: irregular and regular discharges, respectively. An approximate division between the afferent nerves from the hair cells is summarized in Table 1.1 (Goldberg, 1991).

Table 1.1 Some characteristics of vestibular nerve afferents.

Irregularly discharging	Regularly discharging
Calyx form	Bouton form
In striolar zone of macula	In peripheral zone of macula
Innervating *type I hair cells*	Innervating *type II hair cells*
Phasic response	*Tonic* response

A relevant property in our study is the functional subdivision in the phasic cells (type I) sensitive to velocity of otolith displacement, and the tonic cells (type II) sensitive to otolith displacement. When the Bode diagram of the otoliths are derived in the next sections, this subdivision will reoccur.

1.2.2 Physical dimension of otolith input

The dimension of the otolith stimulus is:

$$G = \text{specific force} = \text{resulting external force per mass unit}$$

which is expressed in $m \cdot s^{-2}$. The unit for specific force is "g", which has the value $g = 9.8\ m \cdot s^{-2}$. Exposure to specific force is called "G-load"; G levels above 1g are briefly indicated as "hypergravity".

The condition of "weightlessness" is defined by $G = 0g$, and thus by the absence of any external force. It occurs in free-fall, in parabolic flight, and in orbital motion. Occasionally, the condition $G = 0g$ is indicated by "microgravity". We must be aware that the terms "hypergravity" and "microgravity" are formally not correct, because the earth's *gravitational* field is hardly different in these conditions, or not different at all.

niet
strikt
juist

Although G has the dimension of $m \cdot s^{-2}$, it is not an acceleration. The difference between G and acceleration can be made more clear in a few examples. When a subject is stationary on the earth's surface, he experiences a specific force G = 1g. Yet, his acceleration to the earth's centre is zero. On the other hand, when a subject is in the free-fall phase of parabolic flight, he experiences G = 0g while accelerating to the earth's surface with $9.8\ m \cdot s^{-2}$.

Current knowledge on otolith responses to changes in specific force will be reviewed from two different model approaches: otolith mechanics and a black box analysis.

1.2.3 Model based on otolith mechanics

In this section a model of otolith physiology is presented, where the roles of viscosity, elasticity, and mass-density differences are to be quantified in terms of a differential equation. From this equation the transfer function is to be determined. Because sustained hypergravity is a non-physiological stimulus for the otoliths, specific attention is paid to possible saturation at unphysiologically high force levels.

Differential equation of otolith dynamics

A diagram of the otoconial layer with its associated forces is shown in Fig 1.3 (Grant and Best, 1987).

In this figure the x-direction is in the plane of the otoconial layer, with the coordinate system origin attached to the sensory cell base which moves with the skull. Thus x is the relative displacement of the otoconial membrane measured with respect to the skull. In the dynamics the viscous endolymph damping V is described by $V_x = B\dot{x}$, with $\dot{x}$ being a short notation for the first derivative to time. The gel layer elastic force E is expressed by $E_x = Kx$. The force due to the displaced endolymph fluid is given by $B_x = m_{df}(g_x - a_x)$, with m_{df} indicating the mass of displaced fluid. Note that the forces V_x, E_x and B_x are acting in the -x direction. The system's differential equation is treated here in more detail, because it is the base for the frequency response of the otolith system, and it will also be applied in the model calculations to be presented later in our study.

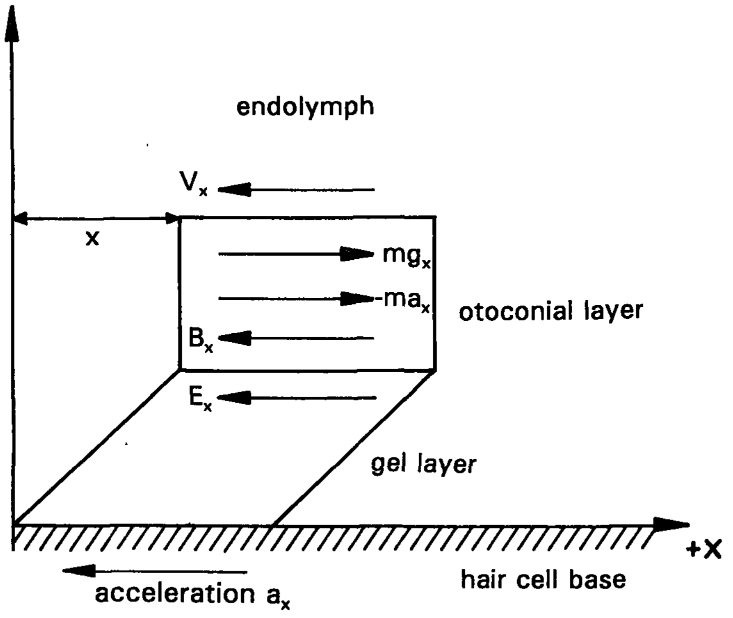

Fig. 1.3 Forces acting on the otoconial layer in the x-direction. E_x = elastic force from the gel layer; V_x = viscous force from the endolymph; B_x = force due to displaced endolymph fluid; g_x = gravitational force per mass unit; x = displacement of otoconial layer with respect to the hair cell base; a_x = acceleration of the hair cell base (from Grant and Best, 1987, modified).

Following the procedure of Grant and Best (1987), we start by applying Newton's second law to the otoconial layer:

$$m\ddot{x} = mg_x - ma_x - V_x - E_x - B_x$$

where $\ddot{x}$ represents the second derivative to time and the right-hand member of the equation equals the summation of all forces acting upon the otoconial layer. Substitution $V_x = B\dot{x}$, $E_x = Kx$, $B_x = m_{df}(g_x - a_x)$, and division by otoconial mass m:

$$\ddot{x} = g_x - a_x - \frac{B}{m}\dot{x} - \frac{K}{m}x - \frac{m_{df}}{m}(g_x - a_x)$$

The quotient m_{df}/m is equal to d_e/d_o, with d_e = density of endolymph and d_o = density of otoconial layer. The terms depending on x are then transferred to the left-hand side of the equation, yielding:

$$\ddot{x} + \frac{B}{m}\dot{x} + \frac{K}{m}x = \left(1 - \frac{d_e}{d_o}\right)(g_x - a_x) \tag{I}$$

The equation (I) relates the system dynamics (left side) to the input of force per mass unit (right side). The term $(1-d_e/d_o)$ represents system sensitivity. The equation is presented as a diagram in Fig. 1.4.

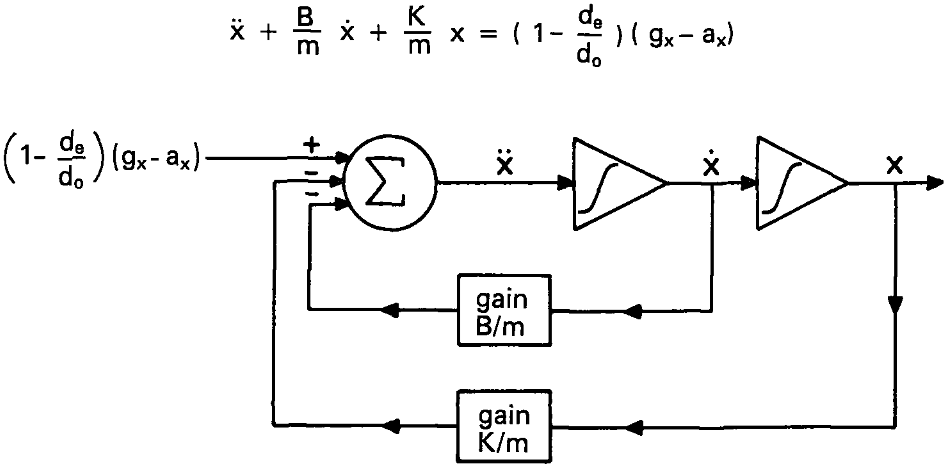

Fig. 1.4 Approximate model of otolith dynamics (Grant and Best, 1987). The system is described by a second order model. Stimulus is the force per mass unit (g_x-a_x); the system dynamics is expressed by a second order differential equation. d_e = density of endolymph; d_o = density of otoconial layer, $d_e/d_o = 0.5$; g_x = component of gravity; a_x = component due to acceleration of the head; m = mass of the otoconial layer; B = viscous damping coefficient; K = spring stiffness coefficient; x = displacement of the otoconial layer relative to the macula. Numerical values from perception measurements (Mayne, 1974): $(B/m) = 1.69\ [s^{-1}]$; $(K/m) = 0.285\ [s^{-2}]$.

Transfer function of the otolith hair cells

This analysis aims to determine the frequency response and the sensitivity to high G forces in man. Equation (I) needs further evaluation in order to perform these calculations. The following procedure has been applied by Grant and Best (1987):

(a) Rewrite (I) in Laplace notation:

$$\frac{X(s)}{[G-A](s)} = \left(1-\frac{d_e}{d_o}\right) \cdot \frac{1}{s^2+\frac{B}{m}s+\frac{K}{m}} \qquad \text{(II)}$$

(b) Factorize the denominator at the right-hand side in (II) in order to identify time constants:

$$\frac{X(s)}{[G-A](s)} = \left(1-\frac{d_e}{d_o}\right) \cdot \frac{T_1T_2}{(1+T_1s)(1+T_2s)} \qquad \text{(III)}$$

where $T_1T_2 = m/K$ (IIIa), and $T_1+T_2 = B/K$ (IIIb).

(c) Substitute in (III) time constant values obtained from other research. $T_1 = 10s$ from perceived specific force experiments, and in an estimation $T_2 = 0.0002s$ from a theoretical analysis of the otolith organ. These time constants correspond to corner frequencies of 0.016 and 800 Hz, respectively. This presentation of the equation will allow us to perform numerical calculations in Chapter 6.

(d) The resulting Bode plot for type II hair cells, sensing otoconial displacement, is presented in the upper diagram in Fig. 1.5. The transfer function for type I cells, sensing otoconial velocity, was obtained by multiplying equation (III) with s. The corresponding Bode plot is shown in the lower diagram in Fig. 1.5.

Based on the time constant values $T_1 = 10s$ and $T_2 = 0.0002s$ for the sensor cells, the values of the viscous and elastic damping terms (B/m and K/m in equation I) are approximated from equations IIIa and IIIb. From (IIIa) it follows that $K/m = 1/(T_1T_2) = 500$ [s^{-2}]. Because $T_1 >> T_2$ we may approximate from (IIIb) that $T_1 = B/K$. Substitution in (IIIa) yields $B/m = 1/T_2 = 5000$ [s^{-1}]. These viscous and elastic terms, derived by Grant and Best, are much larger than the values given by Mayne (1974), based on measurements of perceived specific force: $B/m = 1.69$ [s^{-1}] and $K/m = 0.285$ [s^{-2}]. Grant and Best (1987) explain their larger values by noting that the sensor cells are much faster than subjective recordings of specific force. The large difference between the values of Grant and Best, and those of Mayne, emphasizes that the model parameters are dependent on initial assumptions and experimental conditions.

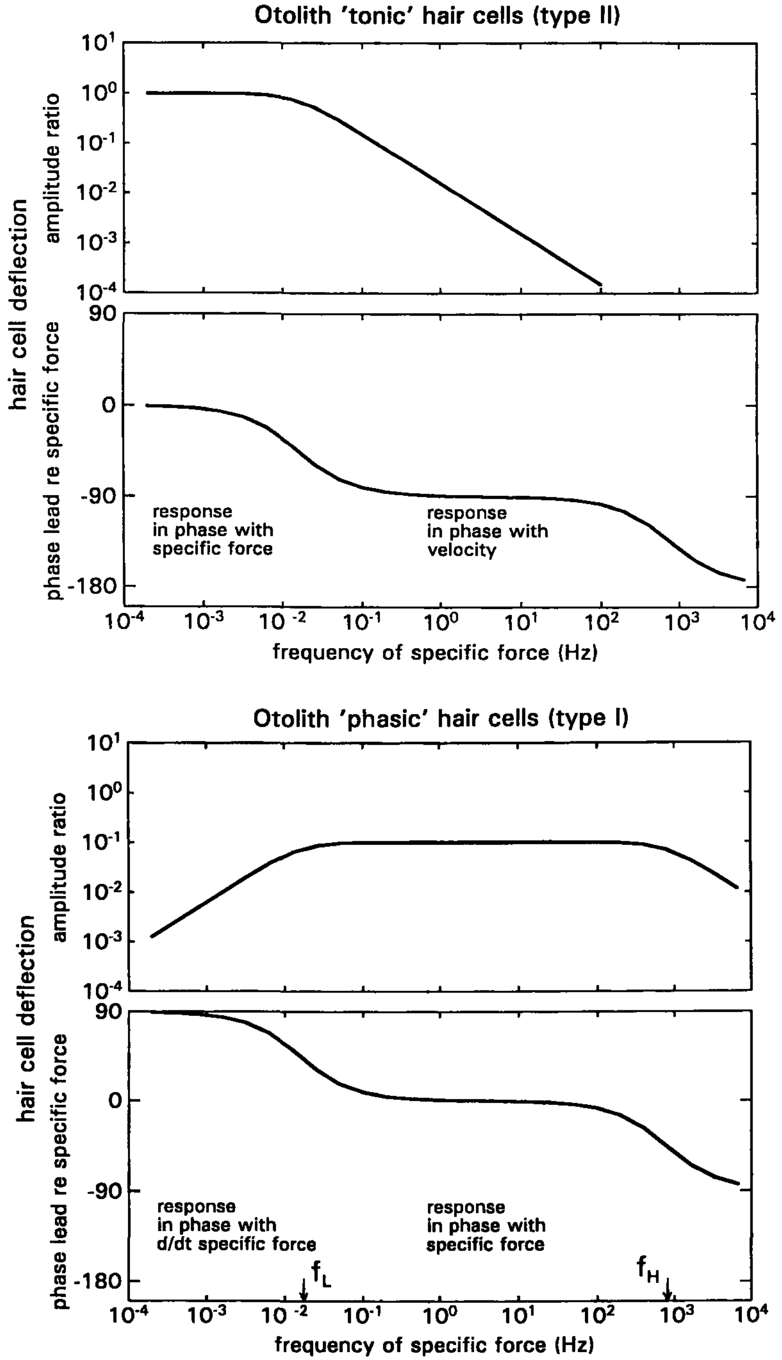

Fig. 1.5 Frequency responses of the hair cells, as predicted by the model of Grant and Best (1987). The corner frequencies are $f_L=0.016$ Hz, and $f_H=800$ Hz. The "tonic" cells (upper diagram) respond in phase with specific force in the frequency range below f_L, and in phase with velocity in the mid-frequency range. The "phasic" cells (lower diagram) are responding in phase with the derivative of specific force below f_L, and in phase with specific force in the mid-frequency range.

Non-linear dynamics at sustained increased specific force

Grant and Best (1987) showed that for a 1g increase in gravity the output would result in a maximum deflection of about 10 mm, which is beyond physiological limits. The prediction of this large deflection could be avoided by assuming that the spring stiffness K of the gelatinous layer is increasing with increasing deflection. Thus, for large-amplitude deflections, which would occur during low-frequency or static periods, system linearity is no longer applicable; the system stiffness may increase by a factor of 10^3.

However, model analysis indicated that this large increase in gel stiffness would cause oscillations. In order to prevent these oscillations, Grant and Cotton (1991) proposed to attribute a viscous term not only to the endolymph, but also to the dynamics of the gel layer. This extension of otolith dynamics with a visco-elastic gel layer resulted in calculated displacements which were within the physiological limits of displacement. The calculated otoconial displacement was 3 μm per g. With the maximum displacement being 25 μm, it may be concluded that from otolith mechanics a dynamic response to hypergravity can be expected.

1.2.4 Black box approach

In this approach the otolith transfer function is investigated starting from input-output analysis. Two output dimensions will be discussed here: the discharge rate of neurons innervating the otolith hair cells, and perceived specific force.

Action potential recording

The physiology of the afferent neurons innervating the otolith organs was investigated by Fernandez and Goldberg (1976, I,II,III) in monkeys, anaesthetized with barbiturate. A centrifugal force was generated by rotating the monkey in a centrifuge. Output was defined as the discharge rate of action potentials in the afferent neurons [spikes $\cdot$ s^{-1}].

During an extended period of constant stimulation, the discharge rate tends to return to the resting level, and this adaptation is most prominent in the phasic cells (type I). Adaptation to long-duration 1.23g centrifugal force was characterized by per-stimulus response decline and post-stimulus secondary response, with time constants between 50 and 150 s.

S-shaped force-response functions were obtained in the stimulus range of ±5g. In general, these functions were approximately linear up to ±3g, and the response levelled off at ±5g. There were individual fibres with a dynamic range up to a higher level.

A frequency-domain analysis was performed on responses to sinusoidal forces in the frequency range from DC to 2 Hz. The phase of the response was derived from the histogram of action potentials plotted over the cycles of stimulation, and referred to specific force. The response of regularly discharging nerves innervating type II cells was predominantly tonic; a small phase lead with respect to specific force was found at frequencies below .1 Hz, and a small lag at higher frequencies. Irregular units from type I cells (phasic) showed phase leads of about 40° at .1 Hz, and of about 20° at 2Hz. Comparing these data with the Grant & Best model in Fig. 1.5, there is a similar trend of increasing phase lag over frequency, but quantitatively there are differences.

We adopt the Grant & Best model, but we should keep in mind that there are different quantitative results from other approaches.

The *perceived specific force* is affected by somatosensory and cognitive cues, and therefore these must be considered before assigning responses to otoliths only. The experimental data are obtained from subjective perception of velocity during sinusoidal linear acceleration, and thresholds to constant acceleration. Both phase lead and phase lag with respect to specific force input have been reported. Young and Meiry (1968) explain the phase lead in terms of neural processing, and the phase lag as caused by a mechanical threshold. Hosman and Van der Vaart (1978) measured perception thresholds to specific force in a flight simulator, and found a modulus of the otolith transfer function in accordance with models of Fernandez and Goldberg (1976, III), and Young and Meiry (1968). The concept of an integrating accelerometer, reporting head velocity in the frequency range of head movements (Fig. 1.5, type II cells) has been proposed by Benson (1986). It describes motion perception on a linear track.It seems in general justified to conclude that the results from perceived specific force are qualitatively confirming the findings from otolith physiology shown in Fig. 1.5.

1.2.5 Summary of otolith models

Otolith models have been reviewed from two different lines. In the physiological approach the otolith displacement is the output parameter, and in the black box approach the output is defined by the frequency of action potentials in the afferent nerve. Despite the fact that the numerical constants in the models are differing between authors, common findings from both approaches can be indicated:

Linear dynamics

The transfer function of the otolith organ is characterized by two time constants with order of magnitude T_1 = 10 s and T_2 = .0002 s. In the frequency response these time constants are corresponding with a lower and a higher corner frequency, enclosing the frequency range of normal head movements. In this range, the type I sensor cells ("phasic") are responding in phase with specific force, and the type II cells ("tonic") in phase with velocity. We have adopted the Grant & Best model, but the model parameters may be dependent on experimental conditions.

Non-linear dynamics

Starting from the properties of the otolithic system, there are no indications that the system fully saturates below G=5g. We may conclude that the dynamic range of otolith responses in man extends to G levels of at least 5g.

1.3 Otolith-ocular responses

1.3.1 Otoliths and vestibular nystagmus

This section will focus on vertical and horizontal eye movements. Observations on nystagmus provoked by linear acceleration were reported by Jongkees and Philipszoon (1962), Lansberg et al. (1965), and Niven et al. (1965).

The neuro-anatomical pathway has been described in detail by Kelly (1981) and Collewijn (1986). For this study it is relevant that the otolith-ocular reflex is basically a three-neuron reflex arc. Nystagmus induced by utricular stimulation has been observed by Gernandt (1970) in cats and monkeys. A long-lasting mechanical stimulation by air-puffs of the isolated utricle evoked a primary nystagmus, followed by a secondary nystagmus at cessation of stimulation. Fluur and Mellstrom (1970a; 1970b) have determined eye movement responses by electrical stimulation (square waves, 300 Hz) in the cat. Stimulation of the utricle evoked eye movements in upward, downward, or horizontal direction, in dependence of the location where the electrical stimulus was applied. For the saccule the eye movement directions were upward, downward, or torsional. However, in a study by Curthoys (1987) using electrical stimulation in the maculae of guinea pigs, there were no differences in eye movement directions corresponding to different hair cell orientations. These findings are thus in contrast to those of Fluur and Mellstrom.

The hair cells are innervated by the primary vestibular afferent neuron, which projects to the vestibular nucleus. After synapsing to a second neuron the signal is transferred via the medial longitudinal fasciculus to the oculomotor nucleus, where eye movement commands are generated (Ranalli and Sharpe, 1988), as shown in Fig. 1.6.

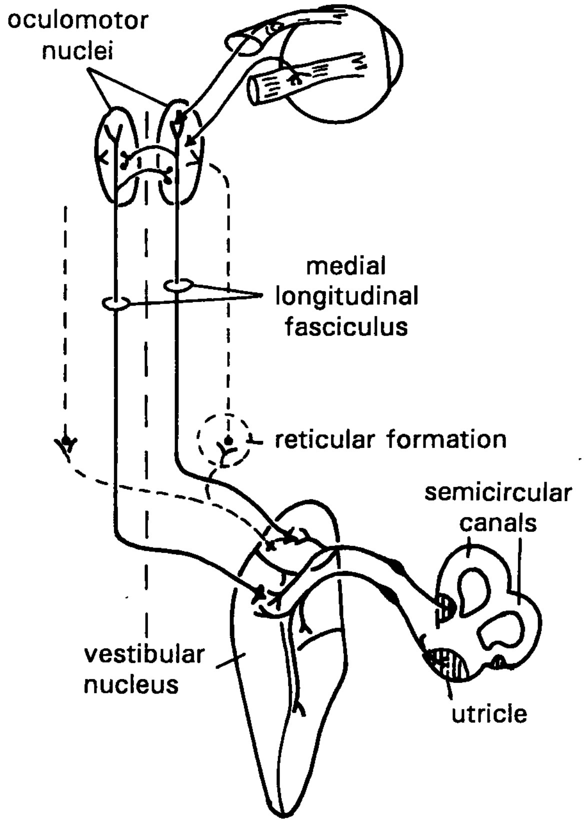

Fig. 1.6 Diagram of the primary vestibular fibres that project from the canals and utricle to the vestibular nuclei VN and synapse with fibres that affect ocular motility (modified from Brodal, 1981).

In our study it is important to note that a similar three-neuron arc exists from the semicircular canals to the oculomotor nuclei. It means that in any study of vestibular eye movements the otolith- and canal-contribution should be discriminated from each other. This consideration will be important in the design of our centrifuge experiment.

Vestibulo-ocular reflex (VOR)

The VOR basically consists of compensatory eye movements generated by the vestibular system in order to maintain visual fixation during acceleration. It gives to man the capability to move and see simultaneously. Referring to the Bode plots in Fig. 1.5, the integrating action of type II cells in the frequency range of head movements has an important functional significance: In stabilizing the retinal-image, the eyes must follow the target velocity, rather than the target acceleration.

The vestibular nystagmus consists of a slow compensatory component generated by the vestibular system, and a fast component induced by the saccadic system. More details about fast-component generation are given by Collewijn (1986). Fast-component eye movements might also have some vestibular input (Berthoz and Israel, 1988). Usually however the slow-component velocity (SCV) is regarded as a signal generated by the vestibular system. The SCV parameter quantifies nystagmus, as well as compensatory eye movements of any form (e.g. sinusoidal during pitch head movements).

Vertical VOR in man

During active pitch head movements in the frequency range from 0.25 to 2 Hz vertical VOR was found to be up-down symmetric, and independent of frequency (Ranalli and Sharpe 1988). The otolith contribution to this VOR is however not immediately clear. In the applied frequency range the eye movements represent the sum of otolith responses to changes in gravity direction, and canal responses to head angular acceleration. Baloh and Demer (1991) reported that during voluntary pitch head movements, otoliths are not critical for functioning of the VOR. It seems that the pure otolith influence cannot be determined from the VOR in response to physiological pitch movements, because there is confounding input from semicircular canal stimulation. An otolith influence on eye movements can be measured in ocular counterrolling in response to static tilt. Ocular torsion however is out of the scope of our study, and the reader is referred to Diamond and Markham (1983), De Graaf (1990), and Bles and De Graaf (1991). The otolith influence on horizontal and vertical eye movements becomes manifest on a parallel swing and on a linear track, which are discussed in the next sections.

1.3.2 Otolith responses on a parallel swing

The parallel swing has the advantage that the movements are linear, which excludes any confounding with canal stimulation. Human otolith responses to inertial force were investigated on a parallel swing by Oosterveld (1970). Bles and Kaptein (1973) observed a sinusoidal eye movement response at the frequency of sled movement, although the amplitude of response was highly variable between subjects. In addition, responses of twice the frequency of the swing were observed, and it was suggested that this response was induced by the vertical accelerations with an amplitude of 0.014 g. This finding was confirmed by Baloh et al. (1988) with scleral coil eye movement recordings. With swing frequency 0.3 Hz the vertical acceleration at twice the swing frequency ranged from 0.03 g to 0.34 g. The response defined as vertical eye velocity divided by vertical swing velocity was 4 $\text{deg} \cdot \text{m}^{-1}$ at 0.6 Hz, or equivalently 10 $\text{deg} \cdot \text{s}^{-1}$ per g unit. Horizontal eye movement responses were comparable in amplitude if the swing displacement was along the subject's interaural axis.

1.3.3 Mechanism of the Linear Vestibulo-Ocular Reflex

The otolith-ocular response to linear acceleration is briefly indicated as linear VOR. In a functional concept the otoliths are inducing a compensatory eye movement during lateral acceleration in order to maintain retinal fixation of visual targets (Niven et al., 1965; Shelhamer, 1990). The influence of target distance d was investigated by Schwarz et al. (1989) in monkeys. Both the linear VOR and the visually induced eye velocity were measured in dependence of viewing distance of an imagined target. A single step input of acceleration was applied. It was found that the vestibularly as well as the visually induced eye velocity responses were inversely proportional to viewing distance d. A model concept showing the proposed relation between the vestibular and visual pathways is shown in Fig. 1.7.

The factor k_2 contains the response for an infinite distance. The variable multiplication factor, k_1/d, gives the linear VOR its dependence on proximity, needed to transform velocity information from Cartesian to polar coordinates. This transformation is needed because the eye movement response is a rotation. The visual pathway also needs an increased sensitivity when the visual target is nearby, because at near distance the increasing retinal-image velocity ("blurring") tends to saturate the effectiveness of the visual pathway in inducing an adequate eye velocity. Reference to this proximity concept will also be made in the following discussion on OKN modulation.

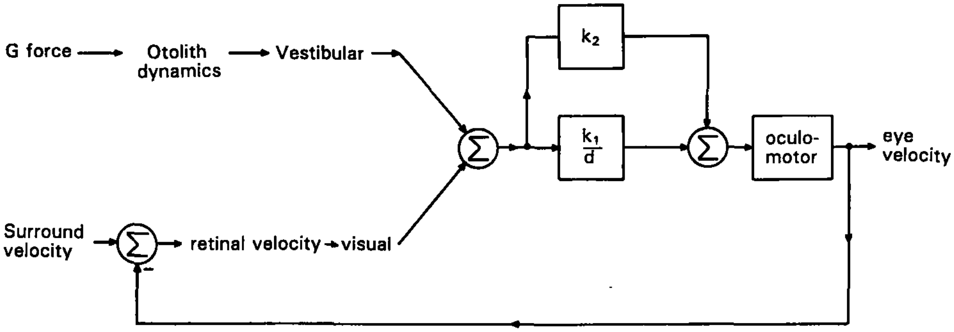

Fig. 1.7 Proposed model showing the effect of variable viewing distance d. The vestibular response to G force and the visual response to linear surround velocity are added. The variable element, k_1/d, makes the ocular response inversely proportional to viewing distance. k_1 and k_2 are constants (modified from Schwarz et al., 1989).

1.3.4 Otolith influence on canal-induced nystagmus

Additional evidence for an otolith-ocular pathway was obtained from two experiments where a canal-induced nystagmus is modified by otolith influence: (1) Suppression of post-rotatory nystagmus by tilt movements, and (2) Continuation of nystagmus during off-vertical axis rotation. The mechanisms of these otolith effects, reviewed in Benson (1974), will be summarized below.

Tilt suppression. A post-rotatory nystagmus in man decays in darkness with a decay time constant of about 20 s. If the subject tilts the head forward, just as the post-rotatory nystagmus begins, the time constant drops to about 7 s, presumably by dumping of stored velocity information (Zee, 1988). The underlying cause for this dumping could be an intravestibular conflict: The preceding rotation has been signalled by the canals, which normally induce a post-rotatory nystagmus for at least 20s. However, with the head tilted the otoliths are denying any continuation of rotation, and thereby they could suppress the post-rotatory nystagmus. It was shown by Igarashi (1980) in monkeys that this effect of tilt-angle disappeared after bilateral otoconial ablation, which provided evidence that indeed the otoliths are responsible for the suppression of nystagmus.

During *off-vertical axis rotation* the opposite effect occurs: while canal signals have faded away because angular velocity remains constant, the otoliths are sensing continued rotation because the direction of gravity is continuously changing with respect to the head (Guedry, 1974; Raphan and Schnabolk, 1988). In this case the otoliths might produce a gravity-related velocity command, which could be responsible for a persisting nystagmus. There is a sustained bias component with a superimposed cyclic modulation component of the slow-phase eye movement velocity. These two components are not present during rotation around an earth-vertical axis, and might be considered as dynamic otolith output signals. Steer (1970) suggested however that density-differences between endolymph and perilymph are creating a travelling constriction around the membranous ring, stimulating the semicircular canals by a pumping action. The role of semicircular canal stimulation in this condition is still in discussion.

1.3.5 Summary of otolith-ocular responses

On the parallel swing a pure otolith-induced vertical nystagmus was observed, with a subject-dependent amplitude of about 10 deg $\cdot$ s^{-1} per g unit. These manifest eye movement responses were induced by a specific force vector amplitude in the range from .03g up to .34g. Considering that eye velocity was far from saturated, larger otolith-ocular responses are to be expected in hypergravity. The underlying mechanism of the linear VOR was explained with a current concept of compensatory eye movements during lateral acceleration. In this view, the amplitude of the linear VOR is inversely proportional to the target distance. Additional evidence for otolith induced modulation of nystagmus in man is obtained from tilt-suppression and off-vertical axis rotation.

1.4 Models of vestibulo-ocular responses

1.4.1 Optokinetic Nystagmus (OKN)

Current models predict that a simultaneous input of specific force and optokinetic stimulation provides a tool to make the otolith effect more manifest through modulation of the optokinetically induced nystagmus (OKN). OKN is a reflex pattern of eye movements, elicited by a moving visual pattern, aimed at reducing the velocity of the image on the retina; the "slip" velocity. When the optokinetic stimulus velocity ranges between about 30 deg $\cdot$ s^{-1} and 90 deg $\cdot$ s^{-1}, the eye does not quite follow the stimulus; the "gain" of the optokinetic eye velocity response is smaller than 1. Gain values are about 0.9 at 30 deg $\cdot$ s^{-1}, and 0.6 at 90 deg $\cdot$ s^{-1} optokinetic stimulus velocity (Buizza et al., 1980). Imperfect stimulus tracking allows any other effect to superimpose on the response.

The optokinetic response is due to a combined action of two neuronal subsystems (Van Die, 1983; Collewijn, 1985): (a) a direct pathway, probably used by the smooth pursuit system, is mainly stimulated by patterns restricted to the central part of the visual field, and (b) an indirect pathway that includes the vestibular nucleus. It is through this central interaction that vestibular stimulation might be more manifest in OKN response (Fig. 1.8).

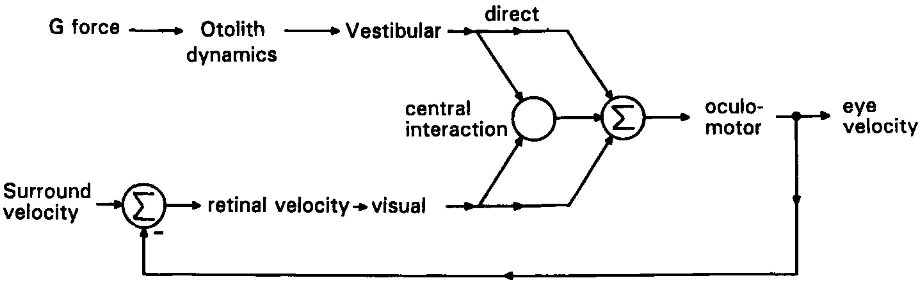

Fig. 1.8 Basic model of a central interaction between otolith stimulation and visual input, in generating the eye velocity signal. It is hypothesized that the otolith output becomes more manifest through a central interaction with the visual optokinetic signal. Both the direct vestibular pathway and this central interaction will be investigated in the experimental set-up.

1.4.2 OKN modulation through central interaction

The general concept of central interaction means that otolith-ocular and canal-ocular responses are not only three-neuron reflex arcs, but that they are also modulated by processes at higher levels in the central nervous system. The following mechanisms of central interaction can be identified:

(a) The proximity cue of the OKN stimulus;
(b) Addition of OKN and VOR;
(c) Velocity storage.

The proximity cue of OKN

In section 1.3.3 it was shown that the proximity cue of an imagined target enhances the linear VOR in response to stepwise acceleration. A limitation of this approach is the possible interference of cognitive factors with the pure vestibular response. The advantage of optokinetic stimulation, above fixed targets, is that a well defined proximity cue is provided, while there is no visual fixation.

Addition of OKN and VOR

Waespe and Henn (1977) measured that the discharge rate of neurons in the vestibular nucleus of monkeys responded transiently to rotation in the dark, and in a sustained way to optokinetic stimulation. Using these data, Robinson (1977) showed by model calculations that optokinetic and semicircular signals are combined by linear addition. In our experiments this assumption of linear addition will be applied in the analysis of responses.

Buizza et al. (1980) confirmed the usefulness of optokinetic stimulation. With sinusoidal lateral acceleration (0.2Hz, amplitude 0.16g) on a linear track the induced modulation of OKN eye velocity was reported to be 20 $\deg \cdot s^{-1}$ peak-to-peak. This modulation amplitude is equivalent to 61 $\deg \cdot s^{-1}$ per g unit. Clement et al. (1986) reported vertical OKN modulation in parabolic flight, to be treated in Chapter 4. Similar findings on vertical OKN were obtained in tilt studies by Clement and Lathan (1991).

Velocity storage

In this section on OKN modulation another mechanism of central interaction cannot be ignored. This is a neural process that preserves or "stores" slow-component velocity, the "velocity storage" integrator. It was postulated (Raphan et al., 1979; Matsuo and Cohen, 1984) that a common velocity storage integration is used for producing semicircular canal-induced vestibular nystagmus, OKN and OptoKinetic After Nystagmus (OKAN). Evidence was found in the similar time course of vestibular nystagmus and OKAN, and their linear summation. These concepts were extended by Bles et al. (1985) for somatosensory nystagmus. The velocity storage model will have relevance in the design and interpretation of our centrifuge and sled experiments.

An influence of the 1g gravity vector on OKN was measured by Raphan and Cohen (1988) in tilt studies on monkeys: they observed that the rotation axis of horizontal OKN tends to align with the earth's gravity direction, rather than being fixed to the head of the monkey. The phenomenon was modelled in terms of three-dimensional velocity storage, aimed to control optokinetic following around an earth-vertical axis. It is not known how this velocity storage responds to hypergravity; this important issue will be treated in Chapter 6.

1.4.3 Summary of vestibulo-ocular reflex models

The central interaction concept suggests that the otolith-ocular effect becomes more manifest through interaction with a visual pathway. The following mechanisms of central interaction are relevant to our study:

(a) A proximity cue, which enhances the sensitivity of the otolith-ocular reflex. The optokinetic stimulus provides this proximity cue, without enabling visual fixation.

(b) Addition of OKN and VOR.

(c) The central integrator of the velocity storage model.

1.5 Conclusions from current models

Recent experimental data and model concepts on otolith-ocular responses have been reviewed. With regard to the responses to specific force the following may be concluded:

(a) From otolith physiology the dynamic force-response range is estimated to extend up to at least 5g.

(b) Otolith-induced eye movements in man have been observed in several laboratory conditions. On a parallel swing the vertical otolith-ocular reflex was reported to have a sensitivity of about 10 $\mathrm{deg} \cdot \mathrm{s}^{-1}$ per g unit.

(c) On a linear acceleration track the otolith-ocular reflex can be enhanced by proximity cues. Application of optokinetic stimulation provides a technique to measure a more manifest otolith response.

(d) The central processing of velocity information is described by the current concept of velocity storage.

Chapter 2

Methods and experimental conditions

2.1 Definition of coordinate system

We start with a brief review of the input stimulus for the otoliths: the specific force G. Specific force has been defined in Chapter 1 as the resulting external force per mass unit. "Hypergravity" is commonly used to indicate conditions where the specific force is increased; "microgravity" means that specific force is near zero. We are aware that the notions hyper- and microgravity are formally incorrect, because the gravitational field is hardly different in these conditions. However, we occasionally apply these terms because they are widely used.

The components of specific force are specified in the head-based coordinate frame indicated in Fig. 2.1.

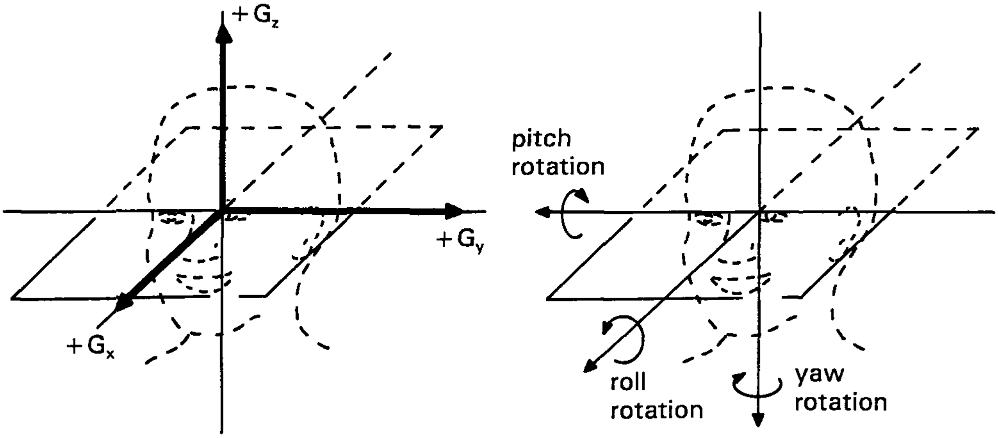

Fig. 2.1 *Definition of coordinates.* The components of specific force (left diagram) and angular velocity (right diagram) are defined with respect to the subject's head.

The indices x, y, and z refer to the orthogonal frame defined with respect to the subject's head: x represents the naso-occipital axis; y the interaural axis and z the spinal axis (Hixson et al., 1966). Vector polarity of the specific force components G_x, G_y, and G_z in Fig. 2.1 is consistent with the right-hand screw convention.

The angular velocity directions yaw, pitch and roll are also defined in Fig. 2.1 with respect to the head. Horizontal and vertical eye movement directions are referred to the head of the subject. In our study, we define rotations rightward and upward as positive.

In the same head-based coordinate frame three orthogonal planes are defined: the sagittal plane through the X-Z axes, the frontal plane through the Y-Z axes, and the transversal plane through the X-Y axes. The semicircular canals will be treated in terms of the "idealized" system, as if they were oriented exactly in these orthogonal planes (Benson, 1988). For example, an angular acceleration "effectively in the sagittal plane" of the subject is equivalent to angular acceleration in "pitch" of the subject, and induces vertical eye movements. These conventions regarding the coordinate system are useful in the description of our centrifuge experiment.

2.2 Outline of experiments

This section gives a general presentation of the experimental conditions in chronological order. First, we shall explain why the finding of a sustained vertical nystagmus in the centrifuge needed extension and confirmation in other experimental situations.

A general methodological point of concern is the separation of otolith responses from semicircular canal responses. Whenever large specific forces are created in a rotating laboratory device, such as the centrifuge, the subject is also exposed to angular accelerations which stimulate the semicircular canals. The otolith response can be separated from the response evoked by the semicircular canals when we assume linear superposition of both responses. However, an experimental confirmation of the linearity assumption, based on experiments with less or absent canal stimulation, is required.

The outline of experiments (Table 2.1) shows laboratory experiments (centrifuge, rotating chair, linear track or "sled"), and a field experiment (the parabolic flight manoeuvre). The G_z load ranges from 0g (parabolic flight) up to 3g in the centrifuge. The angular velocity is ranging from zero (linear track), up to 150 $\text{deg} \cdot \text{s}^{-1}$ in the human centrifuge. The angular *acceleration* in the subject's sagittal plane amounts up to 31 $\text{deg} \cdot \text{s}^{-2}$ both in the centrifuge and on the rotating chair. This acceleration is certainly above-threshold for the semicircular canals.

Table 2.1 The motion environment in the experimental conditions, described by approximate values of G force and angular velocity. (a): including gravity, (b): perpendicular to gravity.

	G range [g]	Pitch angular velocity [deg · s^{-1}]
Centrifuge	1 - 3 (a)	150
Rotating chair	0 (b)	150
Parabolic flight	0 - 2 (a)	0
Linear track sinus 0.2 Hz	0.2 (b)	0

The relations between these experiments can be summarized as follows: a hypergravity effect was discovered during $+3G_z$ in the *centrifuge*, in the form of a sustained vestibular slow-component downward nystagmus. However, in this experiment otolith- and canal-responses had to be separated, assuming linear superposition of the responses. The *rotating chair* experiment yields only the angular acceleration effect, by placing the subject's head in the centre of rotation. This condition serves as a 1G-reference measurement to the centrifuge study. The *parabolic flight* presents the opportunity to measure pure otolith responses, because angular acceleration can be minimized. In addition, it provides the 0g condition. Because in the centrifuge no sustained nystagmus had been found in response to G values below 3g, the phenomenon of vestibularly induced OKN modulation is used to obtain a more sensitive otolith response. However, the observed modulation in flight was considerably less than was expected from data in the literature, which was an incentive to us for studying OKN modulation in more detail on a linear track. The *linear track "sled"* could provide a laboratory reference test for findings obtained in the centrifuge and in flight. The acceleration profiles of the sled are sinusoidal. The phase of the otolith-ocular response is determined, and compared to the theoretical phase diagrams of the otolith sensory cells, as presented in Chapter 1. The sled might thus provide a link between the theoretical otolith models discussed in the introduction, and our experimental data.

Chapter 6 is dedicated to the modelling of vestibulo-ocular responses to G forces. An attempt is made to integrate the findings from our different experiments. These are linked with the current model concept of velocity storage.

2.3 Data acquisition

2.3.1 Measurement of stimulus parameters

A general survey of the recording-path is presented in Fig. 2.2. The potential stimulus inputs are G force, angular velocity, and optokinetic velocity (parabolas, sled).

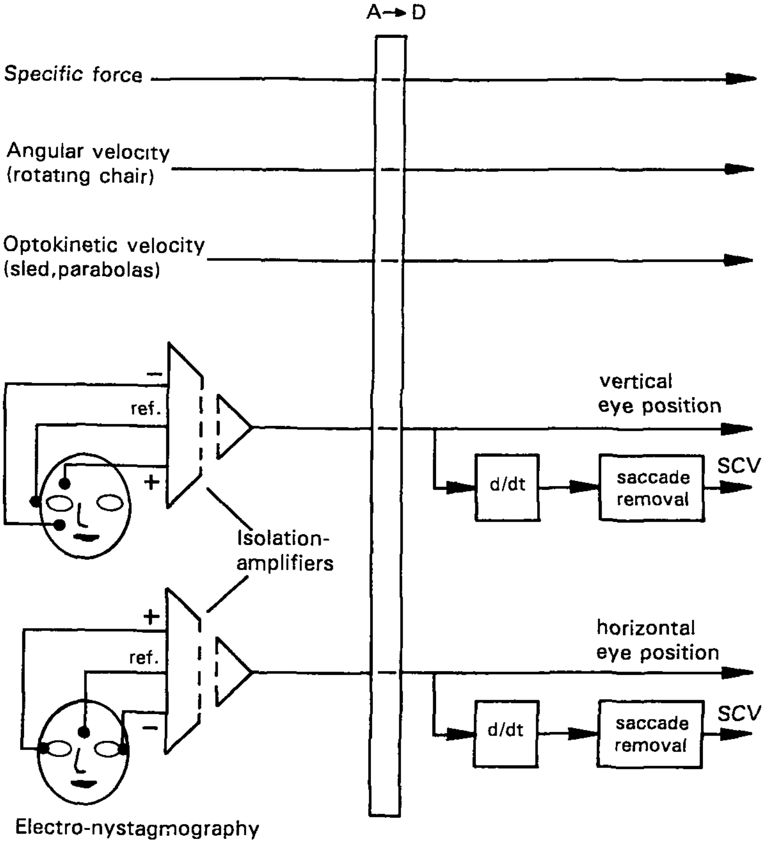

Fig. 2.2 Basic general diagram of *data acquisition*. The potential stimulus inputs are G force, angular velocity (rotating chair and centrifuge), and optokinetic stimulus velocity (parabolic flight and sled). Responses are horizontal and vertical eye movements, as measured by ENG.

In the centrifuge, the G signal was sampled from the computer that controls the device. Angular velocities in the centrifuge were calculated from this G profile by applying basic mechanics. On the rotating chair, angular velocity was sampled from the control-computer. In parabolic flight, we obtained the G signal with a separate sensor for specific force (Entran, type Egax-5). On the sled, the G signal was derived from the sled-position signal, that we obtained from the electronic control system of the sled.

When optokinetic stimulation was applied, the optokinetic-velocity signal was usually sampled from the optokinetic control system.

2.3.2 Measurement of eye movement responses

The eye movements were measured by Electro-Nystagmography (ENG). The ENG method is based on the existence of a difference in electrical potential between the anterior and posterior part of the eye. The ENG signal was picked-up by disposable silver-silverchloride electrodes (Medicotest). The electrode-positioning for horizontal and vertical eye movement measurements is shown in Fig. 2.2.

The horizontal signal was derived bitemporally by electrodes placed at the outer canthus of each eye, with the reference electrode on the centre of the forehead. The vertical signal was derived from the right eye by electrodes directly above and below the eye, centred on the pupil with the eye in the primary position. The reference electrode for the vertical signal was placed behind the right ear. Calibration was obtained with visual targets, located in the centre and at off-centre angles above, below, to the right and to the left. The subjects were instructed to keep their eyes open throughout all eye movement recordings. The signals were sampled at 100 Hz. In the parabolic flight experiment, data had been stored on FM-tape before sampling.

Data-analysis was focused on the slow-component velocity SCV, which is described in the next section. The eye position signal was systematically measured and inspected, in order to check for electrode-drift or gaze-shifts, which could interfere with the SCV measurement. The potential effects of ENG artifacts (noise, drift, calibration shifts, motion artifacts) will be considered in the discussions of the separate experimental results. It is emphasized here that in all experiments both horizontal and vertical eye movements were recorded.

2.4 Slow-component velocity

The slow-component velocity (SCV) curve was calculated by means of an interactive computer program, allowing saccades and eye-blink artifacts to be rejected (Barnes, 1982; Skalar Medical, 1991). It is a semi-automated version of the procedure described by the C.H.A.B.A.-Committee (1992). The procedure is demonstrated in Fig. 2.3.

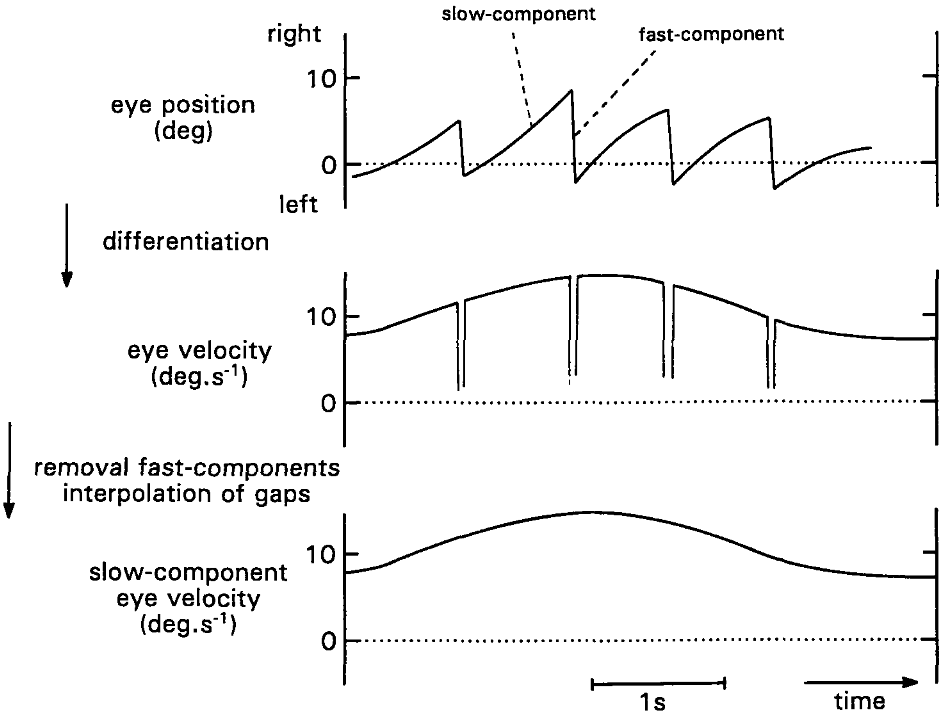

Fig. 2.3 *Procedure of SCV calculation.* The time derivative of eye position is calculated by digital differentiation. Subsequently the fast-component outliers in the velocity trace are rejected.

In this example a horizontal nystagmus is shown. In the eye position trace two different components can be seen: a slow-component to the right, and a fast-component resetting the eyes to the left. The first step in the SCV calculation is digital differentiation of the calibrated eye position signal, yielding eye velocity. In the eye velocity signal the slow-component is interspersed with brief high-velocity spikes of reversed polarity, representing the differentiated fast-components. In the second step, thresholds are set below and above the slow-component curve. Fast-components are recognized because their sample points lie outside the thresholds. They are automatically discarded.

The resulting slow-component trace is inspected by the operator, who checked whether all fast-components had indeed been rejected. If this was not the case, the rejection procedure was repeated with more narrow threshold settings. At this point in the analysis, there is thus necessarily an operator-dependent element in the rejection of fast-components.

Finally, the "gaps" in eye velocity caused by this process are filled in with a linear interpolation between neighbouring slow-component values, at the same sampling times where fast-components had been removed. The SCV data thus obtained are equally-spaced in time, which will enable us to average across different SCV curves. The constant time spacing will also be helpful in frequency analysis of SCV.

Occasionally, the term "Slow-Phase Velocity" (SPV) will be used as a synonym for SCV. Also the terms "upbeat" and "downbeat" nystagmus are sometimes used as synonyms to SCV-down and SCV-up nystagmus, respectively. However, according to the C.H.A.B.A.-Committee (1992), the correct term to quantify amplitude and direction of nystagmus is the SCV.

The potential effects of gaze-shifts (a slowly varying baseline of the ENG) on the slow-component velocity are discussed in Chapters 4 (the parabolic flight experiment) and Chapter 5 (the sled experiment). These effects are also called the effects of "range" or "beating field".

Acknowledgments

Bos, J.E. & Kistemaker, N. (1991). Interactive software for the analysis of eye movements. Personal communication from the Department of Medical Physics, Free University, Amsterdam.

Chapter 3

Vestibulo-ocular responses in man to $+G_z$ hypergravity

(*Aviation, Space, and Environmental Medicine* 61, 1990, 631-635)

Abstract

The influence of high $+G_z$ gravito-inertial force on the vestibular system in man was investigated in a centrifuge (radius 4 m) with a freely swinging gondola. The G_z profile was: acceleration $+.2G_z \cdot s^{-1}$, $+3G_z$ sustained for 3 minutes, deceleration $-.2G_z \cdot s^{-1}$. The subject was exposed to this profile in two conditions in randomized order: facing forward and facing backward. Under these conditions the effective angular velocity in the plane of the vertical semicircular canals is opposed. Adding the slow phase velocity responses from these conditions yields the G_z effect only; subtracting yields the angular velocity effect only. Vertical vestibular nystagmus was analyzed with five subjects. Results indicate that $+3G_z$ induced a subject-dependent vertical nystagmus with slow phase downwards. The average amplitude of this nystagmus reached a maximum of 27 deg $\cdot s^{-1}$ at 16 s from G onset, and was 11 deg $\cdot s^{-1}$ after 3 minutes of sustained $+3G_z$. The vestibular stimulation by $+G_z$ could result in false subjective perception of attitude, and could play a major role in spatial disorientation in flight.

3.1 Introduction

The aim of this study was to evaluate the influence of sustained high $+G_z$ gravito-inertial force (= G_z load) on the vestibular system. The $+G_z$ acceleration was generated by means of a centrifuge; the vestibular function was evaluated by analysis of the vertical nystagmus induced by the angular and linear acceleration of the centrifuge gondola.

In the centrifuge high G_z load is always inherently coupled with high angular velocity. In high performance aircraft, however, the pilot experiences high G forces, but without the high angular velocities that occur in the centrifuge. Thus in order to determine the G effect from centrifuge data it is necessary to separate the effects of angular velocity and G.

3.2 Method

Subjects were male civilian university students, aged 18-25 years. Baseline measurements at 1G were performed on ten naive subjects. The high G centrifuge data were obtained from another group of five naive subjects[1]. These underwent routine medical examination and were made familiar with experimental conditions in the centrifuge. They wore an anti-G protection suit, and were instructed not to make any head movements during the centrifuge run. In all runs the gondola was darkened to eliminate light sources for visual fixation, and the eyes were kept open throughout nystagmus recordings. Vertical vestibular nystagmus was measured with DC-electronystagmography, with high frequency cut-off at 100 Hz. The nystagmus slow phase velocity (SPV) was computed by means of a semi-interactive computer program, allowing eye blink artifacts to be rejected. SPV values were linearly interpolated at time intervals of 0.5 s in order to obtain continuous curves.

The centrifuge with radius 4 m is located at the National Aerospace Medical Centre, Soesterberg, The Netherlands. The gondola is fixed in pitch mode, but freely swinging in roll, so that the test subject within the gondola experiences a z-axis acceleration that is aligned with the resultant of the centrifugal and gravitational accelerations. For this coordinated turn calculations show that the largest effective angular acceleration impulse occurs in the subject's sagittal plane, because during the onset of G_z this plane rotates nearly into the plane of rotation (see Table 3.1). The semicircular canals will be described in terms of the idealized system, as if the canals would be oriented exactly in the subject's sagittal, transversal and frontal planes. The vertical canal will denote here the idealized vertical canals in the subject's sagittal plane. The plots of G_z and angular velocities are presented in Fig. 3.1.

---

[1] The centrifuge experiment started with 11 subjects, from which 6 subjects had to be disregarded. One suffered severe motion sickness; in five subjects the vertical eye movement recordings were disturbed frequently by blinking, or large offset shifts in acceleration. In two of these five subjects a sustained SPV-down nystagmus during 3G was nevertheless observed in parts of the data, with amplitudes of 10 and 14 deg · s^{-1}. The unbalanced number of five centrifuge subjects was left for detailed analysis. The centrifuge volunteers could not participate in the 1G control test, because of time scheduling reasons.

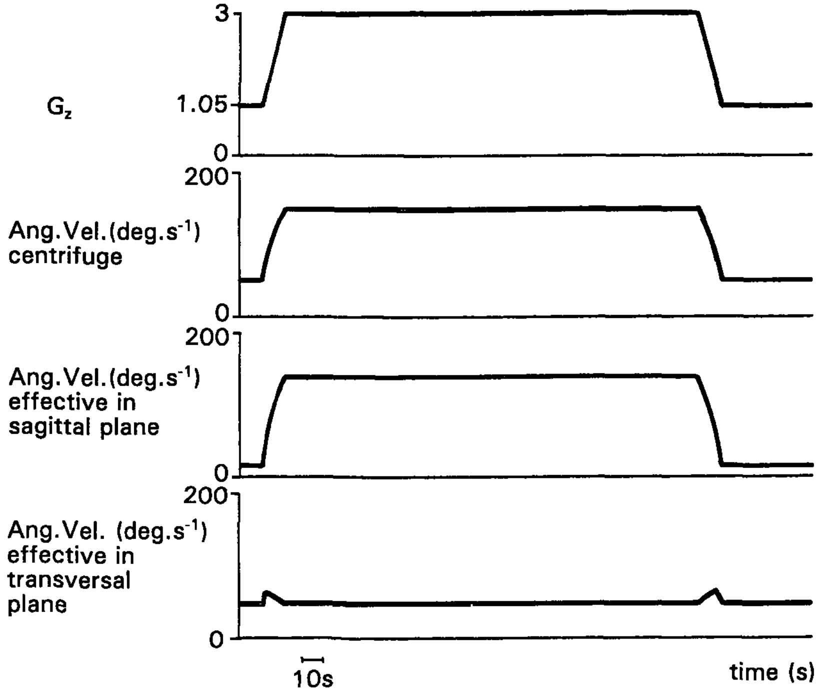

Fig. 3.1 The motion environment that the subject within the gondola experiences. The 1.05 G_z interphase started 60 s before the onset of the $+3G_z$ load in order to damp out the effect of the initial acceleration effective in the transversal plane that occurs during the transition from 1 to 1.05 G_z. In the transition from 1.05 to 3 G_z the largest angular acceleration is effective in the subject's sagittal plane.

Table 3.1 The computer-controlled $3G_z$ profile; the corresponding angular velocity of the centrifuge, and the angular velocities effective in the sagittal and transversal planes of the subject's head.

Time [s]	G_z [g]	Ang.Vel. Centrifuge [deg · s^{-1}]	Ang.Vel. Sag. plane [deg · s^{-1}]	Ang.Vel. Transv.plane [deg · s^{-1}]
0	1.05	51	15	48
60	1.05	51	15	48
70	3.00	151	142	50
250	3.00	151	142	50
260	1.05	51	15	48
320	1.05	51	15	48

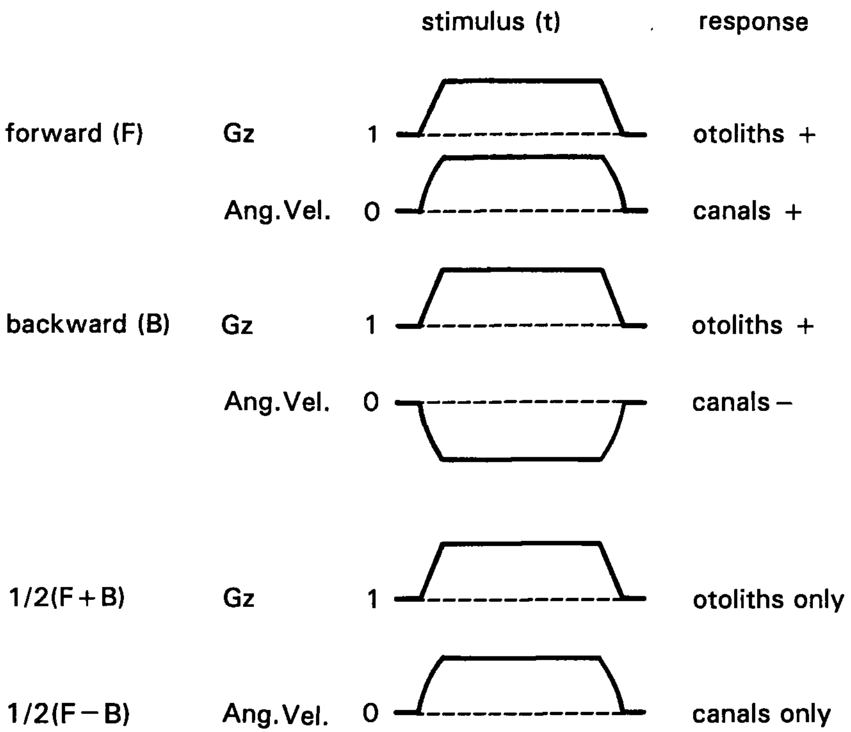

Fig. 3.2 Symbolic diagram illustrating the stimuli and responses in centrifuge runs with the subject facing Forward, and Backward. The gondola swings freely in roll; thereby in the Backward condition the angular velocity profile effective in the sagittal plane is equal in amplitude, but opposed in direction. Adding of responses yields the presumed otolith effect only; subtraction yields the canal effect only. In the experiment, G_z was ranging from 1.05 to 3 G, and the angular velocity in the sagittal plane from 15 to 142 $\text{deg} \cdot \text{s}^{-1}$.

Given the linear G profile, the non-linear angular velocity profiles were calculated applying basic mechanics. The interphase of 1.05 G_z was applied in order to reduce the Coriolis stimulation, due to the roll movement of the gondola during acceleration and deceleration. Peak angular acceleration is effective in the subject's sagittal plane, amounting to about 31 $\text{deg} \cdot \text{s}^{-2}$. The angular acceleration effective in the subject's transversal plane, calculated over the range from 1.05 till 3 G_z, is less than 1 $\text{deg} \cdot \text{s}^{-2}$, because the transversal plane rotates nearly out of the plane of rotation. (It is assumed here that the small upward deflection in the transversal angular velocity curve at 1.4 G_z has no net effect.)

Separation between G effects and angular velocity effects was obtained by applying the same G_z profile on each subject in two conditions: the subject facing forward (F), and the subject facing backward (B). To accomplish this, the chair in the gondola was rotated through 180 deg in yaw between measurement runs. The angle between the head support and the z-axis in the gondola in both conditions was inclined 15° backwards for the subject. The sequence of forward and backward runs was randomized among subjects. In the facing forward condition the angular velocity profile in the sagittal plane is positive (upward for the subject). In the facing backward condition the angular velocity profile is equal in amplitude, but inverted: see Fig. 3.2. Thus by adding the responses from both conditions only the G effect remains, presumably induced by the otoliths; by subtracting the backward from the forward response only the angular velocity effect remains, induced by the canals.

This technique of addition and subtraction of responses is only valid if there is no physiological asymmetry between up- and downbeat nystagmus. The up- and down-responses at 1G were investigated by positioning subjects on their side on a rotating platform. The head was in the centre of rotation, in order to minimize centrifugal forces acting on the vestibular sensors. The computer-controlled platform generated the same non-linear angular velocity profile in the sagittal plane of the subject's head, as the centrifuge did during the 3G run. It should be noted that in this 1G baseline condition the direction of the gravity vector is parallel to the subject's y-axis (lateral).

3.3 Vestibular nystagmus data

3.3.1 The 1G baseline data

In Fig. 3.3 the 1G baseline data are presented, averaged over 10 subjects.
Addition of Forward and Backward responses, the trace 1/2(F+B), results in a zero line (except for noise). These data suggest that the angular acceleration responses are up-down symmetric. Therefore it seems justified in the centrifuge analysis to eliminate the angular acceleration effect by adding forward and backward responses, yielding the G effect only. The data from 10 subjects are presented in Table 3.2. The decay time constant has been determined by measuring the time interval between peak SPV amplitude and decay to (1/e) of peak value.

Table 3.2 Vertical nystagmus slow phase velocity data during the 1G baseline measurement (10 subjects). Amp is amplitude, and Tc is decay time constant. The individual responses to angular acceleration and deceleration were obtained from the individual curves 1/2(F-B); from these values the average and standard deviation were calculated.

	Ang.Acc. response from 1/2(F-B)		Ang.Dec. Response from 1/2(F-B)	
	Amp [deg · s^{-1}]	Tc [s]	Amp [deg · s^{-1}]	Tc [s]
Average	69	6.4	57	6.5
Stand.dev.	12	2.3	13	2.3

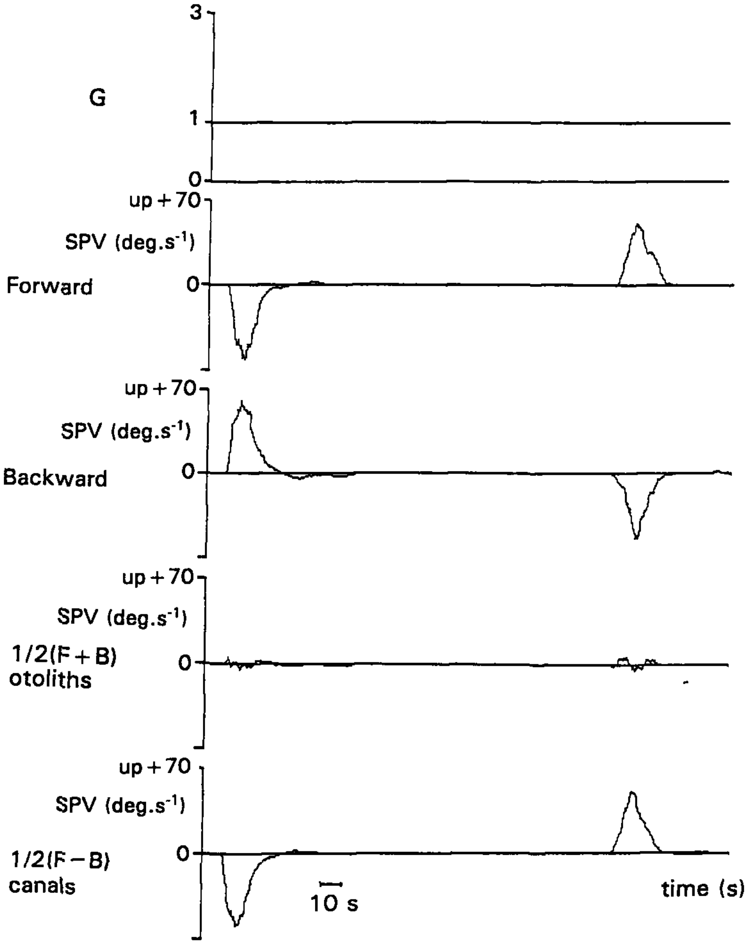

SPV = vertical nystagmus Slow Phase Velocity

Fig. 3.3 Baseline measurements of vertical nystagmus at 1G, averaged over 10 subjects. Subjects were lying on their side on a rotating platform.

3.3.2 The 3G data

The recordings of horizontal eye movements indicated a very low transient response during the transition between 1.05 and $3G_z$, as was expected from the low angular acceleration effective in the subject's transversal plane (Fig. 3.1). No sustained horizontal nystagmus was observed in any subject.

The addition and subtraction technique, as illustrated in Fig. 3.2, has been applied on the vertical slow phase velocity responses. Results in Fig. 3.4 are averaged curves over 5 subjects.

Note in the backward condition the reversal of SPV direction from upwards to downwards. This already suggests an otolith path, because the canal-induced eye movements have a SPV-upwards. The trace 1/2(F+B) denotes the half sum of forward and backward SPV-curves, and thereby, as demonstrated in Fig. 3.2, the pure G_z effect presumably induced by the otoliths. This averaged otolith curve reaches a maximum SPV value of -27 deg $\cdot$ s^{-1}, 16 s after G onset, and then gradually decreases to -11 deg $\cdot$ s^{-1} at the end of the $3G_z$ load. This could be a manifestation of rate-sensitivity, and adaptation. Subtraction of forward and backward SPV-curves and division by 2 yields the trace 1/2(F-B); only the angular velocity effect remains, induced by the canals. The individual responses to G_z and to angular acceleration and deceleration are presented in Table 3.3.

Table 3.3 Vertical nystagmus slow phase velocity data during the $3G_z$ centrifuge run. The response to $+G_z$ was derived from the individual curves 1/2(F+B), measuring after 3 minutes of sustained $+3G_z$. The responses to angular acceleration and deceleration were obtained from the individual curves 1/2(F-B).

Subject	$3G_z$ response from 1/2(F+B)	Ang.Acc. response from 1/2(F-B)		Ang.Dec. response from 1/2(F-B)	
	Amp [deg $\cdot$ s^{-1}]	Amp [deg $\cdot$ s^{-1}]	Tc [s]	Amp [deg $\cdot$ s^{-1}]	Tc [s]
1	0	108	6	116	8
2	-10	40	8.5	54	4.5
3	-8	85	9	91	5
4	-14	45	7.5	44	4.5
5	-21	121	7	81	7
Average	-10.6	80	7.6	77	6.5
Stand.dev.	6.9	33	1.1	26	1.5

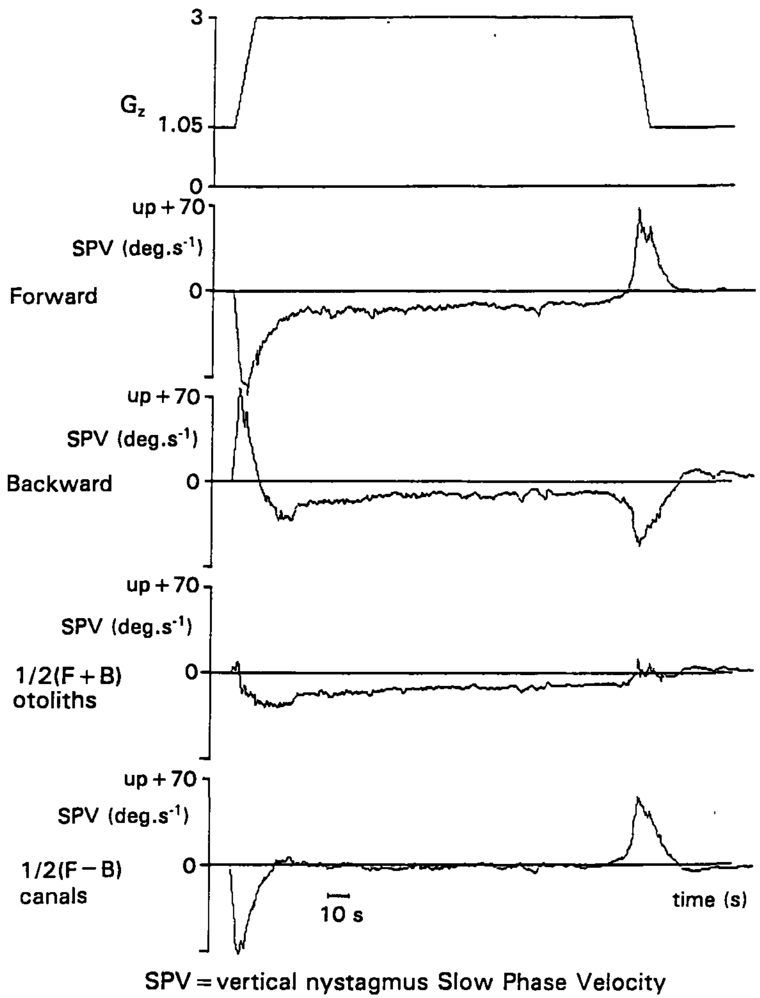

Fig. 3.4 Vertical nystagmus slow phase velocity (SPV) curves, obtained from the 3G centrifuge runs, averaged over 5 subjects. Conditions and analysis are corresponding with Fig. 3.2. Adding the forward and backward responses yields the pure G_z response, probably induced by the otoliths; subtracting yields the pure canal response.

Averaging individual amplitudes of angular responses yields larger values (80, 77) than the down- and up amplitudes of the averaged curve (Fig. 3.4, lower trace), because subjects give their maximum responses at different times.

3.3.3 Comparison 3G data vs 1G baseline

The canal response to angular acceleration and deceleration, derived from centrifuge data, is compared with the 1G canal response. It is assumed that the time constant is the most important parameter for this comparison. The decay time constants Tc from the 1/2(F-B) curves, obtained from the centrifuge and from the 1G rotating platform, are presented in Table 3.4. No systematic difference between canal responses from the centrifuge and the 1G platform was observed, which suggests that the subtraction of the centrifuge responses 1/2(F-B) does yield the pure canal response.

Table 3.4 Time constants of angular responses calculated from the 1/2(F-B) curves, in the conditions 1G and $3G_z$. An independent samples t-test was applied on time constants grouped by G. No significant difference was found for the acceleration responses ($p = 0.235$), nor for the deceleration responses ($p = 0.514$).

	1G (n=10)		$3G_z$ (n=5)	
	Tc [s]	St.dev.	Tc [s]	St.dev.
Ang.Acc.response	6.4	(2.3)	7.6	(1.1)
Ang.Dec.response	6.5	(2.3)	6.5	(1.5)

3.4 Discussion

3.4.1 Influence of linear acceleration on nystagmus

Benson (1974) and Lansberg et al. (1965) exposed subjects seated in a centrifuge with fixed gondola to a centrifugal y axis component G_y. A sustained horizontal nystagmus was observed, with the resultant slow phase opposed to the direction of G_y.

Young (1967) made a further analysis of the Lansberg data obtained from the subject seated in the fixed gondola, in the conditions facing forward and backward. In these conditions the angular stimulation is equal, and the linear G_y stimulus is opposed. Subtraction of horizontal nystagmus responses thereby yielded twice the linear acceleration sensitive component, called the "L" nystagmus. This experiment is complementary to the present study in the free swing gondola, where in the forward and backward conditions the angular stimulation is opposed, and the linear G_z stimulus equal. The L-nystagmus is consistent with the sustained slow phase down nystagmus during $+G_z$, observed in the present study.

3.4.2 Indications for otolithic origin of $+G_z$ response

The response amplitudes to G_z and to angular acceleration in this study are not correlated (see Table 3.3; the correlation coefficient = 0.2), which suggests that the G_z response is initiated by other sensors than the canals.

The set of experiments performed by Lansberg in the fixed gondola centrifuge contains two conditions which allow a further determination of the sensors. A comparison was made between two conditions in which the subject was recumbent. In one position the subject's head was pointing away from the centre of rotation, resulting in a 2.2 G centrifugal component acting in the subject's -z axis. In the second position the subject's head pointed towards the centre of rotation, resulting in a centrifugal component of about the same amplitude acting in the subject's +z axis. A sustained vertical upbeat nystagmus of about 5 $\text{deg} \cdot \text{s}^{-1}$ was only found during the $+G_z$, and not during the $-G_z$ force. It is unlikely that this could be explained with stimulation of proprioceptors or cupulae; the 1G measurements in this study have confirmed that the canal response is symmetric. Thus the direction-dependence indicates that the otoliths are responsible for the L nystagmus in the fixed gondola.

Fluur and Mellstrom (1971) and Gernandt (1970) have applied selective mechanical stimulation of exposed utricles in animals. During lasting stimulation a strong nystagmus was evoked. These findings support the concept of a direct connection from the otoliths to the nystagmus centre in the central nervous system.

In a previous centrifuge experiment a prolonged decay time of slow phase down nystagmus had been observed in $3G_z$ runs with the subject facing forward (Marcus et al., 1989). Considering the new data from forward and backward runs (Fig. 3.4, lower two traces), the interpretation should be that a decaying otolith G_z-response is superimposed on a normal canal response to the initial angular acceleration impulse.

3.5 Conclusions

1 The vertical nystagmus induced by semicircular canal stimulation only is up-down symmetric.

2 Pure canal responses in the centrifuge do not differ significantly from canal responses in the 1G baseline condition.

3 At +$3G_z$ a slow-phase-down nystagmus is observed, which reaches an averaged maximum amplitude of 27 $\deg \cdot s^{-1}$ at about 16 s from G onset. This response, probably otolithic in origin, is superimposed on the normal transient canal response.

3.6 Practical implications

A vertical nystagmus induced by +$3G_z$ has been observed in a coordinated turn. This condition is similar to a turning aircraft, which usually aligns itself to the resultant of gravity and centrifugal forces also. In high performance aircraft both the G_z onset rate and the G_z level used in our experiment are often exceeded considerably. Recent modelling of the otolith mechanics does not indicate saturation above 3G (Grant and Best, 1987). Thus even stronger nystagmoid eye movements are to be expected in flight.

The G_z effect, presumably induced by the otoliths, could have a major impact on the aviator's task performance. Incomplete suppression of nystagmus will lead to impaired visibility of instruments. In addition, inflight experiments have indicated that the G vector can contribute to a false perception of the aircraft attitude (Fulgham and Gillingham, 1989).

The slow phase down nystagmus provoked by +G_z could lead to the elevator illusion (Gillingham and Wolfe, 1986; Niven et al., 1963; Whiteside et al., 1965): during +G_z force the eyes are driven downward when visual cues are poor or absent. Attempting to stabilize the instrument panel visually, causes this panel to appear to shift upward when the G force is increased. An aviator who is sensitive to this vestibular illusion could be inclined to compensate by pitching downward.

Acknowledgments

The authors express their thanks to Dr. A.J. Benson and Dr. M.P. Lansberg MD, for their valuable advice and encouragement.

Chapter 4

Otolith responses in man during parabolic flight

(Submitted to *Experimental Brain Research*, 1992)

Abstract

The influence of the varying specific force (G_z) during parabolic flight on the human otolith function was investigated experimentally. It was hypothesized that a varying G_z force profile initiates an otolith-ocular response that manifests itself in modulation of optokinetic nystagmus slow-component eye velocity (OKN-SCV). Six subjects were seated in the ESA-Caravelle, facing perpendicular to the aircraft's longitudinal axis. The G_z profile was subsequently: 1.8 G_z pull-up, 0 G_z and 1.8 G_z recovery, each phase lasting about 20 s. Vertical eye movements were recorded with electro-nystagmography throughout the parabolic manoeuvre. Conditions were: (1) visual fixation, (2) darkness, and (3) optokinetic stimulation at 50 deg $\cdot$ s^{-1} in upward or downward direction, from a cylindrical screen at .6 m viewing distance. The otolith responses were evaluated by analyzing the modulation of slow-component eye velocity during the G_z conditions. No consistent nystagmus or gaze shift was measured in darkness. With optokinetic stimulation, however, ANOVA revealed downward enhancement of OKN-SCV by 5 deg $\cdot$ s^{-1} in 1.8 G_z hypergravity, as compared with the 0 G_z condition and the 1 G_z condition. It is concluded that an otolith-ocular pathway modulates optokinetic eye movements in parabolic flight.

4.1 Introduction

4.1.1 Rationale of the parabolic flight study

In the centrifuge study it was observed that $+3G_z$ specific force induced a sustained vertical nystagmus with slow component down (Marcus and Van Holten, 1990). In the centrifuge, however, fast G_z transitions are always inherently coupled with high angular accelerations in the subject's sagittal plane. These angular accelerations are not representative of normal flight patterns. Moreover, they induce responses of the semicircular canals confounded with otolith responses. The otolith responses recorded in the centrifuge were separated from canal responses by addition of the slow component velocity (SCV) responses obtained from forward and backward runs. This separation technique, however, was based on the assumption of linear superposition of otolith and canal responses. In order to confirm and extend our knowledge about the otolith system, the otolith-ocular responses should thus be measured in conditions with only specific-force input, without any canal stimulation.

A pure linear acceleration can be generated with a linear acceleration track such as the ESA "sled". Limitations of this device, however, include small amplitude of acceleration, up to a maximum of 0.2g for sinusoidal movements, and a permanent bias of the earth's gravitational field.

The parabolic flight manoeuvre provides conditions of fast G_z transitions, without a dominant vestibular canal stimulation. Even minor canal responses can be separated from otolith responses in parabolic flight, by positioning the subject such that the angular acceleration and the potential G_z influence are effective in mutually orthogonal planes. From the centrifuge data, the amplitude of vestibular nystagmus SCV was found to be 5 $\text{deg} \cdot s^{-1}$ per g unit change with respect to the $1G_z$ gravitational force (Marcus and Van Holten, 1990). In parabolic flight the G_z value ranges from 0g to 1.8g. Assuming linearity, the vestibular SCV amplitude evoked by the parabolic flights might thus be expected to reach only 5 $\text{deg} \cdot s^{-1}$.

4.1.2 Optokinetic Nystagmus as a tool for measuring otolith responses

When the visual field moves at a velocity greater than about 20 $\text{deg} \cdot s^{-1}$, the tracking eye velocity will lag behind the stimulus. The gain of optokinetic nystagmus (OKN), defined as the ratio of eye velocity to stimulus velocity, will thus be smaller than unity (Van den Berg and Collewijn, 1988; Murasugi and Howard, 1989). Several studies indicate that otolithic activity may show up as changes in this gain.

On a linear track Buizza et al. (1980) measured the influence of linear acceleration on the otoliths in the form of a modulation of the OKN. In monkeys, it was shown by Raphan and Cohen (1988) that otolith responses to gravity can become manifest in the tendency of the OKN rotation vector to align itself with the direction of gravity. In man, Clement et al. (1989) applied OK stimulation during parabolic flight. They observed a downward shift in the range of eye movement (the "beating field") upon entering microgravity. In man, an otolithic effect was also manifest in the effects of static tilt on OKN (Clement and Lathan, 1991).

4.1.3 Hypothesized effect in parabolic flight

The downward SCV induced by $+G_z$, as observed in the centrifuge, might appear in the form of an additive factor in the optokinetically induced eye movement. In parabolic flight this factor may be added in the 1.8 G_z phase, and subtracted in the 0 G_z phase. Thus, the driving force of the otoliths on eye movement might be demonstrated by simultaneous application of vertical optokinetic stimulation during a complete parabolic flight manoeuvre. The predicted modulation of the slow-component velocity (OKN-SCV) is presented in Fig. 4.1.

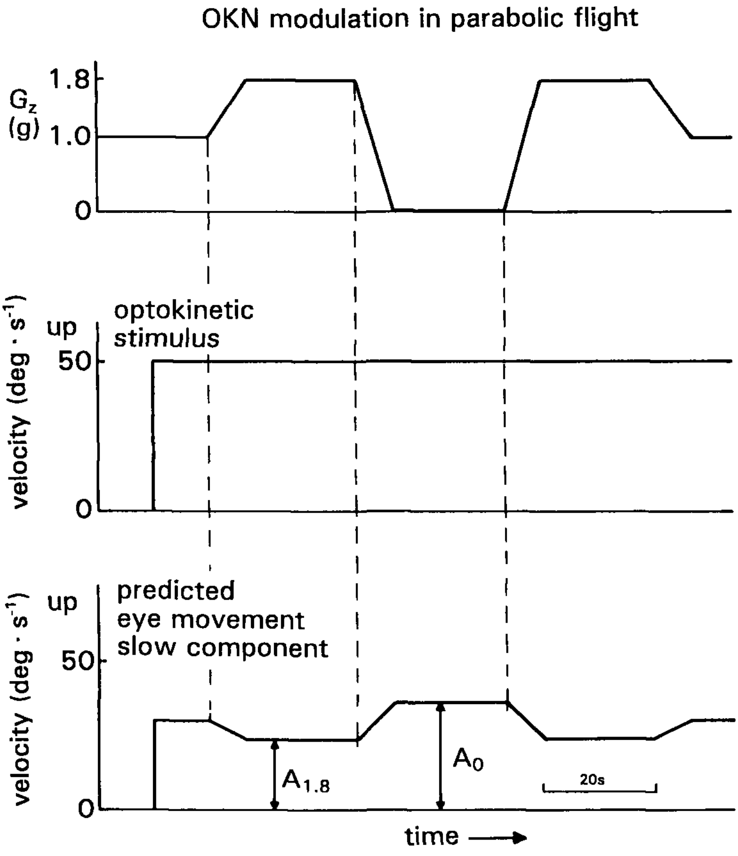

$$\text{modulation index} = \frac{A_0 - A_{1.8}}{A_0 + A_{1.8}}$$

Fig. 4.1 Hypothesized OptoKinetic Nystagmus (OKN) modulation in parabolic flight. With the applied vertical stimulus velocity of 50 deg · s^{-1} the gain of the OKN slow-component velocity is smaller than 1. The predicted modulation implies a downward drive in +1.8 G_z hypergravity and an upward drive in 0 G_z microgravity. In calculating the modulation index, $A_{1.8}$ is the mean OKN-SCV value from the 1.8 G_z pull-up and the 1.8 G_z recovery phases.

4.2 Methods

4.2.1 Parabolic manoeuvres

Parabolas were flown with the ESA "zero G" Caravelle, based at the Centre d'Essay en Vol in Brétigny, France. Microgravity ($G_z=0$) in the aircraft is obtained by entering a free-fall curve. This curve is a parabola because it takes place in a small volume where the earth's gravitational field can be treated as uniform, as seen in Fig. 4.2. In the beginning of the manoeuvre, the aircraft pulls up from straight and level flight, entering a 1.8 G_z hypergravity phase lasting 20 s. At 50-deg nose-up the pilot starts the microgravity phase. This moment is indicated as "injection", because at this point the aircraft is "injected" into a parabolic flight path. After about 20 s, at 50-deg nose-down, the aircraft enters the recovery phase with, again, 1.8 G_z hypergravity during 20 s.

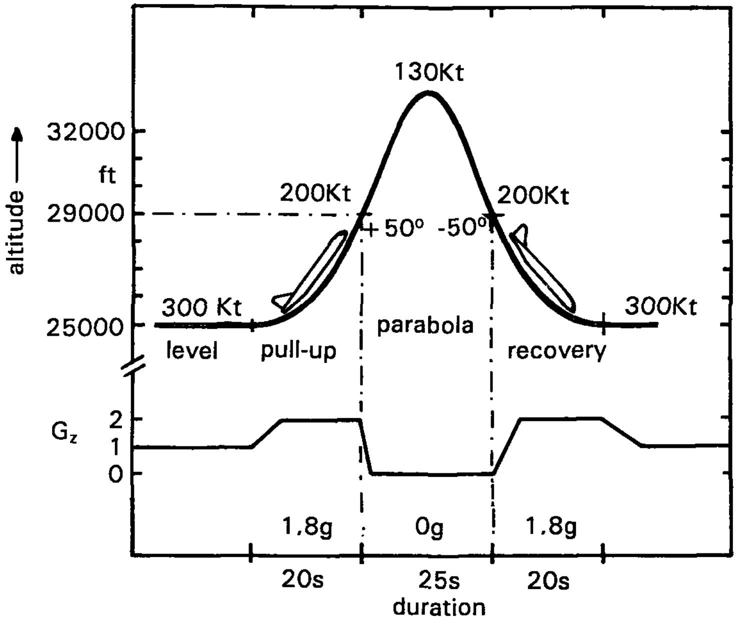

Fig. 4.2 Parabolic flight manoeuvre. The aircraft trajectory and the G_z level in the aircraft are plotted over time (from ESA documentation, modified). The resultant specific-force vector is continuously aligned with the aircraft's z-axis (within a 3 deg error range).

The G_z value at the subject's location was continuously recorded with a z-axis accelerometer type Entran Egax-5, range ± 5 G, frequency range 0-100 Hz.

4.2.2 Orientation of the specific force vector

In this chapter we use the current terms "hypergravity" and "microgravity", because these descriptions are widely used. However, in flight there is hardly any change in the earth's gravitational field. Hypergravity means in fact an increase of the specific force, generated by the lift force of the wings of the aircraft. Microgravity implies that the specific force is near zero. Thus we describe the otolith stimulation in terms of the specific force vector. This vector is defined within the aircraft's orthogonal reference frame x (afterward-forward), y (lateral), and z (up-down). Fig. 4.2 serves to illustrate that the resultant G vector during pull-up and pull-out is always aligned with the aircraft's z-axis.

The z-orientation of the G vector was verified by continuous measurements. The G_z vector value was stored on our data-recorder simultaneously with the eye movement data. In addition, the G_x, G_y, and G_z vector components were continuously measured throughout the parabolas by the flight engineer. The G_x vector had a maximum value of +0.1g, and this value was only reached during the 1.8 G_z pull-up phase. The G_y vector was always less then 0.02g. Thus the resultant G vector is well aligned with the z-axis of the aircraft during the entire parabolic manoeuvre, within an error of about 3 deg. The subject, strapped in a chair and with his head supported, did not experience any swing of the resultant vector direction.

4.2.3 Method of optokinetic stimulation

The projection screen was homogeneous, white, and cylindrically curved subtending a visual angle of 80 deg horizontally and 95 deg vertically (see Fig. 4.3).

The bar pattern was generated by means of an Osram 8.5 V DC, 6A tungsten bulb (type Wi 9) with a 5-cm linear filament, inside a rotating cylinder. The wall of the cylinder contained 15 slits parallel to its main axis, enabling projection of dark and light bars (12 deg each) by shadow casting. The luminances of the light and dark bars were 10 and .5 $cd \cdot m^{-2}$, respectively. The applied angular velocity of the cylinder was 50 $deg \cdot s^{-1}$ upward or downward. The stimulus projector above the head was off-axis with respect to the axis of the cylindrical screen, implying a slight non-uniformity of pattern velocity vertically across the screen. The chair-screen combination was surrounded by non-reflecting black curtains.

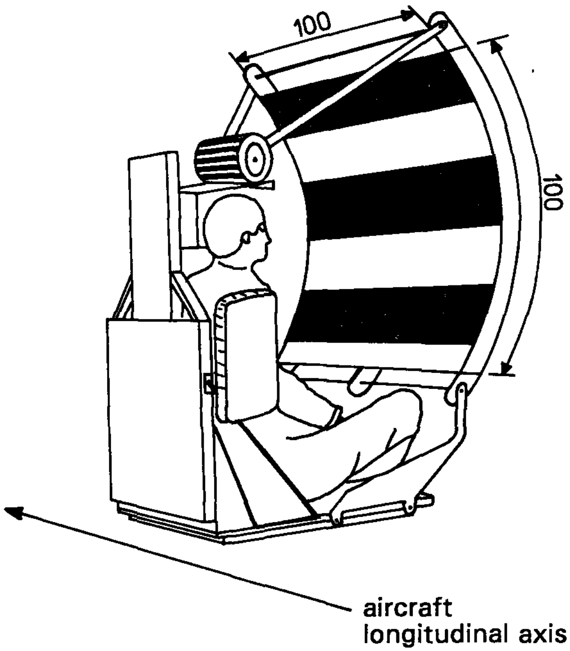

Fig. 4.3 The subject is sitting in front of a cylindrical projection screen, with .6 meter radius of curvature. Viewing distance is .6 m. The combination of chair, screen and projection cylinder has been fixed to the bottom of the aircraft. The subject is facing perpendicular to the aircraft's longitudinal axis. Thus the angular velocity of the aircraft during parabolas is effectively in the subject's frontal plane, and is not expected to influence the nystagmus in the subject's sagittal plane.

4.2.4 Protocol

In one flight, 2 sets of 15 parabolas each were flown. On board were a subject and an operator, who exchanged roles after the first set. Stimulus conditions besides the OK stimulation were: visual fixation at the stationary bar pattern, and darkness.

The *fixation* condition was applied in parabolas 1 and 10 in order to measure a possible drift in the ENG eye position signal, for example due to electrode offset shift or vasovegetative reactions of the subject. The projection lamp was switched on, the rotor switched off, and the subject fixated at the edge in front of him during the complete parabola. In the *darkness* condition the projection lamp was switched off, and an additional black curtain was placed in front of the subject's eyes, which were kept open. This condition was applied to measure the gaze shift and a potential vertical nystagmus of vestibular origin only, which both could influence the OKN-SCV. The planned sequence for each subject was as follows ("ok" = optokinetic stimulus):

Parabola number	*Condition*	*Parabola number*	*Condition*
1	fixation	9	ok down
2	dark	10	fixation
3	dark	11	dark
4	ok up	12	dark
5	ok down	13	ok up
6	ok up	14	ok down
7	ok down	15	ok up
8	ok up		

The optokinetic stimulus started 10 s before pull-up and was kept constant during the complete G_z profile. Between 2 subsequent parabolas there was an interval of straight and level flight lasting for 2 minutes.

4.2.5 Subjects

Six male subjects (ages 26-47 yr) underwent medical tests and hypobaric chamber training according to ESA requirements. They signed informed-consent forms of the experiment protocol, and did not use any medication. They were familiarized with the optokinetic stimulus before the flights. Their instructions were to keep their gaze in the middle of the screen within deviations of about 15 deg, and not to pursue any missed bar.

4.2.6 Eye movement analysis

Vertical and horizontal eye movements were measured with electro-nystagmography (freq. range of amplifiers: .1 Hz - 100 Hz), and recorded on a FM data-recorder. Calibration of the eye-movement signals was performed before take-off. The FM recorded (0-1 kHz) signals were low-pass filtered with the cutoff frequency at 50 Hz, and subsequently sampled at 100 Hz. The optokinetic nystagmus slow-component velocity (OKN-SCV) was analyzed off-line in subsequent steps:

1 Determination of eye velocity by differentiation of eye position.

2 Removal of the fast components in eye velocity, and interpolation of SCV during the fast components. This was performed by an interactive computer program that recognizes fast components whenever threshold limits in eye velocity are exceeded (Barnes, 1982; Bos and Kistemaker, 1991). This procedure was described in chapter 2. In this way a continuous SCV curve over time was obtained, throughout each parabola for each subject. Fig. 4.4 offers an example of eye position and velocity during the transition to microgravity.

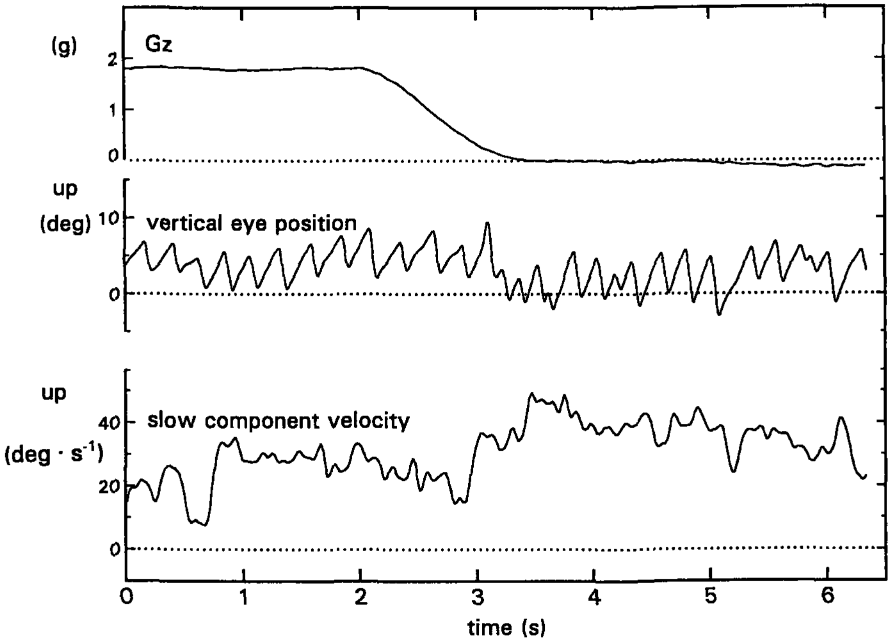

Fig. 4.4 Example of eye movement analysis during the transition from 1.8 G_z to 0 G. The eye position signal (middle trace) is differentiated in order to obtain the velocity signal. The outliers of fast-component velocity are then removed, and the slow-component velocity (SCV, lower trace) is interpolated over the time intervals of the fast components. During $G_z=0$ the SCV is enhanced in the upward direction.

3 Synchronization of the SCV curves from different parabolas at the time of "injection". Subsequently these curves were averaged across parabolas, by subject and OK direction (OK up and OK down). Fig. 4.5 illustrates the effect of averaging for the upward OKN-SCV traces: the signal to noise ratio is enhanced. OKN responses were not obtained from all scheduled parabolas

with OKN stimulation, the main reason being motion sickness (subjects 2, 4, 6). For subject 1, the sequence of parabolas was interrupted and discontinued because the aircraft had insufficient fuel. For these reasons the number of separated measures varied between 1 to 4 parabolas.

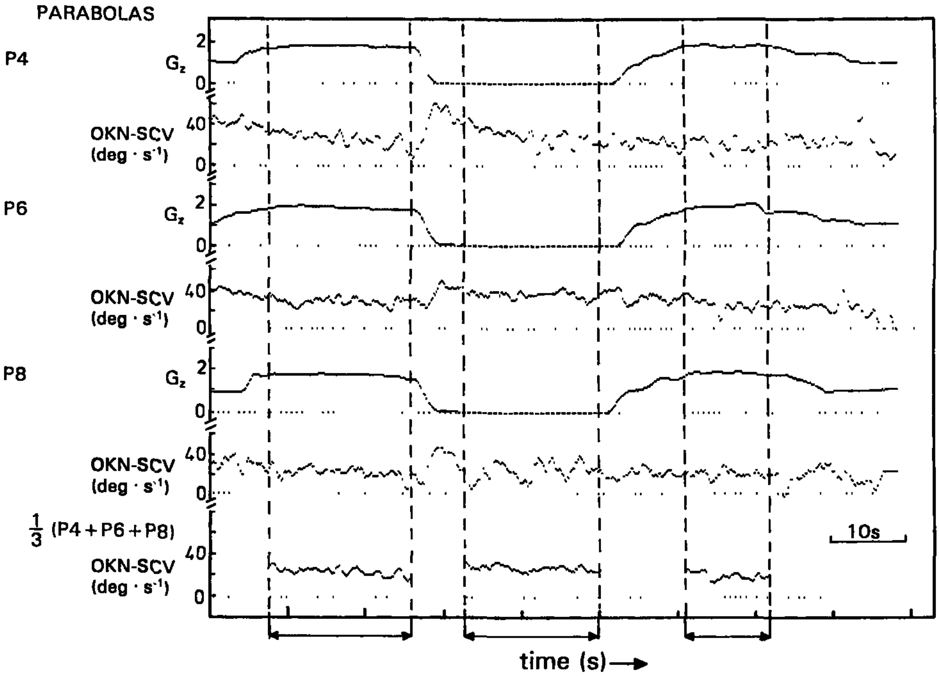

Fig. 4.5 Averaging of upward OKN-SCV traces over parabolas 4, 6, and 8, for subject 2. For each separate parabola the G_z profile and the SCV response are shown. The curves were synchronized at the time of injection, and subsequently they were averaged. The vertical broken lines delineate the time intervals in which the response was calculated for each G condition of the averaged trace 1/3(P4+P6+P8).

4 Calculation of mean SCV value and standard deviation over time during each G_z condition: 1 G_z, 1.8 G_z pull-up, 0 G_z, 1.8 G_z recovery. The averaged SCV response within each G condition is calculated over the time interval starting at least 5 s after the G transition, and for as long as the G value is in a steady state (± .1 g).

5 Analysis of Variance on these mean SCV values, obtained from 6 subjects, 2 OK conditions and 4 different G conditions. In this analysis, the subjects were regarded as a random variable. It was already mentioned that for some subjects the planned sequence of measurements was not completely fulfilled.

Therefore, one averaged SCV curve for each OKN condition was considered for each subject, in order to give each subject the same weight in the analysis.

6 From the SCV curves obtained in step 2, the modulation index (introduced in Fig. 4.1) was calculated for each subject in each separate parabola. This normalized measure facilitates a comparison between the modulation in separate parabolas, in order to check whether modulation is consistent within subject. The mean SCV response amplitudes at 0 G_z and 1.8 G_z are denoted A_0 and $A_{1.8}$, with $A_{1.8}$ determined by the mean of the 1.8 $G_{z,\text{pull-up}}$ and 1.8 $G_{z,\text{recovery}}$ responses. An index of modulation is defined as a function of A_0 and $A_{1.8}$:

$$\text{Modulation index} = \frac{A_0 - A_{1.8}}{A_0 + A_{1.8}}$$

This definition of the index has the important advantage of being independent of ENG calibration.

4.3 Results

4.3.1 The fixation condition

Random drift artifacts occasionally occurred after the moments of injection and recovery, with amplitudes equivalent to 20 deg eye position. However, these changes in ENG offset were not systematic in any one direction.

4.3.2 The darkness condition

Offset shifts equivalent to 20 deg were observed, most markedly during G_z transitions. These shifts, however, were not systematic in the upward nor in the downward direction. Only subject 4 showed a systematic 20 deg downward gaze shift, after injection to 0 G_z. Vestibular nystagmus was observed in subject 2 during pull-up and recovery, with a SCV of 4 $\text{deg} \cdot \text{s}^{-1}$ downward.

4.3.3 The optokinetic condition

The horizontal eye movement recordings did not reveal any consistent gaze shift nor nystagmus. This finding is in agreement with the absence of any tilt vector. The averaged vertical OKN-SCV values are given in Table 4.1.

Table 4.1 OKN-SCV and standard deviation over time in deg · s^{-1}, by subject, averaged over n parabolas.

		UPWARD OK			
Subject	1 G_z	1.8 $G_{z,\text{pull-up}}$	0 G_z	1.8 $G_{z,\text{recovery}}$	n
1	35 ± 3	30 ± 5	36 ± 6	21 ± 5	3
2	36 ± 1	24 ± 3	28 ± 3	21 ± 3	3
3	42 ± 4	45 ± 3	40 ± 4	46 ± 3	4
4	30 ± 3	18 ± 5	19 ± 5	10 ± 5	1
5	31 ± 5	16 ± 5	23 ± 4	18 ± 4	4
6	29 ± 6	16 ± 4	20 ± 4	14 ± 5	3
		DOWNWARD OK			
Subject	1 G_z	1.8 $G_{z,\text{pull-up}}$	0 G_z	1.8 $G_{z,\text{recovery}}$	n
1	-45 ± 8	-55 ± 2	-51 ± 4	-52 ± 4	2
2	-44 ± 4	-49 ± 3	-44 ± 3	-50 ± 2	2
3	-46 ± 3	-45 ± 3	-52 ± 3	-53 ± 2	4
4	-19 ± 4	-22 ± 4	-15 ± 2	-15 ± 5	3
5	-43 ± 1	-52 ± 5	-34 ± 5	-46 ± 5	4
6	-36 ± 2	-41 ± 4	-30 ± 3	-33 ± 3	3

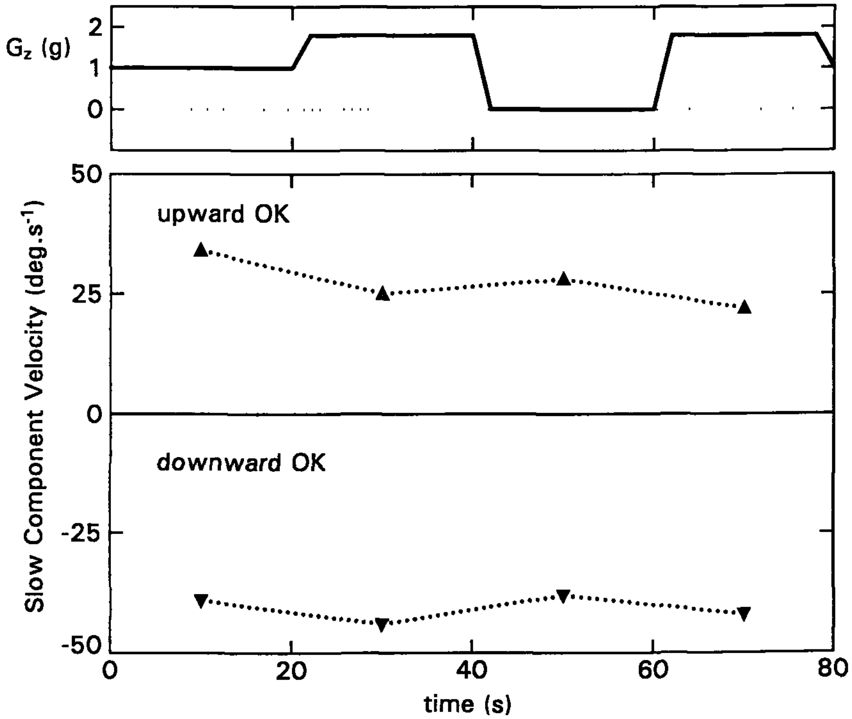

Fig. 4.6 OKN-SCV averaged across parabolas and 6 subjects. The time-averaged values are given for each G-level, showing that the G_z profile induces a similar modulation for both the up- and downward OK directions.

Fig. 4.6 presents a graph of SCV values averaged across subjects (Table 4.2). In our evaluation of the data, we start with the assumption that vestibular and optokinetic signals add linearly, as was proposed by Robinson (1977) for angular acceleration input. As Fig. 4.6 suggests, the G_z force induces a modulation of OKN-SCV in the same direction for both up- and downward OK stimulation, in agreement with the assumption of linear superposition. In view of this result, analysis of variance was performed on the average SCV values of Table 4.1, for the *combined* set of upward and downward OK stimulation. OK direction was considered as a separate dimension. A main effect due to G level was observed ($F=9.4$; $df=3,15$; $p<0.01$; 0.7% variance explained).[1] In the combined up/down dataset the interaction between up/down and G level was found to be insignificant. This finding confirms the approach of combining the up- and down-responses.

Post-hoc Newman-Keuls analysis (Winer, 1962) revealed significant differences ($p<0.05$) between the SCV values (combined for upward and downward OK) at 1.8 G_z (pull-up as well as recovery) and those for 1 G_z and 0 G_z. However, no significant difference was observed between 1 G_z and 0 G_z. Table 4.2 presents the mean SCV values.

Table 4.2 OKN-SCV [deg · s^{-1}] values derived from Table 4.1, averaged across subjects.

	1 G_z	1.8 $G_{z,\text{pull-up}}$	0 G_z	1.8 $G_{z,\text{recovery}}$
Upward	+33.8	+24.8	+27.7	+21.7
Downward	-38.8	-44.0	-37.7	-41.5
Average	-2.5	- 9.6	-5.0	-9.9

4.3.4 G modulation indices from separate parabola responses

In the analysis so far, the responses have been averaged across subsequent parabolas. The question remains whether SCV modulation is consistent for each subject, from one parabola to the next. In order to quantify the modulation, the modulation index as defined in Fig. 4.1 is applied. The values are given in Tables 4.3a and 4.3b.

---

[1] The small percentage of explained variance is due to the large difference between the SCV's for upward and downward OK stimulus, explaining 89% of variance.

Table 4.3a The G modulation indices for responses in separate parabolas.

Subject	UPWARD OK stimulation G modulation indices	DOWNWARD OK stimulation G modulation indices
1	.16 ; .16 ; .21	-.01 ; -.07
2	.16 ; .09 ; .07	-.07 ; -.04
3	-.03 ; -.04 ; -.11 ; -.13	.0 ; .04 ; .04 ; .06
4	.19	-.10 ; -.08 ; -.10
5	.03 ; .08 ; .18 ; .19	-.06 ; -.12 ; -.40 ; -.11
6	.16 ; .19 ; .14	-.19 ; -.10 ; -.16

Table 4.3b The G modulation indices for responses averaged across parabolas.

Subject	UPWARD OK stimulation G modulation index	DOWNWARD OK stimulation G modulation index
1	.18	-.04
2	.11	-.06
3	-.08	.04
4	.19	-.09
5	.12	-.17
6	.16	-.15

The modulation index values in Table 4.3a show that for each subject the sign of the modulation is highly consistent from one parabola to the next. As was hypothesized in Fig. 4.1, the value of A_0 is larger than $A_{1.8}$ during upward OKN, resulting in a positive index; the reverse holds true for downward OKN. Subject 3 shows indices with a sign contrary to the prediction, both for upward and downward OK stimulation. Because of the consistency of the effect in the other 5 subjects, the overall effect remains significant for the group of 6 subjects, as was revealed earlier by the ANOVA on the OKN-SCV data in Table 4.2. OKN-SCV for subject 2, who was the only subject with a vestibular nystagmus response in the darkness condition, did not differ from the results for subjects 1, 4, 5, and 6.

Table 4.3b shows the averaged index values. For the upward-OK indices a one-tailed T-test versus zero revealed that the values are larger than zero ($p<0.025$). Similarly, the downward-OK indices are smaller than zero ($p<0.025$). These results provide confirmation of the G effect. If there was no G effect, then the index values would be randomly distributed around zero.

Motion sickness was developing in subjects 2, 4, and 6. However, no difference in response was found between these subjects and the three other subjects resistant to motion sickness.

4.4 Discussion

4.4.1 Potential artifacts of arousal, fatigue and offset shifts

Arousal and fatigue are known to influence the nystagmus response. A differentiation must be made between these factors and the presumed G_z effect. Shifts in gaze and ENG calibration might also interfere with our measurements of SCV. These potential artifacts will be discussed.

(1) Arousal

Since 5 of the 6 subjects were undergoing their first parabolic flight, arousal might occur when entering the 0 G phase, possibly resulting in the observed increase in amplitude of upward SCV. However, the enhancing effect of arousal is independent of nystagmus direction (Collins, 1974), and thus the same arousal effect should cause an increase in the downward SCV when entering 0 G_z, which is not the case.

(2) Fatigue

A subject's oculomotor system might be fatigued by the long duration of sustained optokinetically induced eye movements, extending over more than 60 s. Such fatigue could cause a continuous decline in SCV response irrespective of its direction; it cannot, however, explain the increased upward SCV during 0 G_z, nor the increased downward SCV during 1.8 G_z recovery.

(3) Shifts in gaze

A systematic gaze shift ("range effect") during the G_z profile might influence the results, because of the slight deviation in pattern velocity across the screen. This potential artefact, however, should cause the same amplitude effect on up and down SCV, which would cancel itself out in the combined up/down dataset.
If gaze would be influenced by the OK stimulus direction and OKN gain would be dependent on gaze, then this would cause an overall amplitude difference between OKN-up and OKN-down. However, such a general gain shift could not interfere with a G induced modulation. Our modulation index, as defined in the method section, is not sensitive to a gain factor.

(4) Shifts in ENG calibration

ENG electrode artifacts might have influenced the offset or the gain of the ENG signal during a parabola. The "fixation" condition was applied to observe any ENG offset artifacts. Eye position data showed these shifts, but they were not systematic in terms of direction at a particular G level. If systematic shifts in ENG calibration factor had occurred during a parabola, these would have caused the same change in absolute value of OKN velocity in both the up- and downward direction, but these changes would have had opposite polarity. Thus, this modulation would be cancelled out when taking up- and down-responses together.

Summary of potential artifacts

In summary, it is unlikely that any artefact can account for the observed effects. Artifacts would potentially induce an *amplitude-effect* on OKN-SCV, while the combined set of up- and down-OK responses, as shown in Fig. 4.6, exhibits a *direction-effect* on OKN-SCV induced by the G_z vector.

4.4.2 Vectorsum of G-induced and OK-induced SCV contributions

The directional G effect on OKN-SCV may be expressed by the vectorsum of G-induced SCV and OKN-SCV, as shown in the tentative model in Fig. 4.7.

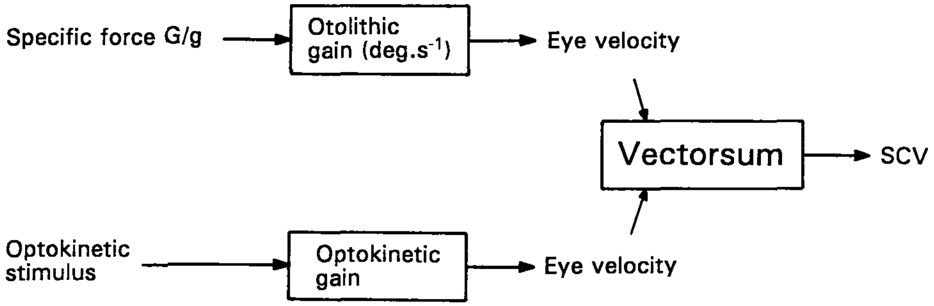

Fig. 4.7 Basic model of the generation of slow-component eye velocity (SCV) by otolithic and optokinetic pathways, which are added by vector summation. The vectors are defined with respect to a head-fixed coordinate system.

This proposed model indicates that the specific force G is sensed by the otoliths, which induce an eye velocity signal in the direction compensatory to the

G vector. The sensitivity of this otolith-ocular reflex, expressed in deg · s^{-1} induced modulation per g unit, is, in our experiment, about 3 deg · s^{-1}. The model can qualitatively account for the results shown in Fig. 4.6. The G-induced modulation of the OKN-SCV does not depend on the direction of OK stimulation.

In order to test the general validity of this vectorsum-concept, some references will be given from other experimental conditions.

4.4.3 Observations related to the vectorsum-concept

The G_z effect in the centrifuge was revealed in a vestibular downward SCV, with a mean amplitude of 5 deg · s^{-1} per g (Marcus et al., 1989; Marcus and Van Holten, 1990). The vestibular nystagmus of 4 deg · s^{-1} in darkness, observed in subject 2 of the present parabola experiment, is quantitatively quite consistent with the centrifuge SCV. The mean G modulation of OKN in parabolas amounts to about 3 deg · s^{-1} per g, indicating that the OKN modulation per g unit in flight may be lower than the amplitude of the nystagmus of vestibular origin in the centrifuge. The direction of modulation however is consistent with the centrifuge data.

The directional effect is also consistent with data of Clement et al. (1989) in a study on 2 subjects in parabolic flight. They observed a decrease of OKN-SCV down and an increase of OKN-SCV up during the transition to free-fall. Clement and Lathan (1991) applied the method of static tilt about the roll-axis. They observed in man that the gain of upward vertical OKN was increased in 90 deg roll position. In terms of vectors, the otolith-induced SCV is opposed to OKN-SCV in the upright subject, and orthogonal to OKN-SCV in the 90 deg roll position. The increased upward gain in roll can be explained by the release of the downward otolith-induced SCV component with respect to the subject's head.

DiZio and Lackner (1992) found that, in parabolic flight, vertical vestibular nystagmus (induced by angular acceleration) showed no effect of G level on peak SCV amplitude. In their experiment, however, the subject was lying on his side, with the right-ear down to the floor of the aircraft. The subject therefore must have experienced the G force along his lateral y-axis, orthogonal to the vertical SCV direction, which probably explains the lack of a significant G effect on vertical SCV amplitude. These results seem to be consistent with the proposed vectorsum model.

It was shown by electro-physiology in cats that responses to vertical linear acceleration are initiated by the otoliths (Xerri et al., 1987). Fukushima and Fukushima (1991) reported that otolith-induced SCV responses in cats are about in phase with specific force G. These data also support the model in Fig. 4.7, with regard to the otolith-ocular pathway.

Raphan and Cohen (1988) have described another mechanism where velocity storage plays a role in the orientation of optokinetic following with respect to the earth's 1g gravity. This mechanism however cannot account for the hypergravity effect. Extended studies on the three-dimensional nature of the otolith-ocular reflex, and its influence on velocity storage, are continuing (De Jong and Oosterveld, 1987; Angelaki et al., 1991; Gizzi et al., 1991; DiZio and Lackner, 1992).

4.4.4 Functional implications

During OK stimulation in parabolic flight there could arise some conflict between visual and vestibular perception. For example, when the subject is entering hypergravity during upward OK, he could experience upward acceleration due to the $+G_z$ increase, but acceleration downward due to the upward moving visual stimulus. The most striking change in the subjects' perception, however, was not a conflict, but an apparent change in pattern velocity during the parabola. It is still a question, whether this percept is primarily due to direct input from the vestibular system, or secondarily due to vestibularly induced changes in eye velocity. Further research is needed to clarify the functional implications of the simultaneous input of OK stimulation and changes in the G force.

4.4.5 Comparison between 1 G_z and 0 G_z responses

In our data the G effect was manifest in the difference between 1.8 G_z and 0 G_z. At this point an explanation for the apparent lack of difference between the 0 G_z and the 1 G_z condition is still missing. It may be due to the absence of an immediate transition between 1 G_z and 0 G_z. The "high-G barrier" between the two conditions may offset the system. Perhaps a difference between 1 G_z and 0 G_z might indeed be found if the transitions between 1 G_z and 0 G_z were made more direct. This approach would, however, require another flight manoeuvre.

4.5 Conclusions

During parabolic flight, the otolith responses to the G_z profile were measured by analyzing the vertical slow-component eye velocity. In darkness, vertical vestibular nystagmus was observed in only one out of six subjects. With vertical optokinetic stimulation, however, the otolith responses were manifest in modulation of the vertical optokinetic slow-component velocity.

Statistical analysis revealed:

1. In 1.8 G_z hypergravity the amplitude of upward OKN-SCV is decreased, and the amplitude of downward OKN-SCV is increased. This holds true for the comparison between 1.8 G_z and 1 G_z, and between 1.8 G_z and 0 G_z.
2. No significant difference, however, was found between the 1 G_z and 0 G_z condition.
3. No significant interaction was found between the OK stimulus direction (up or down), and the G level.
4. The G effect on OKN-SCV can be qualitatively expressed by the vectorsum of G-induced SCV and OKN-SCV. However, this concept can not account for the lack of difference between the responses at 1 G_z and 0 G_z.

Acknowledgements

Drs. A. Kuipers MD (ESTEC) was co-investigator in the flight experiment. Prof. Dr. G.F. Smoorenburg has made an important contribution to the correction and improvement of this manuscript. Additional financial support was provided by the Space Research Organization Netherlands (SRON). The technical support of the Dept. of Medical Physics, Free University Amsterdam, is highly appreciated. Dr. Mathew Sandor (ESTEC) has made suggestions for improving the English text.

Chapter 5

Eye movements in man induced by sinusoidal acceleration on a linear track

Abstract

(1) Normal human subjects (n=8) were exposed to sinusoidal acceleration on a linear track, directed along their interaural axis, with amplitude of 2 m · s^{-2} and frequency of 0.176 Hz. (2) During this acceleration, horizontal Opto-Kinetic Nystagmus (OKN) was induced by horizontally moving patterns produced by two different devices: one based on projection on a cylindrical screen at .6m distance and fixed with respect to subject position, the other on head-mounted binoculars. Opto-Kinetic (OK) stimulation was applied in the right- and leftward direction, at velocities of 40, 60, and 80 deg · s^{-1}. (3) The Slow-Component Velocity (SCV) of eye movements was measured by electro-nystagmography in complete darkness, and with OK stimulation. The effects of sinusoidal linear acceleration were analyzed by determining the modulation of the SCV induced by the acceleration. Discrete Fourier Transformation yielded the amplitude of induced modulation, and the phase referred to the subject's velocity. (4) In darkness the averaged amplitude of acceleration-induced SCV was 1.5 deg · s^{-1}, and its phase was -190 deg. With OK stimulation, the amplitude of modulation ranged from 3 to 7 deg · s^{-1}, equivalent to a sensitivity to translation (peak eye velocity/peak subject velocity) of 1.7 to 4 deg · m^{-1}. The mean phase ranged from about -180 deg to -90 deg. Analysis of variance revealed significant effects of OK velocity on the amplitude and phase of modulation. (5) Less coherence in modulation was found with the projection OK-stimulator, than with the binocular stimulator. (6) In an additional test, the subjects were tracking an after-image (AI) in darkness. SCV modulation was found with averaged amplitude of 2.4 deg · s^{-1} and phase of -82 deg. (7) In darkness, the phase of modulation confirms the concept of an otolith-induced SCV response compensatory to subject velocity. With OK stimulation and AI tracking, visual-vestibular interactions might be responsible for the phase leads of modulation, relative to the phase of modulation in darkness.

5.1 Introduction

This study was initiated in order to obtain an otolith test in the laboratory, which should provide a reference to otolith-induced human eye movements measured in a centrifuge (Chapter 3 of this thesis) and in flight (Chapter 4). The basic laboratory tools for studying otolith-induced horizontal and vertical eye movements are provided by a linear acceleration track and a parallel swing. In these stimulators there is no angular acceleration, excluding any confounding semicircular canal stimulation.

Nystagmoid eye movements induced by horizontal linear acceleration along the interaural axis have been observed in man by Jongkees and Philipszoon (1962). Niven et al. (1966) reported quantitative data on otolith-induced nystagmus, but the amplitude of the applied sinusoidal acceleration input was as high as 0.58g, which cannot be attained in most laboratory settings. On a parallel swing, smooth eye movements induced by linear acceleration were observed by Baarsma and Collewijn (1975) in rabbits. Also on a swing, Baloh et al. (1988) applied the scleral search coil technique for measuring otolith-ocular responses in man. The scleral coil technique, however, is sensitive to disturbances like motion and electromagnetic fields, and moreover it is difficult to implement in a centrifuge or aircraft environment. Therefore, we used the more suitable Electro-Nystagmo-Graphy (ENG) recording technique.

The eye movements induced by linear acceleration, however, have a low amplitude (order of 5 $\text{deg}\cdot\text{s}^{-1}$ per g unit), which at low acceleration values could easily be buried in eye movement noise when measured by ENG. For this reason a more sensitive test for otolith-ocular responses is desired. Current literature indicates that simultaneous optokinetic and vestibular stimulation provides such a technique. For details of optokinetic stimulation, specifically the neuro-anatomical pathways, the reader is referred to Collewijn (1985). For angular acceleration the vestibulo-optokinetic interaction was described by Robinson (1977) in terms of linear addition of the optokinetic and vestibular signals. Buizza et al. (1980) applied the technique of OptoKinetic (OK) stimulation using sinusoidal acceleration on a linear track. They reported that otolith-induced eye movements are manifest in modulation of the OptoKinetic Nystagmus Slow-Component Velocity (OKN-SCV), rather than in a direct response in darkness.

The present study also concerns otolith-ocular responses to sinusoidal acceleration on a linear track. Our experiment addresses the following questions:

a In which visual conditions (e.g. darkness, OK stimulation) is the human otolith-ocular response most manifest and consistent?
b Can we explain the basis of these otolith-ocular responses, in terms of otolith physiology and vestibular-visual interaction?

In our design the acceleration stimulus was kept constant, while the visual conditions were varied.

This study is supplemented by experiments on after-image (AI) tracking during acceleration. Recently this technique was proposed by Shelhamer and Young (1991) for obtaining an amplified otolith-ocular response. In this study, we will measure, in the same group of subjects, the eye velocity responses in darkness, with OK stimulation and with after-image tracking. We will try to relate our data to the findings of Buizza et al. (1980), Baloh et al. (1988), and Shelhamer and Young (1991).

5.2 Methods

5.2.1 Acceleration profile

The linear track, "sled", has been provided to our laboratory by the European Space Agency, ESA. It consists of a chair and head restraint mounted on a cart which is guided along two rails. A cable attached to both sides of the cart is wound around a pulley at one end and a winch drum at the other. In our experiment the subject is sitting in upright position, facing sidewards with respect to the track (Fig. 5.1). The subject is restrained by a five-strap harness, with the head stabilized by means of a biteboard. The sinusoidal acceleration is directed along the subjects interaural (y-) axis, and will be briefly denoted as G_y. The symbol "G" stands for specific force, defined as the resulting force per mass unit, and expressed in "g" which is the specific force induced by gravity on the earth's surface ($1g = 9.8 \text{ m} \cdot \text{s}^{-2}$). In our study, the computer-controlled acceleration profile consists of 6 cycles of sinusoidal G_y acceleration at a frequency of 0.176 Hz. Position amplitude is 1.6m, velocity amplitude $1.77 \text{ m} \cdot \text{s}^{-1}$, and acceleration amplitude $1.96 \text{ m} \cdot \text{s}^{-2}$ (equivalent to 0.2g). The + signs of position, velocity, and acceleration refer to the right-hand side of the subject. Starting position is at +1.6m.

5.2.2 Optokinetic stimulation

Projection

In the projection mode the stimulus consists of bright and dark bars (12 deg each) projected on a homogeneous white screen, subtending a visual angle of 80 deg horizontally and 60 deg vertically (Fig. 5.1).

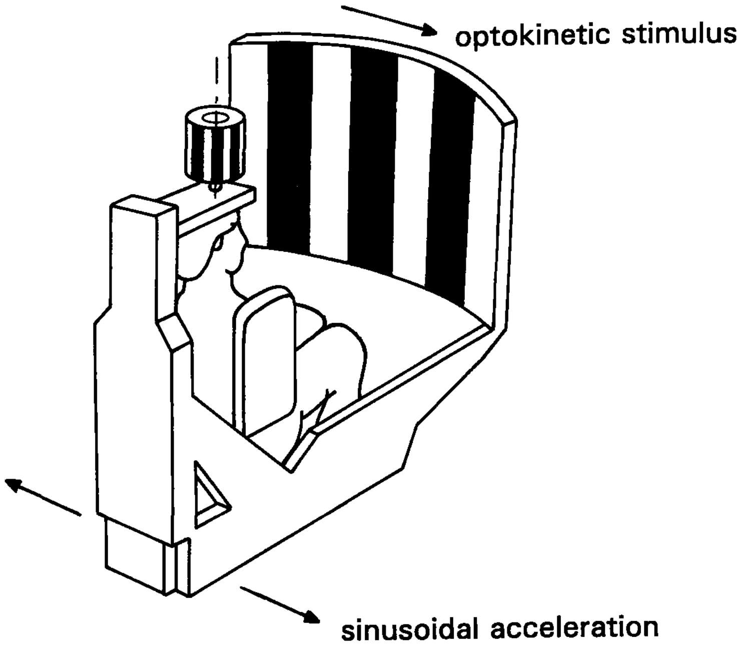

Fig. 5.1 Experimental set-up of the subject moving on the linear track, "sled". In this figure the projection system of Opto-Kinetic (OK) stimulation is mounted, with OK stimulus velocity to the right.

The subject's eyes are in the axis of the cylindrical curve of the screen, at .6m viewing distance. The bar pattern is generated by means of an Osram 8.5 V DC 6A tungsten bulb, type Wi 9, with a 5 cm linear filament aligned to the axis of a rotating cylinder. The wall of this cylinder contains slits parallel to its main axis, enabling projection of dark bars by shadow casting. The luminance of bright and dark bars is 10 and .5 $cd \cdot m^{-2}$ respectively; the luminance transients were sharp, less than 0.5 deg.

Binoculars

The binocular optokinetic stimulus system was kindly provided by Dr. A. Berthoz from the Lab. de Physiologie Neurosensorielle (C.N.R.S.) in Paris. It has been first developed for experiments aboard the MIR space station. The stimulator is tightened directly on the subject's head. It provides OK stimulation by a horizontally moving black and white checkerboard pattern (squares of 4x4 deg visual angle). The pattern was lightened by red light-emitting diodes (650 nm wavelength) and viewed through Fresnel lenses in front of each eye for focusing.

The size of the visual field is about +/- 40 deg in the horizontal and vertical direction.

Stimulus velocity

The two different optokinetic devices were used in the same group of subjects. In order to enable a comparison between the binocular and the projection system, we used the same angular velocities in both optokinetic devices. Stimulus velocities were 40 deg · s^{-1}, 60 deg · s^{-1} and 80 deg · s^{-1} both to the left and to the right. In this velocity range the OKN Slow-Component Velocity (OKN-SCV) is smaller than the stimulus velocity, which allows any modulation of the OKN-SCV (Buizza et al., 1980) as shown in Fig. 5.2.

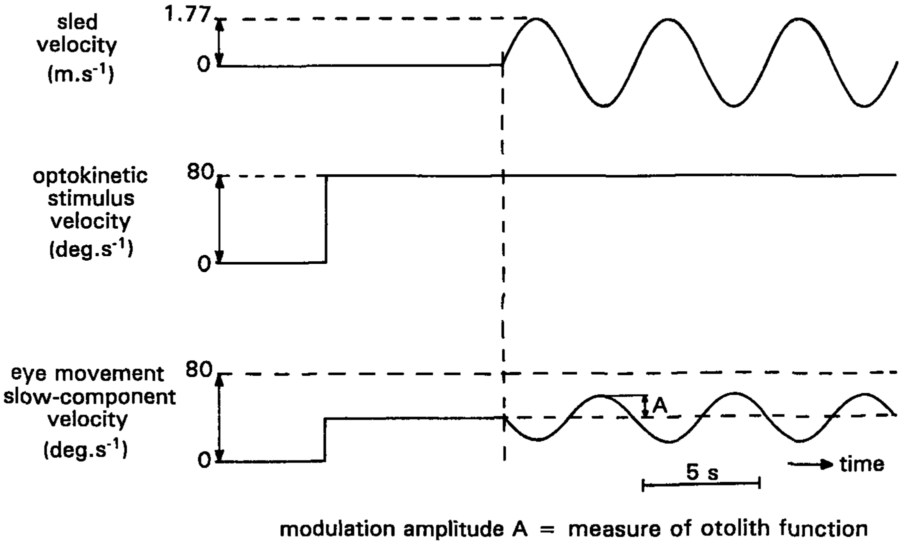

Fig. 5.2 Predicted modulation of Opto-Kinetic Nystagmus Slow-Component Velocity (OKN-SCV), induced by sled velocity. This diagram shows 3 cycles of sled motion, and OK stimulation at 80 deg · s^{-1}. The gain of OKN-SCV is smaller than one, allowing modulation of the SCV. In the lower trace the phase lag of eye velocity is 180 deg, as if eye velocity was exactly compensatory to sled velocity.

The instruction to the subject during OK stimulation was: "Try to keep your gaze in the middle third of the pattern, look at every subsequent bar or square, do not pursue any missed one". In all conditions the subjects were constantly kept mentally alert by talking to them.

5.2.3 Balancing of conditions

The subjects (n=8) were non-selectively recruited, naive, 20-25 years of age, males (3) and females (5). One subject had been replaced by an additional subject because of motion sickness, and another because of poor OKN performance. The letters "B" and "P" will denote OK stimulation with Binoculars and Projection, respectively. Tables 5.1a,b present the experimental conditions.

Table 5.1a Survey of experimental conditions.

Code	Stimulus condition
OK/B	optokinetic only, with binoculars
SLED-OK/B	sled moving, optokinetic with binoculars
OK/P	optokinetic only, with projection
SLED-OK/P	sled moving, optokinetic with projection
SLED-DARK	sled moving, darkness
SLED-FIX	sled moving, light, fixation at subject-fixed target
AI	after-image tracking in darkness
SLED-AI	sled moving, after-image tracking in darkness

Table 5.1b Sequence of OK and SLED-OK conditions for subjects 1 through 8.

1,5	OK/B	SLED-OK/B	OK/P	SLED-OK/P
2,6	OK/P	SLED-OK/P	OK/B	SLED-OK/B
3,7	SLED-OK/B	OK/B	SLED-OK/P	OK/P
4,8	SLED-OK/P	OK/P	SLED-OK/B	OK/B

For subjects nrs. 1,2,3,4 the velocity sequence was 40R,40L,60R,60L,80R,80L $\text{deg} \cdot s^{-1}$, where R and L denote OK stimulation to the right and to the left. Subjects 5,6,7,8 had the same sequence of OK and SLED-OK conditions, but the reverse velocity sequence: 80R,80L,60R,60L,40R,40L $\text{deg} \cdot s^{-1}$. OKN is specified in terms of the slow-component direction. The measurements OK/B and OK/P were performed with the subject mounted on the sled, strapped in security belts and the head fixed with a biteboard. Thus the only difference with the SLED-OK conditions was the movement on the sled.

Each set of six SLED runs was followed by two reference SLED conditions with the subject still fully mounted:

1 SLED-FIX, visual fixation at a screen-fixed target that was stationary with respect to the subject. This condition was applied in order to measure any electrode shift artefact.
2 SLED-DARK, darkness with eyes opened, in order to measure a Vestibulo-Ocular Reflex in response to Linear acceleration (LVOR).

After-image tracking

Finally, measurements of after-image tracking are performed. An electronic photo-flash was offered at .6 m and at 3 m distance (sequence balanced) before moving the sled. The subject was instructed to keep looking at the after-image in darkness. After the flash the sled started to move (condition SLED-AI). The reference condition was after-image tracking on a non-moving sled (condition AI).

5.2.4 Procedure of eye movement analysis

Eye velocity

Eye movements were recorded by Electro-NystagmoGraphy (ENG). The horizontal measurements were bitemporal; the vertical measurements were from the right eye and were used to check whether or not any vertical nystagmus component occurred. These eye movement recordings were sampled on-line (100 Hz/ch), simultaneously with signals of sled position and OK stimulus velocity. Eye movements were quantified by the Slow-Component Velocity, SCV (C.H.A.B.A.-Committee, 1992). The horizontal SCV was calculated by an interactive computer program consisting of differentiation of the horizontal eye position signal, and subsequent rejection of fast-components by threshold settings (Barnes, 1982; Bos and Kistemaker, 1991; see also Chapter 2, Fig. 2.3). The gaps in the eye velocity data string, caused by fast-component rejection, were then filled by linear interpolation. The velocity was calculated by this procedure in all conditions, including the SLED-DARK and SLED-AI cases where eye movements were usually not nystagmoid.

The analysis aims to quantify the modulation of eye velocity induced by the sled, sinusoidally moving at a well-defined single frequency. The Discrete Fourier Transform (DFT) was used for calculating the response to this specific frequency component. A DFT analysis was performed on SCV responses during the sled cycles 2 through 6, covering an integral number of 5 cycles. The reference sinusoid is sled velocity. The amplitude (symbol "A") of SCV modulation is defined as 0.5 times the peak-to-peak amplitude at the frequency of the sled. The phase of SCV modulation is defined with reference to sled velocity. In the conditions without sled movement (OK/B, OK/P and AI) this analysis was carried out on SCV, covering a time interval of the same length (28.4 s) as the duration of 5 sled cycles. Averaging across subjects was performed by vector-averaging, in order to take both amplitude and phase of modulation into account. The results will be denoted by SCV modulation, also in the SLED-DARK and SLED-AI conditions (where we usually did not observe fast-components of nystagmus).

Influence of changes in gaze on the observed SCV modulation

In many recordings, the baseline of the ENG-signal was not constant, but it showed a slow sinusoidal wave with a frequency corresponding to sled movement. Thus, nystagmus was superimposed on gaze-changes of the eye. The *velocity* of this change in gaze, SCV_{gaze}, contributes to the observed SCV (If not specified, SCV will always be $SCV_{observed}$). The "true" slow-component velocity, that would be found for a steady baseline (no changes in gaze), is indicated by SCV_{true}. Thus we can write the observed $SCV_{observed}$ as the sum of contributions of gaze and true slow-component velocity:

$$SCV_{observed} = SCV_{gaze} + SCV_{true}$$

The SCV_{gaze} was calculated as follows: The change in gaze was determined by Fourier analysis of the eye position signal itself (without differentiation and fast-component rejection). DFT yielded the component at the frequency of the sled movement (f_{sled} = 0.176 Hz). The time segment of raw ENG signal, over which the DFT was applied, was always covering the sled cycles 2 through 6 (the same time interval over which the SCV is calculated). The amplitude of the change in gaze is denoted by A_{gaze} (in degrees). We note that the frequency of individual nystagmus beats is usually higher than about 1 Hz, and thus individual beats are not contributing to the amplitude A_{gaze} at the frequency of the sled.

Once A_{gaze} has been determined, we are able to determine the *velocity* of the change in gaze. If the gaze is given by $A_{gaze} \cdot \sin(\omega t)$, then the velocity of change in gaze, SCV_{gaze}, equals $\omega \cdot A_{gaze} \cdot \cos(\omega t)$. This is the contribution of gaze-changes to the observed SCV.

Calculation of velocity modulation

Subsequently, we calculate the "true" velocity modulation. This is relevant for our Chapter 6 on modelling, where we are only concerned with velocity signals.

The **vectors** representing amplitude and phase (referred to sled velocity) of SCV are denoted in bold characters. The vector $\mathbf{SCV}_{\mathbf{true}}$ is calculated by the vector-subtraction:

$$\mathrm{SCV}_{\mathrm{true}} = \mathrm{SCV}_{\mathrm{observed}} - \mathrm{SCV}_{\mathrm{gaze}}$$

This calculation of $\mathbf{SCV}_{\mathbf{true}}$ has the additional advantage that the electrode-shift artefact is rejected, because this artefact is equally present in $\mathbf{SCV}_{\mathbf{observed}}$ and in $\mathbf{SCV}_{\mathbf{gaze}}$. Thus by the above subtraction this artefact vanishes.

Statistics

The individual data from the OK and SLED-OK conditions were subjected to analyses of variance. The MANOVA-module of the SPSS/PC+ package was used for calculation of univariate analyses (Norusis, 1990). Independent variables are sled movement (moving and non-moving sled), subjects (n=8), the type of OK stimulus device (binoculars and projection), OK stimulus direction (left- and rightward) and OK stimulus velocity (40, 60, and 80 deg · s^{-1}). Dependent variables are mean SCV, and amplitude and phase of **SCV**. The same MANOVA-module was used for multivariate analyses. The Tukey test procedure (Winer et al., 1991) was applied to determine effects of OK velocity differences.

5.2.5 Rejection of electrode-shift artefact

This artefact could be induced by changes in skin pressure during the periodical motion of the subject. Slight motion-induced changes in the impedance of the soft tissue around the eyes will cause periodical changes in the measured ENG signal, which are particularly misleading because they are locked with the sled movement, and thus have the same frequency as the eye movement responses that we are interested in. In the SLED-FIX condition, with lights on, we instructed the subject to fixate accurately on a point target that was fixed relative to him. Any ENG signal measured in this SLED-FIX condition was thus considered to be an electrode-shift artefact. We measured amplitude and phase of this artefact for each subject, and corrected the observed modulation in the conditions SLED-OK, SLED-DARK and SLED-AI for this artefact by vector-subtraction.

In summary, we have described two different methods for rejecting the electrode-shift artefact: (1) Using the data measured in the SLED-FIX condition, and (2) Calculation of the vector $\mathbf{SCV}_{\mathbf{true}}$ (see previous section). Whenever we perform artefact-rejection, we will inform the reader about the applied method.

5.3 Results

5.3.1 Effect of sled movement

No vertical slow-component velocity was found in any condition; therefore data-analysis concerns horizontal eye movements only. In a first approach, a statistical analysis will be made of the combined dataset of OK (non-moving sled) and SLED-OK data. Dependent variables are mean OKN-SCV velocity, and the amplitude of SCV modulation at the frequency of the sled movement. For each subject a complete dataset has been obtained, which means that each cell in the analysis is filled with one element. Table 5.2 shows the results.

Table 5.2 Univariate analysis of variance of the mean OKN-SCV, and OKN-SCV modulation amplitude, for the combined dataset of OK and SLED-OK conditions. "n.s." stands for non-significant.

		Average	p-value	Tukey test
Mean ($deg \cdot s^{-1}$)				
Subjects (n=8)			$p<0.001$	
Sled:	Moving	48.6	$p<0.001$	
	Non-moving	34.1		
OK device:	Binoculars	38.8	n.s.	
	Projection	43.9		
OK velocity:	40 $deg \cdot s^{-1}$	30.2	$p<0.001$	40-60: $p<0.01$
	60 $deg \cdot s^{-1}$	42.0		40-80: $p<0.01$
	80 $deg \cdot s^{-1}$	51.8		60-80: $p<0.01$
OK direction:	Left	40.9	n.s.	
	Right	41.9		
Amplitude ($deg \cdot s^{-1}$)				
Subjects (n=8)			$p<0.01$	
Sled:	Moving	4.4	$p<0.001$	
	Non-moving	2.0		
OK device:	Binoculars	3.6	n.s.	
	Projection	2.9		
OK velocity:	40 $deg \cdot s^{-1}$	2.6	$p<0.001$	40-60: n.s.
	60 $deg \cdot s^{-1}$	2.8		40-80: $p<0.01$
	80 $deg \cdot s^{-1}$	4.3		60-80: $p<0.01$
OK direction:	Left	3.4	n.s.	
	Right	3.1		

The mean SCV

Main effects on mean SCV are induced by sled movement ($p<0.001$), and by OK velocity. Only one interaction was found to be significant: "Sled movement by OK velocity" ($p<0.01$). The mean SCV values were averaged across subjects, and plotted in Fig. 5.3 for the two stimulus devices, as a function of OK stimulus velocity, and sled movement versus no movement.

Fig. 5.3 Mean OKN-SCV averaged across subjects, obtained with the binocular OK device (upper panel) and the projection OK device (lower panel).

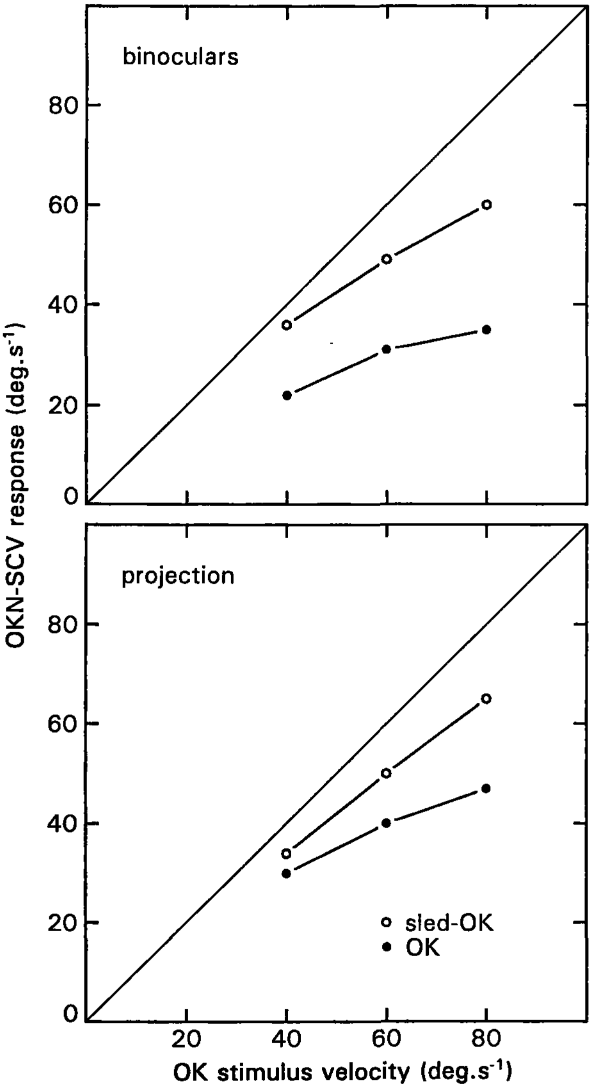

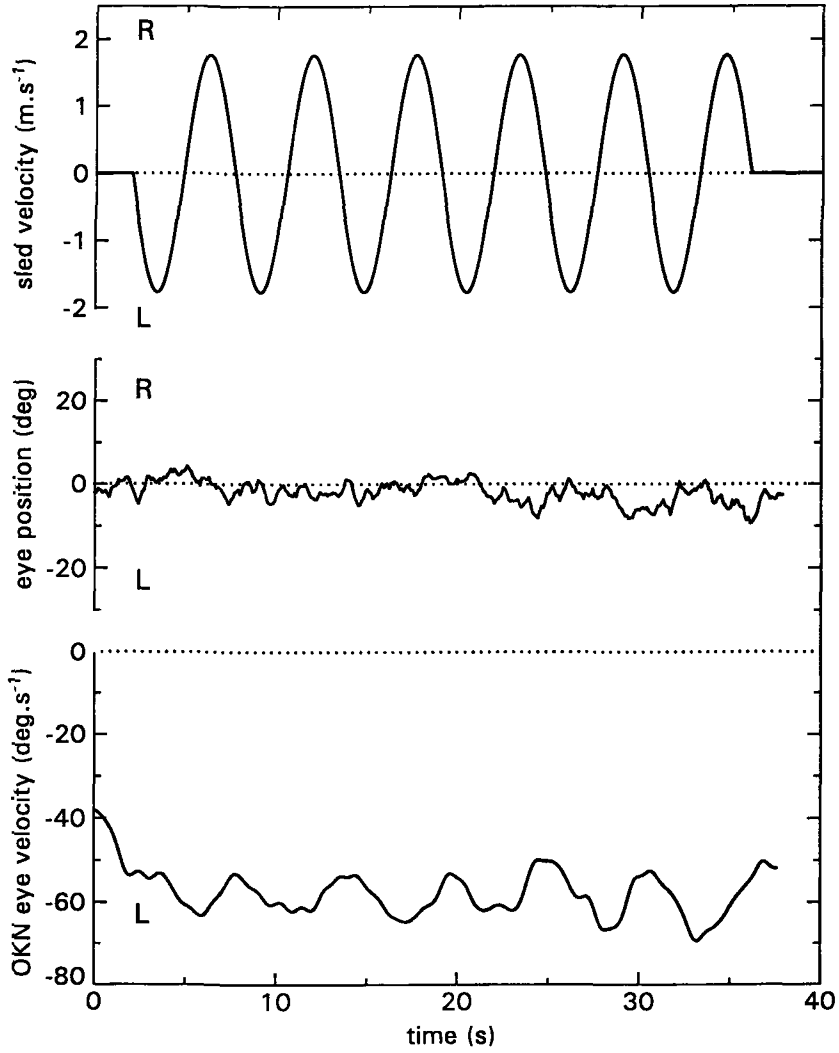

Fig. 5.4 Sled velocity, eye position and slow-component eye velocity averaged across 8 subjects in the condition SLED-OK; OK stimulation with binoculars at 80 deg · s^{-1} to the left. Rightward (R) direction is defined as positive. Prior to averaging all responses had been synchronized at sled onset.

Fig. 5.3 shows that the gain of the OKN-SCV response is decreasing with increasing OK velocity, which illustrates that there is "space" for any modulation to be superimposed on the response. A striking finding is the effect of sled movement on the mean SCV, which increases significantly with OK velocity as was apparent in the interaction "Sled movement by OK velocity". No significant difference between OK devices was found in this analysis. A MANOVA of the combined dataset of modulation amplitude and mean SCV, did not reveal any additional significant effect.

Modulation amplitude

Main effects on modulation amplitude are induced by sled movement ($p<0.001$) and by OK velocity ($p<0.001$). As before, the interaction "Sled movement by OK velocity" was significant ($p<0.05$). This justifies a separate ANOVA of the modulation-amplitude in the SLED-OK conditions. For these conditions we also know the phase of modulation (related to sled velocity). In the next sections the phase-information will be used for a more complete description of our results.

5.3.2 Modulation of OKN Slow-Component Velocity (OKN-SCV)

As an example, the responses from one condition (SLED-OK, binoculars, 80 $\text{deg} \cdot \text{s}^{-1}$ to the left), averaged across subjects are presented in Fig 5.4. The eye velocity trace of Fig. 5.4 shows modulation at the frequency of sled velocity.

Analysis of variance of the individual data from all SLED-OK conditions is summarized in Table 5.3. Phase values are defined in the range between 0 and -360 deg; clusters of phase data were not separated by this choice.

This analysis shows that modulation *amplitude* depends on subject and on OK stimulus velocity. Moreover, *phase*-lag increases with an increase of OK velocity from 40 to 60 $\text{deg} \cdot \text{s}^{-1}$ and from 40 to 80 $\text{deg} \cdot \text{s}^{-1}$, but not from 60 to 80 deg $\cdot\, \text{s}^{-1}$. Only one interaction was significant: "direction by velocity" had an effect on phase ($p<0.001$). In addition to the univariate analysis, a multivariate analysis of variance (MANOVA) was performed on the combined dataset of amplitude and phase. No additional effects were revealed by this MANOVA.

So far, amplitude and phase have been treated as separate quantities, while in fact they are representing one vector. In the next sections amplitude and phase will be presented in polar diagrams, in order to get a complete quantification of the modulation vector.

Table 5.3 Univariate analysis of variance of OKN-SCV modulation amplitude and phase, induced by the sled movement in the SLED-OK conditions. "n.s." stands for non-significant.

		Average	p-value	Tukey test
Amplitude (deg · s^{-1})				
Subjects (n=8)			$p<0.01$	
OK device:	Binoculars	4.9	n.s.	
	Projection	3.9		
OK velocity:	40 deg · s^{-1}	3.6	$p<0.001$	40-60: n.s.
	60 deg · s^{-1}	3.7		40-80: $p<0.001$
	80 deg · s^{-1}	5.9		60-80: $p<0.001$
OK direction:	Left	4.8	n.s.	
	Right	4.0		
Phase (deg)				
Subjects (n=8)			n.s.	
OK device:	Binoculars	-109	$p<0.05$	
	Projection	-142		
OK velocity:	40 deg · s^{-1}	-95	$p<0.01$	40-60: $p<0.01$
	60 deg · s^{-1}	-146		40-80: $p<0.05$
	80 deg · s^{-1}	-135		60-80: n.s.
OK direction:	Left	-115	n.s.	
	Right	-135		

5.3.3 Polar diagrams of modulation

The polar diagram presents modulation amplitude as the modulus, and the modulation phase as the phase angle referenced to sled velocity. In Figs 5.5, 5.6, and 5.7 these diagrams are shown for the conditions: binoculars 80 deg · s^{-1} to the left, projection 80 deg · s^{-1} to the left, and after-image tracking (after-image induced from 3 m distance). These conditions are taken as examples because here the modulation was found to be most manifest. The SLED-FIX data are plotted as a reference. In the individual data, the electrode shift artefact, as apparent from the SLED-FIX condition, has not yet been rejected from the SLED-OK and SLED-AI data.

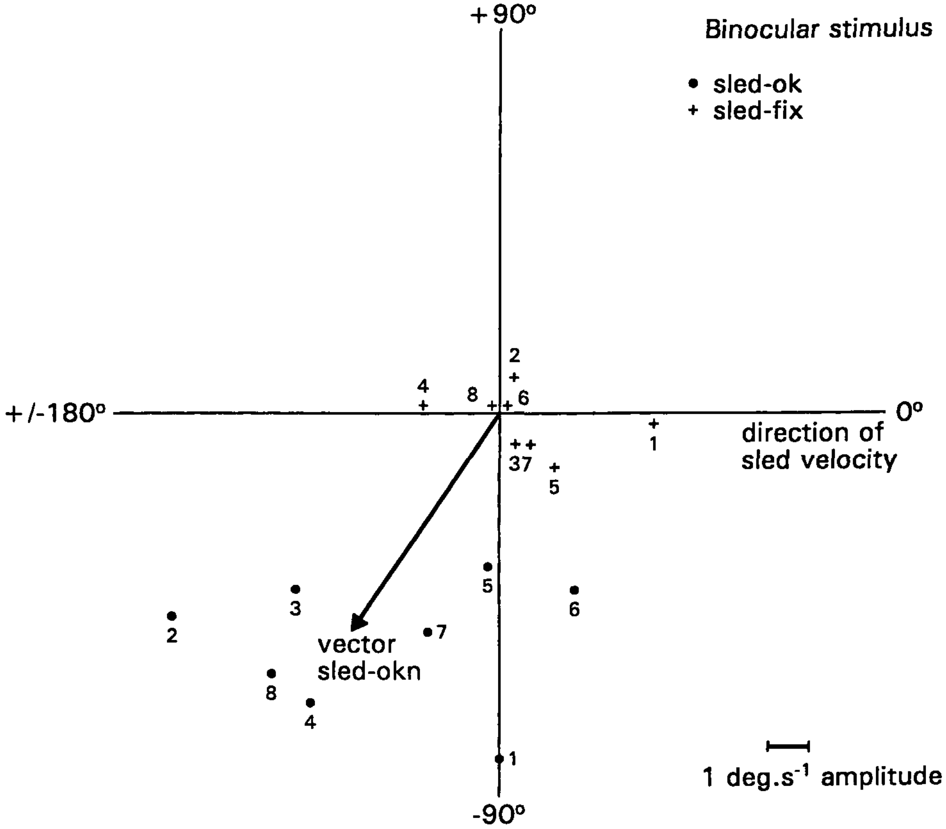

Fig. 5.5 Polar diagram of Slow-Component Velocity (SCV) modulation for 8 subjects, as calculated by discrete Fourier transform analysis. The modulus is the modulation amplitude, and the phase is the phase difference between eye velocity and sled velocity. The conditions are SLED-OK and SLED-FIX. In SLED-OK, OKN is induced with binoculars at 80 deg · s^{-1} to the left. The arrow denotes the vector-average across subjects for the condition SLED-OK, corrected for the electrode shift artefact that is apparent from the sled-fix condition. This vector-average presents the modulation of the averaged velocity trace in Fig. 5.4. The numbers 1 through 8 are referring to the individual subjects.

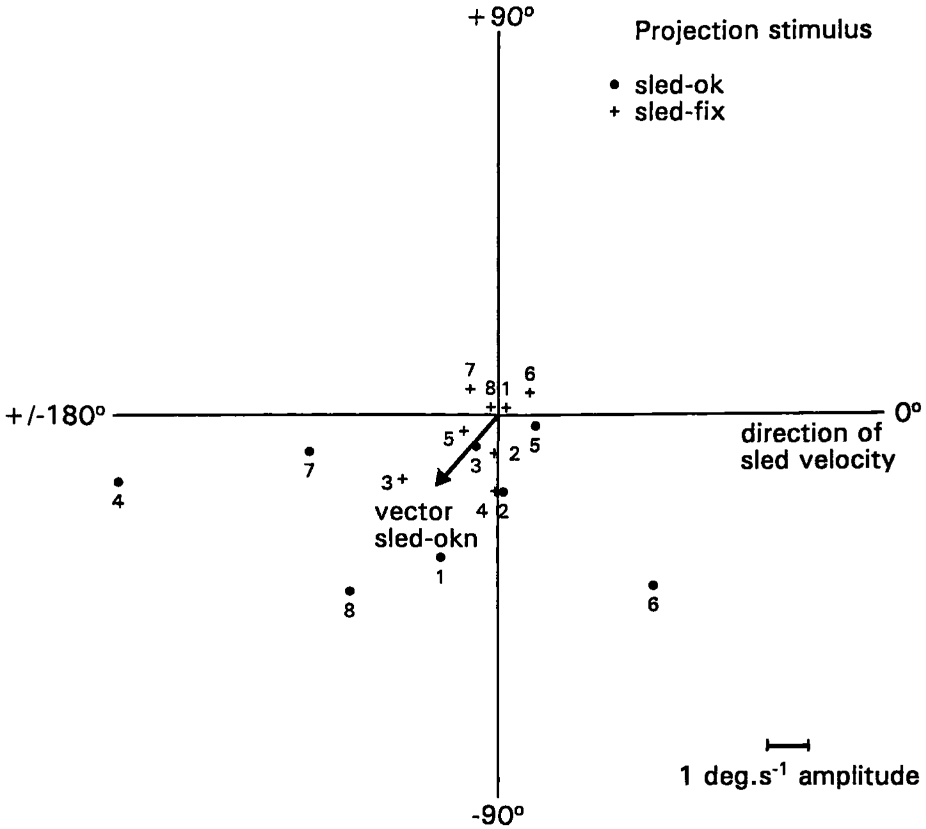

Fig. 5.6 Polar diagram of SCV modulation. OKN is induced with projection at 80 deg · s^{-1} to the left. The arrow denotes the vector-average across subjects for the SLED-OK condition, corrected for the electrode-shift artefact. The numbers 1 through 8 are referring to the individual subjects. For subjects nrs. 3 and 5 the modulation in SLED-OK is not different from SLED-FIX.

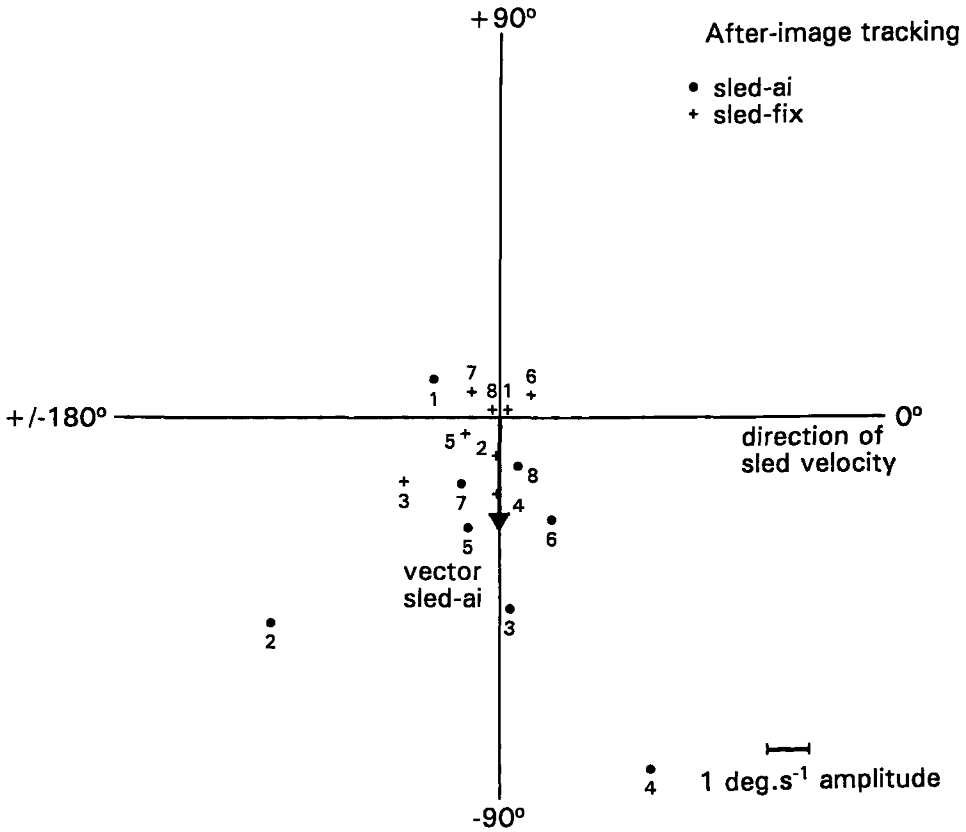

Fig. 5.7 Polar diagram of SCV modulation during after-image tracking (AI). The reference condition is SLED-FIX, as measured when the projection system was mounted. The vector-average is obtained across subjects for the SLED-AI condition, corrected for the electrode-shift artefact. The numbers 1 through 8 are referring to the individual subjects. The photo-flash, that induced the after-image, was at 3m distance in front of the subject.

The plots show phase coherence between subjects in the SLED-OK and SLED-AI conditions. Because of this coherence, there is a prominent average vector. In this average vector, the electrode shift artefact has been rejected. The physical meaning of the vector in Fig. 5.5 can also be interpreted as amplitude and phase of the averaged velocity trace (Fig. 5.4). The coordinates (amplitude; phase) of the average vectors in Figs 5.5, 5.6 and 5.7 are (6.8 deg $\cdot$ s^{-1}; -124 deg) for binoculars, (2.4 deg $\cdot$ s^{-1}; -131 deg) for projection, and (2.9 deg $\cdot$ s^{-1}; -90 deg) for after-image tracking.

5.3.4 Vector averaging across subjects

For all conditions the results of vector averaging are presented in Table 5.4. The observed SCV modulation vectors ($SCV_{observed}$) from the conditions SLED-OK, SLED-DARK and SLED-AI (Table 5.4) have been corrected for the electrode shift artefact (measured in SLED-FIX) by vector-subtraction.

Table 5.4 Amplitude and phase of $SCV_{observed}$, obtained from vector-averaging across 8 subjects. R and L stand for OK stimulus direction to the right and to the left. "Averaged R/L" is the modulation which is vector-averaged across the R and L directions.

	AMP ($deg \cdot s^{-1}$)	PHASE (deg)	AMP ($deg \cdot s^{-1}$)	PHASE (deg)
SLED-OK Binoculars			Averaged R/L	
40 $deg \cdot s^{-1}$ R	2.6	-98	3.4	-99
40 $deg \cdot s^{-1}$ L	4.1	-100		
60 $deg \cdot s^{-1}$ R	2.9	-130	3.6	-119
60 $deg \cdot s^{-1}$ L	4.3	-112		
80 $deg \cdot s^{-1}$ R	4.0	-155	5.2	-135
80 $deg \cdot s^{-1}$ L	6.8	-124		
Overall vector average	3.9	-121		
SLED-OK Projection				
40 $deg \cdot s^{-1}$ R	1.4	-101	1.7	-136
40 $deg \cdot s^{-1}$ L	2.4	-155		
60 $deg \cdot s^{-1}$ R	1.0	-163	1.0	-146
60 $deg \cdot s^{-1}$ L	1.1	-130		
80 $deg \cdot s^{-1}$ R	2.8	-189	2.3	-162
80 $deg \cdot s^{-1}$ L	2.4	-131		
Overall vector average	1.6	-150		
SLED-DARK				
binoculars mounted	1.2	-184		
projection mounted	1.8	-194		
Overall vector average	1.5	-190		
SLED After-Image				
distance .6m	1.9	-69		
distance 3m	2.9	-90		
Overall vector average	2.4	-82		
SLED-Fixation				
binoculars mounted	0.7	-23		
projection mounted	0.7	-132		

The vectors are collected in one plot in Fig. 5.8. For the OK conditions, the averages across right (R) and left (L) OK direction are plotted; for SLED-DARK the average across "binoculars mounted" and "projection mounted"; for SLED-AI the average across the flash-distances of .6 and 3m.

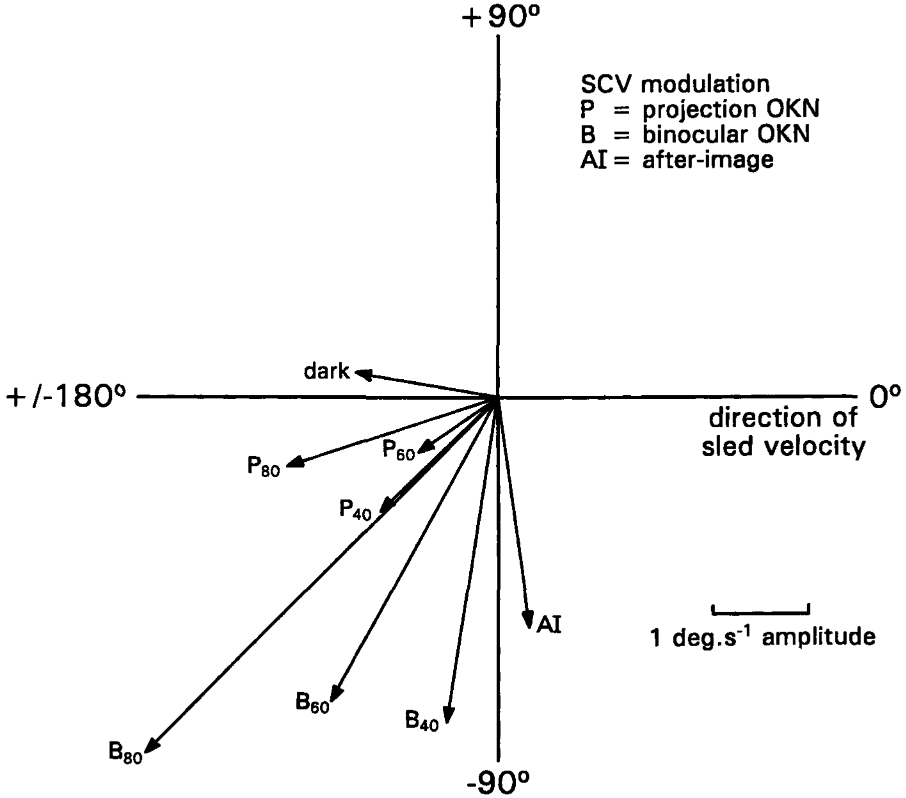

Fig. 5.8 Survey of modulation vectors of Slow-Component Velocity (SCV) averaged across subjects and corrected for the electrode shift artefact (Table 5.4). For OKN, the vectors are also averaged across right- and leftward OK stimulus. "B" and "P" are for binoculars and projection; 40, 60, and 80 are referring to OK stimulus velocity.

The phase relations between SLED-DARK, SLED-OK/P and SLED-OK/B were analyzed by t-tests on paired samples of the phase of modulation.

The results showed that the phase in SLED-OK/B is leading to the phase in SLED-DARK ($p<0.01$). The phase in SLED-OK/B is also leading to the phase in SLED-OK/P ($p<0.05$). This last result is in agreement with the effect of OK device on phase, that was already found in the ANOVA of SLED-OK phase values (Table 5.3). The phase difference between SLED-OK/P and SLED-DARK was found to be not significant.

5.3.5 Contribution of gaze-change to SCV modulation

Amplitude and phase of the change in gaze was calculated in the conditions SLED-OK/B and SLED-OK/P. Subsequently, the vector SCV_{gaze} was determined. SCV_{true} was calculated by vector-subtraction of $\text{SCV}_{\text{observed}}$ and SCV_{gaze}. This result was vector-averaged across subjects. The resulting amplitude and phase values are shown in Table 5.5.

Table 5.5 Amplitude and phase of SCV_{true}, obtained from vector-averaging across 8 subjects. R and L stand for OK stimulus direction to the right and to the left. "Averaged R/L" is vector-averaged across the R and L directions.

	AMP (deg · s^{-1})	PHASE (deg)	AMP (deg · s^{-1})	PHASE (deg)
SLED-OK Binoculars			Averaged R/L	
40 deg · s^{-1} R	2.3	-62	3.0	-69
40 deg · s^{-1} L	3.7	-73		
60 deg · s^{-1} R	2.3	-94	2.8	-83
60 deg · s^{-1} L	3.4	-75		
80 deg · s^{-1} R	1.9	-147	3.4	-117
80 deg · s^{-1} L	5.3	-107		
Overall vector average	2.9	-91		
SLED-OK Projection				
40 deg · s^{-1} R	1.0	-349	0.3	-56
40 deg · s^{-1} L	0.9	-128		
60 deg · s^{-1} R	2.1	-235	0.9	-230
60 deg · s^{-1} L	0.4	-78		
80 deg · s^{-1} R	2.7	-208	2.0	-169
80 deg · s^{-1} L	2.5	-127		
Overall vector average	0.8	-180		

Table 5.5 shows that for OK stimulation with binoculars the amplitude of SCV_{true} is smaller than the values in Table 5.4 (which were not corrected for the gaze-change effect), but we still find modulation of the SCV with a consistent phase. For OK stimulation with projection, however, there is hardly any

modulation left. This means that for OK with projection, the observed SCV modulation is largely due to changes in gaze.

Some individual results, including the values of SCV_{gaze}, are shown in the appendix. For the projection OK device, the phase values of SCV_{true} are dispersed over the range from -9 to -310 deg. This leads to the low amplitude of the vector-averaged SCV_{true}.

5.4 Discussion

5.4.1 Possible artifacts

An increase in SCV modulation amplitude with sled movement does not necessarily imply an effect of the movement itself, but it could be due to a general increase of random eye movements induced by discomfort. This would enhance the amplitude of all frequency components in the SCV rather than only the one related to sled movement.

However, the phase coherence in responses, revealed in the vector-averages, indicates that the increase of the DFT amplitudes in the SLED-OK conditions is not only an effect of an overall increase of activity. In addition, we have checked for one OK velocity whether or not variability increases during SLED-OK, in comparison with OK. Both modulation amplitude and standard deviation (the root-mean-square value) of the SCV were calculated for stimulation with binoculars, 80 deg $\cdot$ s^{-1} to the left. We selected this OK velocity for the test, because the amplitude is largest in this condition. The t-test on paired samples for individual subjects revealed that during SLED-OK the SCV standard deviation is *not* larger than during OK only, while the amplitude is larger ($p<0.005$). Therefore, it is unlikely that the increase of amplitude during SLED-OK is caused by a general increase of random eye movements.

5.4.2 Effect of optokinetic stimulus type

The analysis of variance revealed no effect of OK device on modulation amplitude, while the vector-averaged values in Fig. 5.8 do show larger modulation responses obtained with the binocular "B" system than with the projection "P" system. This indicates that the phases of response are more coherent across subjects when OKN is induced with binoculars. Presumably this difference is caused by a difference in the type of OKN that was induced. We suggest that our projection system evoked a "look-OKN", while the binocular system evoked a "stare-OKN". The idea that the binocular system induces stare-OKN is supported by comparison of the gain of our OKN, induced with binoculars, with the gain of stare-OKN reported by Van den Berg and Collewijn (1988). For horizontal stare-OKN, pooled over right and left OK directions at 57 deg $\cdot$ s^{-1} OK stimulus velocity, they found a gain of 0.54. This is quite comparable with the averaged gain of OKN with binoculars in our study, which is 0.52 at 60 deg $\cdot$ s^{-1} in the OK/B condition (see Fig. 5.3).

The moving checkerboard pattern, that was presented with binoculars, is probably easily lost from foveal vision, inducing a more "lousy" OKN response than the black-and-white bars of 24 deg spatial period in the projection system (gain of 0.67 at 60 deg $\cdot$ s^{-1} in the OK/P condition). Thus there could be a stronger effect of the vestibular system on eye velocity. From a practical point of view, the binocular system seems more suitable than the projection system for studying otolith-induced modulation.

5.4.3 The mean OKN-SCV

An unexpected observation is the increase in mean nystagmus SCV during SLED-OK, as compared with OK only (see Table 5.2 and Fig. 5.3). Buizza et al. (1980) observed the same phenomenon, and attributed it to the acoustical noise related to sled motion. We presume that the main reason is an increase in the subject's arousal state during motion, which could induce the increase in mean SCV. Also, during motion the subject might orient himself more strongly on his visual environment, and therefore perform a better OKN.

5.4.4 The amplitude of SCV modulation

Darkness

For comparison with current literature, we use the unit "sensitivity for translation" (ST) as a measure of the amplitude of modulation. ST is defined as the amplitude of eye velocity [deg $\cdot$ s^{-1}], divided by peak subject-velocity [m $\cdot$ s^{-1}], and the dimension of ST is thus [deg $\cdot$ m^{-1}]. In our experiment, the amplitude of eye velocity modulation is average 1.5 deg $\cdot$ s^{-1} (after correction for the shift artefact), peak subject velocity is 1.77 m $\cdot$ s^{-1}, and thus ST = 1.5/1.77 = 0.8 deg $\cdot$ m^{-1}. Niven et al. (1966) applied an acceleration with 0.58g amplitude and measured ST = 2.1 deg $\cdot$ m^{-1}. Baloh et al. (1988) measured human eye movement responses on a parallel swing. He reported ST values in darkness of 3.8 to 4.7 deg $\cdot$ m^{-1}. Buizza et al. (1980) reported on a linear track a ST of 3.2 deg $\cdot$ m^{-1}. We thus conclude that our ST value in darkness is smaller, when compared with LVOR data reported in literature.

Optokinetic stimulation

Buizza et al. (1980) measured OKN-SCV modulation on a linear track, in an experimental set-up comparable to ours. They applied an acceleration amplitude of 0.16g, and reported modulation amplitudes of at least 10 deg · s^{-1}. Our modulation amplitudes are about 50% smaller, compared with the data of Buizza et al. We suggest that several parameters in the visual environment (e.g. form and dimensions of the screen, spatial properties of the optokinetic pattern), are largely influencing the modulation.

5.4.5 The phase of SCV modulation

Our study has yielded not only the amplitude, but also the phase of SCV modulation, which allows us to discuss the physiological basis of the response.

Darkness

Our phase value of -190 deg in darkness (see Table 5.4) is matching the phase of responses in monkeys on a linear track (Paige and Tomko, 1991). At an acceleration amplitude of 0.36g and frequency of 0.5 Hz, nearly ideal compensatory eye movements were observed. Baloh et al. (1988) measured human eye movement responses in darkness on a parallel swing, and reported phase values of -152 to -160 deg.

An eye velocity purely compensatory to sled velocity would correspond to a phase lag of -180 deg. Our phase value of -190 deg is quite compatible with a response compensatory to velocity. This response in darkness is in agreement with the otolith model of Young and Meiry (1967), which acts as a "velocity transducer" over the mid-frequency range ($0.03Hz < f < 0.24Hz$), which encompasses the frequency of sinusoidal motion that we applied on the sled ($f=0.176Hz$).

Optokinetic stimulation

The phase of modulation in Table 5.4, as obtained from vector-averaging, ranges from -189 deg to -98 deg for OKN, while the phase for AI tracking ranges from -69 deg to -90 deg. For OKN and AI tracking, we thus find a phase lead with respect to the phase measured in darkness. These phase relations *cannot* be explained on the basis of otolith physiology, because the acceleration stimulus of the sled is the same in all conditions with a moving sled. Also, the phase difference between the OKN-SCV modulation with binoculars vs projection, cannot be explained on the basis of otolith cell activity.

At this point we thus conclude that during OKN and AI tracking there should be some visual-vestibular interaction, which is responsible for the phase shift. For OKN, this interaction will be analyzed in Chapter 6. For AI tracking, some concepts about the underlying mechanism are discussed here.

5.4.6 After-image tracking

After-image tracking provides another technique, proposed by Yasui and Young (1975), for amplifying the vestibulo-ocular reflex. It has been applied by Shelhamer and Young (1991) on a linear track. The underlying mechanism is probably different from OKN-SCV modulation, because with AI tracking the visual feedback loop is opened: there is no effect of eye velocity on retinal-image velocity. The after-image is always fixed at the retina. We discuss two alternative mechanisms for the origin of SCV modulation during AI tracking.

The first mechanism is based on the concept of "efferent copy" of the oculomotor system (see Fig. 5.9).

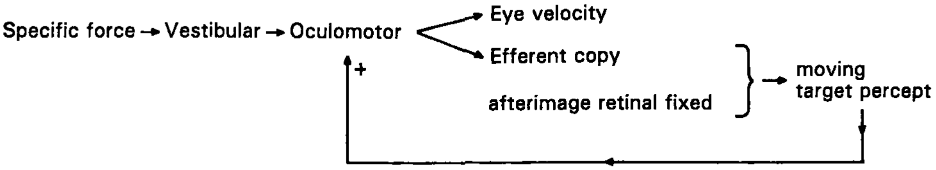

Fig. 5.9 A model of after-image tracking as a technique for enhancing the otolith-ocular reflex. An efferent copy of the oculomotor command, combined with the information that the target is retina-fixed, induces a central percept of a "moving" target. This percept generates positive feedback to the oculomotor system, to keep track of the "moving" target. Some of these concepts were suggested by Collewijn et al. (1981), and Shelhamer and Young (1991).

An after-image is induced, and subsequently the linear acceleration starts while the subject is instructed to track the after-image foveally in a dark environment. Initially a small-amplitude vestibulo-ocular reflex is induced by the otoliths. An efferent copy of the oculomotor command is transmitted to some central level, bringing the message that the eyes are moving. The "central processor" has also the information that the visual target (the after-image) is not moving on the retina. The conclusion for the central processor is necessarily that the target is moving, and thereby that the eye movement must be sustained. The result is a positive perceptual feedback: an internal representation of target velocity is tracked by the oculomotor system. This mechanism was proposed by Collewijn et al. (1981). In our experiment, it would be expected that the after-image evoked at .6m distance would induce a larger SCV modulation than the after-image from 3m distance. Such an effect of viewing distance was predicted by Schwarz et al. (1989). However, in our data no significant effect of viewing distance was found.

An alternative mechanism might also be effective during after-image tracking. Linear acceleration can modify the perceived velocity of a visual scene, in the absence of any eye movement (Pavard and Berthoz, 1977; Berthoz and Droulez, 1982). In this view the percept of velocity is primary, and an efferent copy of the oculomotor system does not play a role. During after-image tracking, subjects might follow their central percept of target velocity, which is induced by acceleration.

So far, we have mentioned two different mechanisms of modulation during AI tracking. Further research should bring more clarity. From a practical point of view, the AI-tracking technique has the advantages that no OK stimulus devices are needed, and that the eye movement response is not nystagmoid, but sinusoidal. This means that no nystagmus-SCV calculations are needed.

5.5 Conclusions

Discrete Fourier Transform analysis of Slow-Component eye Velocity (SCV) has been performed on eye movement responses in darkness, with horizontal optokinetic (OK) stimulation, and with after-image (AI) tracking. Our conclusions are based on the modulation (amplitude and phase) of the SCV, that was induced by subject acceleration. Phase is always referred to subject velocity.

1 During acceleration in darkness, vector averaged eye velocity equals 1.5 deg $\cdot$ s^{-1} at a phase of -190 deg. This is consistent with a compensatory otolith-induced eye velocity.

2 During acceleration with OK stimulation, the observed OKN-SCV is modulated with an average amplitude of 3.9 deg $\cdot$ s^{-1} and average phase of -121 deg for the binocular OK system, and 1.6 deg $\cdot$ s^{-1} and -150 deg for the projection OK system.

3 ANOVA of the SLED-OK data revealed significant effects of OK system and OK velocity on the phase of modulation. Relative to darkness, there was less

phase shift using the projection system than using the binocular system. There was a trend of smaller phase shifts with increasing OK velocity.

4 The phase lead, observed in OK stimulation and AI tracking with respect to the darkness condition, might be explained on the basis of visual-vestibular interactions.

5 Using the projection system, observed OKN-SCV modulation was largely an effect of changes in gaze. Using the binoculars, observed OKN-SCV modulation was mainly a true modulation of the slow component of the nystagmoid signal.

6 During acceleration with AI tracking, SCV modulation is observed at an average amplitude of 2.4 $\deg \cdot s^{-1}$ and average phase of -82 deg. In a current model this is explained by positive perceptual feedback.

Acknowledgments

The binocular optokinetic stimulation device has been kindly provided by Prof. A. Berthoz, Lab. de Physiology Neurosensorielle, Paris.

APPENDIX: The effect of gaze-change on eye velocity

In Table 5.6 below the individual data are given for the observed vector $SCV_{observed}$, the vector of velocity modulation induced by gaze-change SCV_{gaze}, and the vector of the modulation of the slow-component velocity of the nystagmoid signal SCV_{true}. The condition is SLED-OK, with OK stimulus velocity of 80 deg · s^{-1} to the left. The upper part of the table concerns the binocular OK device; the lower part the projection OK device. A is amplitude in deg · s^{-1}; ϕ is the phase, referred to sled velocity, and expressed in degrees. In this table, the electrode shift artefact is included in the values of $SCV_{observed}$ and SCV_{gaze}.

Table 5.6 Individual data of the vectors $SCV_{observed}$, SCV_{gaze}, and SCV_{true}, with OK stimulation of 80 deg · s^{-1} to the left.

BINOCULAR OK DEVICE

Subj.nr.	$SCV_{observed}$		SCV_{gaze}		SCV_{true}	
	A	ϕ	A	ϕ	A	ϕ
1	9	-90	2.2	-197	9.9	-78
2	10	-148	1.1	-69	9.9	-154
3	7	-139	3.3	-151	3.8	-129
4	9	-123	6.6	-159	5.3	-76
5	4	-94	1.1	-69	3	-103
6	5	-67	0		5	-67
7	6	-108	0		6	-108
8	9	-131	2.2	-143	6.9	-127
Vector-average	6.7	-118	1.7	-151	5.3	-107

PROJECTION OK DEVICE

Subj.nr.	$SCV_{observed}$		SCV_{gaze}		SCV_{true}	
	A	ϕ	A	ϕ	A	ϕ
1	4	-112	5.6	-144	3.0	-9
2	2	-86	3.3	-65	1.6	-239
3	1	-125	2.2	-128	1.2	-310
4	10	-170	3.3	-240	9.4	-151
5	1	-16	8.9	-295	8.8	-109
6	6	-48	4.4	-64	2.1	-13
7	5	-169	2.2	-229	4.3	-143
8	6	-130	3.3	-117	2.9	-145
Vector-average	3	-130	0.5	-145	2.5	-127

Chapter 6

Extension of the velocity storage model with a direct otolithic path

Abstract

In experiments in the centrifuge, during parabolic flight and on the linear track ("sled") we have found evidence that G forces contribute to the Slow-Component eye Velocity (SCV) via a direct otolith-ocular pathway. The aim of this chapter is to express these results in one model for the generation of SCV.

For the construction of the model, we use the SCV modulation that we observed on the sled in response to sinusoidal motion. For a number of conditions the amplitude of modulation was computed, as well as the phase with respect to sled velocity. In darkness, the phase lag of LVOR-SCV modulation was compensatory to subject velocity, which is explained by the frequency response of the tonic otolith cells. With OptoKinetic (OK) stimulation, a reduction in this phase lag was observed which is explained by adding a direct otolith-ocular path to the current model of velocity storage. The weighting factor of the storage pathway is calculated from the observed reduction in phase lag of OKN-SCV modulation.

In physiological conditions like walking, the model shows that the otolithic pathway functions in synergy with the visual system to stabilize the gaze. During hypergravity, however, the same pathway may interfere with vertical oculomotor search. The model predicts that proximity cues of visual targets enhance this non-functional otolithic response to increased G-force, and that visual references in the peripheral visual field may suppress this otolithic effect.

6.1 Review of experiments

We have investigated the otolith-ocular responses in man in different force environments: during G=3g hypergravity in a centrifuge, in parabolic flight ("parabolas") and during sinusoidal acceleration on a linear track ("sled"). The otolith responses are expressed in a pure, linear vestibulo-ocular reflex (LVOR) in darkness, or in modulation of OptoKinetic Nystagmus (OKN). We note that the term "linear" in this context refers to the linear (non-rotational) acceleration input, and not to the response of the reflex arc. The otolith-ocular influence is quantified on the basis of the modulation of the Slow-Component Velocity (SCV). Our main findings of the otolithic influence on SCV are summarized in Table 6.1. Because eye *velocity* is the relevant dimension in our model, we included in this table only the "true" velocity modulation for the SLED-OK conditions. It was defined in Chapter 5 that this is the SCV modulation, after correction for the effects of changing gaze. With the projection system we have found that the true modulation of OKN-SCV was hardly above noise level (Chapter 5, Table 5.5). In this chapter we therefore restrict our analysis to the responses obtained with the head-mounted binocular OK stimulus.

Table 6.1 Survey of results of otolith-ocular responses, averaged across subjects. The directions of G_z and G_y have been defined in Chapter 2. V is vertical, H is horizontal eye velocity. "Amp" is the amplitude of response, expressed in deg · s^{-1} *per g unit*. Phase is referred to sled velocity.

Specific force	Otolith-ocular responses	Amp [deg · s^{-1}]	Phase [deg]
Centrifuge, G_z=3g	V-LVOR, in darkness	5	
Parabolas, G_z=0..1.8g	V-OKN modulation	3	
Sled, G_y=0.2g sinus	H-LVOR in darkness	7.5	-190
	H-OKN modulation		
	at 40 deg · s^{-1} OK stim.	15	-69
	at 60 deg · s^{-1} OK stim.	14	-83
	at 80 deg · s^{-1} OK stim.	17	-117

Our experimental results have so far been presented as separated phenomena. This chapter is devoted to the development of model concepts, which might have a wider applicability than the specific conditions of our experiments. We shall try to describe the otolith-ocular responses, observed in these different conditions, in one integrated model.

6.2 Integrated model of responses in the centrifuge, on the sled and in parabolic flight

6.2.1 Velocity storage and a direct otolithic pathway

Velocity storage

We start our model with the current velocity storage concept (Cohen et al., 1977; Raphan et al., 1977). This model quantifies the roles of angular velocity and visual surround velocity in the generation of slow-component eye velocity "V_{eye}".

The model is shown in Fig. 6.1. The input "*surround* velocity" is equivalent to OK stimulus velocity, and thus it is the visual input to the model. The subtraction of surround velocity and eye velocity yields the retinal-slip velocity which is the input to the visual system. The *angular* velocity is the input to the block "cupula dynamics" (Appendix C).

Both the angular and the visual (surround) velocity signals are transferred to the eye velocity signal via two different pathways: a direct path, and an indirect path via an integrating circuit called "velocity storage". This circuit integrates, or "stores" velocity information; it is also called the "central" integrator, because of its neuro-anatomical location in the central vestibular nuclei. The integrator discharges via the feedback gain element h, which thus determines the decay time constant $T_{decay}[s] = h^{-1}$. The value of the feedback gain element h is estimated to be $h = 0.1\ [s^{-1}]$ (Kostelijk, 1982). The weighting factors g_1 and g_2 are determining the weight of the direct and indirect visual pathways, respectively. The direct path involves the cortex and is mainly supported by the foveal region of the retina, while the indirect, subcortical, path is mainly supported by the peripheral retina (Buizza and Schmid, 1982; Murasugi and Howard, 1989). For a more detailed description of the different pathways, the reader is referred to Collewijn (1985).

A direct otolithic pathway

In order to account for the G effects that we observed, we extend the velocity storage model with a direct otolith-ocular connection [suggested earlier by Lansberg et al. (1965) and Young (1967)], as shown by the upper pathway in Fig. 6.1. The specific force input "G force" is sensed by the otoliths, which generate an eye velocity signal "$V_{otolith}$". The model block "otolith dynamics" thus transforms the linear dimension of G input $[m \cdot s^{-2}]$ to the angular dimension of eye rotation $[deg \cdot s^{-1}]$. The direction of eye velocity is expressed by the eye rotation vectors, as defined in Chapter 2. The otolith-ocular path thus induces a pitch eye velocity vector in response to G_z, and a yaw eye velocity vector in response to G_y. The gain of this otolith-ocular reflex is influenced by a proximity cue, as discussed in Chapter 1. The proximity factor has been included in the model of Fig. 6.1.

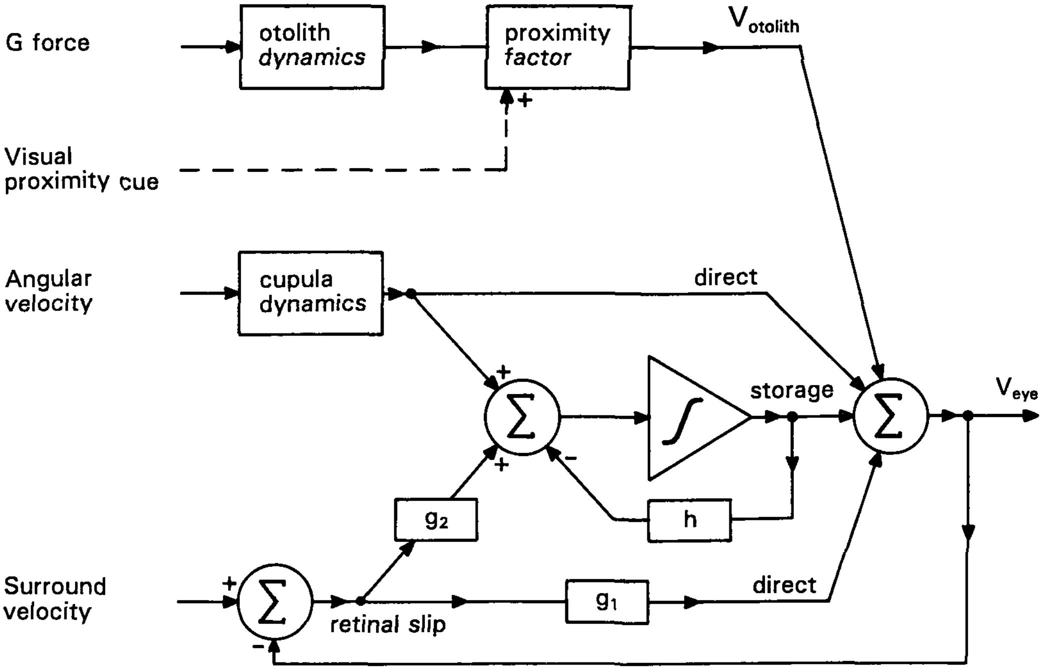

Fig. 6.1 *Integrated model,* accounting for vestibular inputs of G force and head angular velocity, and the visual input of surround velocity. In accordance to the velocity storage concept, the same central integrator is responsible for storing the angular velocity information from the semicircular canals, as well as the visual surround velocity.

For reasons of simplicity we assume that for the vertical nystagmus generation a similar storage mechanism is used as for the horizontal nystagmus. We should be aware that the value of the feedback gain element h may be different for horizontal and vertical directions.

In conclusion: *The effect of specific force on eye velocity is expressed by linking a direct otolithic path to the velocity storage model.*

We will investigate whether the model in Fig. 6.1 can cover our results, and what parameter values in the model can be determined from our data.

6.2.2 The otolithic pathway in the centrifuge experiment

The centrifuge experiment has given evidence for the direct otolith pathway, because we observed a sustained SCV-down nystagmus in response to $G_z = +3g$. The model inputs for this experiment are G force and angular velocity, which is the pitch angular velocity profile of the subject in the gondola. All measurements were made in complete darkness, and so the visual input of surround velocity is absent. In order to verify whether the direct otolith path provides a *complete* description of our centrifuge data, we investigate whether or not there should be additional connections: (1) from the otoliths to the input of the integrator, and (2) from the otoliths to the feedback factor of the integrator.

Both questions can be answered on the basis of the combined dataset of forward and backward centrifuge runs, as described in Chapter 3. Considering the possible otolith-integrator connection (1), we refer to the summation trace (forward + backward) which is the pure otolith response to $+G_z$ (if we assume linear addition of canal- and otolith-contributions). After cessation of the $+G_z$ load, this otolith response stops immediately, which shows that the otoliths did *not* charge the integrator. Considering the possible connection (2), we refer to the subtraction trace (forward - backward), which is the assumed pure canal response during $G_z = +3g$: Comparing this canal response to $G = 1g$ baseline measurements revealed no differences. Thus the otoliths did *not* change the feedback factor of storage in our data.

In conclusion: *Our data from the centrifuge experiment can be explained by taking into account only the direct otolithic path.*

6.2.3 The otolithic pathway in the sled experiment

On the sled, the sinusoidal input of G force provides us with both amplitude and phase of the response. We use these responses for verifying some elements of the model in Fig. 6.1. We start from the LVOR-SCV response in darkness on the sled. In this condition, the observed eye velocity is a pure otolith-ocular response.

The observed phase of the LVOR-SCV modulation is -190 deg (see Fig. 6.2), which means that the SCV response is about compensatory to sled velocity. This matches with the frequency response of the "tonic" otolith cells, which was presented in the introductory chapter, and calculated in Appendix A.

In the *mid-frequency range*, these tonic cells respond in phase with velocity, rather than with acceleration. At the frequency of sled movement the phase lag is calculated at -175 deg. Our observed phase of LVOR-SCV modulation (average value of -190 deg) is not significantly different from this model prediction. In our model considerations we thus proceed with the phase value of -175 deg for the LVOR-SCV modulation.

The idea of "velocity transduction" in the frequency range of natural head movements is confirmed in otolith models based on perceived specific force (Young and Meiry, 1968; Mayne, 1974).

The same otolith model may also serve to describe the response to *sustained* $+G_z$ in the centrifuge. The frequency response of the tonic otolith cells (Chapter 1, Fig. 1.5) shows that the same cells, that are responding in phase with velocity on the sled, are responding in phase with specific force in the low-frequency range. The specific force input in the centrifuge is a steady state input, and thus in the low-frequency range. Hence the same tonic otolith cells, that are responding in phase with velocity on the sled, are responding to specific force in the centrifuge.

In conclusion: *In the model, the phase of modulation of the otolith-induced eye velocity signal $V_{otolith}$ is about compensatory to sled velocity. Responses in darkness on the sled and in the centrifuge can both be explained from the frequency-response of the tonic otolith cells.*

6.2.4 Otolithic and visual pathways in the sled experiment

The phase of OKN-SCV modulation

In this section we continue with the sled-experiment, and consider the modulation of OKN-SCV induced by sled motion. Our model calculations start from the OKN-SCV modulation vector observed with binocular OK stimulation at 80 deg $\cdot$ s^{-1}. This vector has an amplitude of 3.4 deg $\cdot$ s^{-1} and phase of -117 deg (Fig. 6.2). (The modulation vectors at 40 deg $\cdot$ s^{-1} and 60 deg $\cdot$ s^{-1} OK stimulation are discussed later.)

The reduced phase lag of the sinusoidal modulation in OKN-SCV (compared with the phase of LVOR-SCV) cannot be explained on the base of otolith haircell processing, because the otolith stimulus is identical in all conditions with moving sled. Thus the reduction of phase lag in the modulation of OKN-SCV should be understood from properties of the visual pathway. For the explanation of this phase lag reduction, we refer to the model in Fig. 6.1. Inputs are sinusoidal G-force, and constant surround velocity (= OK stimulus velocity). Fig. 6.1 shows that the sinusoidal signal $V_{otolith}$ is transferred to the final summator that yields the eye velocity. An essential property of the model is, however, that this sinusoidal component is also transferred to the visual pathway via the visual feedback, whenever there is surround velocity input. The retinal slip is the difference between surround velocity and eye velocity, and thus any sinusoidal component of V_{eye} is inverted, and transmitted to retinal slip. Subsequently, this signal is partially led through the storage integrator, which shifts the phase. Due to this integrator in the negative feedback loop, the contribution of velocity storage to eye velocity V_{eye} will finally *lead* in phase with respect to $V_{otolith}$. A similar mechanism was suggested by Buizza et al. (1980; 1981).

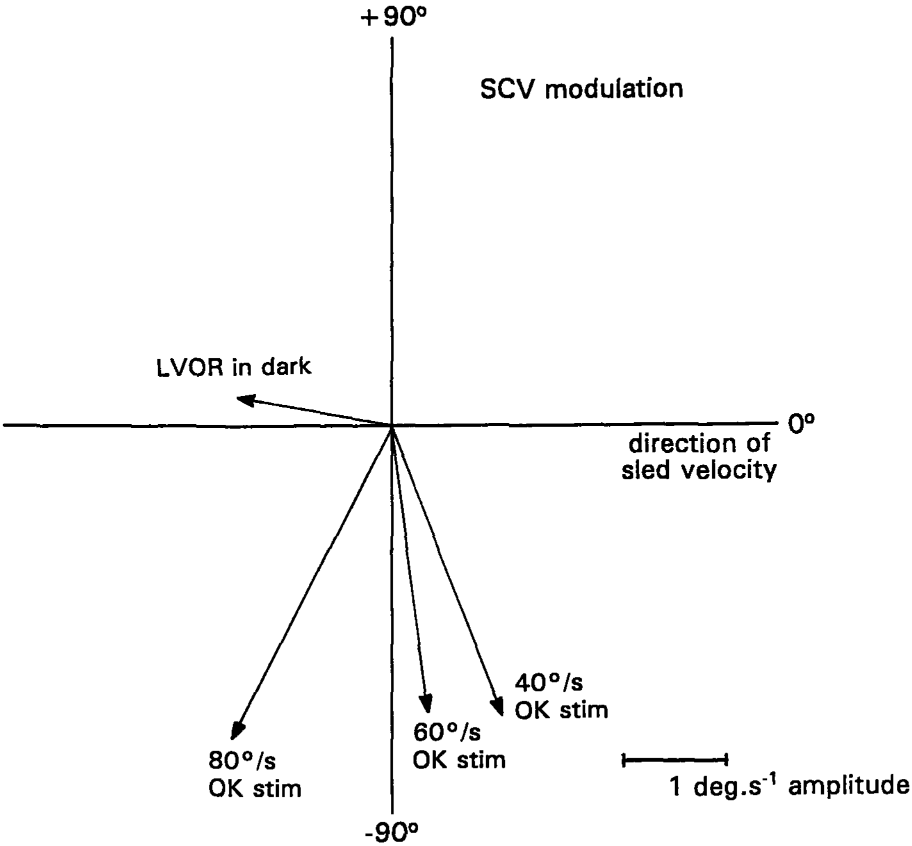

Fig. 6.2 Summarized result from the *sled experiment*, presented in a polar diagram of the modulation of SCV in response to sinusoidal sled movement. The zero-phase axis is aligned with the phase of sled velocity. With OK stimulation by binoculars, only the true SCV modulation is shown which was obtained after correction for changes in gaze. The modulation vectors are averaged across subjects, and across the left- and rightward OK stimulus directions.

Model calculations

In this section we calculate, whether the model can quantitatively predict the reduced phase lag of OKN-SCV modulation. For this purpose, we describe the extended velocity storage model of Fig. 6.1 from a systems-analysis point of view. In this approach we assume that the system is linear, although we are aware that in reality non-linear elements are present (e.g. saturation of OKN response at large OK stimulus velocities).

In the linear approach, the general formula for V_{eye} is written as the sum of the velocity signals induced by otolith stimulation and induced by surround velocity:

$$V_{eye} = H_{storage,\ otolith} \cdot V_{otolith} + H_{storage,\ surround} \cdot V_{surround}$$

This equation is derived in more detail in Appendix B2. Because of the visual feedback path, the transfer function $H_{storage,otolith}$ depends on the system parameters g_1, g_2, and h of the velocity storage mechanism. $V_{surround}$ is constant. The aim of our model calculation is to find model parameters with which the observed phase lead is predicted. Our approach is:

1 Assume fixed values $h=0.1$ and $g_1=0.8$. These values are estimated from simulations of human postrotational nystagmus and optokinetic after-nystagmus (Kostelijk, 1982).

2 Write the parameter g_2 as a function of h, g_1, and the observed phase lead with respect to the modelled phase of the LVOR (-175 deg). This is performed in Appendices B1 through B4.

3 Check whether there is a value of g_2, that satisfies the observed phase lead.

Appendix B4 shows that phase leads up to about 85 deg are predicted, by taking an appropriate value of g_2 (according to eq. 8 in this Appendix). Thus the model can explain the phase of OKN-SCV modulation at OK velocity of 80 $\text{deg} \cdot s^{-1}$. From the observed *phase* of V_{eye} (-117 deg), it follows that the matching g_2 value is 3.8. Finally, from the observed *amplitude* of V_{eye}, the amplitude of $V_{otolith}$ is scaled to 13.6 $\text{deg} \cdot s^{-1}$ (Appendix B5).

For the OK velocities of 40 $\text{deg} \cdot s^{-1}$ and 60 $\text{deg} \cdot s^{-1}$, however, the observed phase leads to LVOR are larger than 85 deg (see Fig. 6.2). Thus for these OK velocities, the observed phase leads cannot completely be explained by our model.

Once all model parameters have been determined, model simulations are performed using the TUTSIM program (Meerman Automation, 1988). The sinusoidal acceleration of the sled induces a sinusoidal $V_{otolith}$. In order to present more clearly the amplitude- and phase relations in the model network, the simulation results are first presented in a polar diagram in Fig. 6.3.

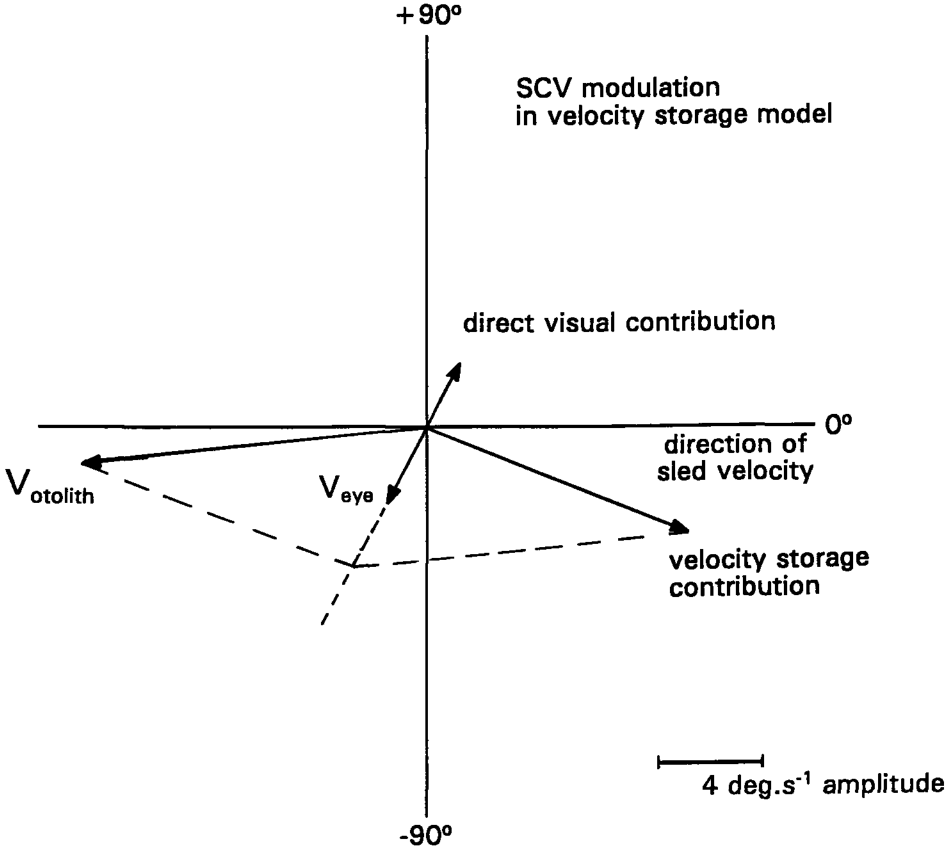

Fig. 6.3 Polar diagram of the different contributions in the *extended velocity storage model.* This diagram shows that the storage contribution induces the phase lead of V_{eye} with respect to the otolith induced velocity signal $V_{otolith}$.

This polar diagram may further clarify the effect of velocity storage: The output of the central integrator ("velocity storage contribution") is responsible for the observed phase lead of V_{eye} with respect to $V_{otolith}$. The outputs of the separate model blocks are shown in Fig. 6.4.

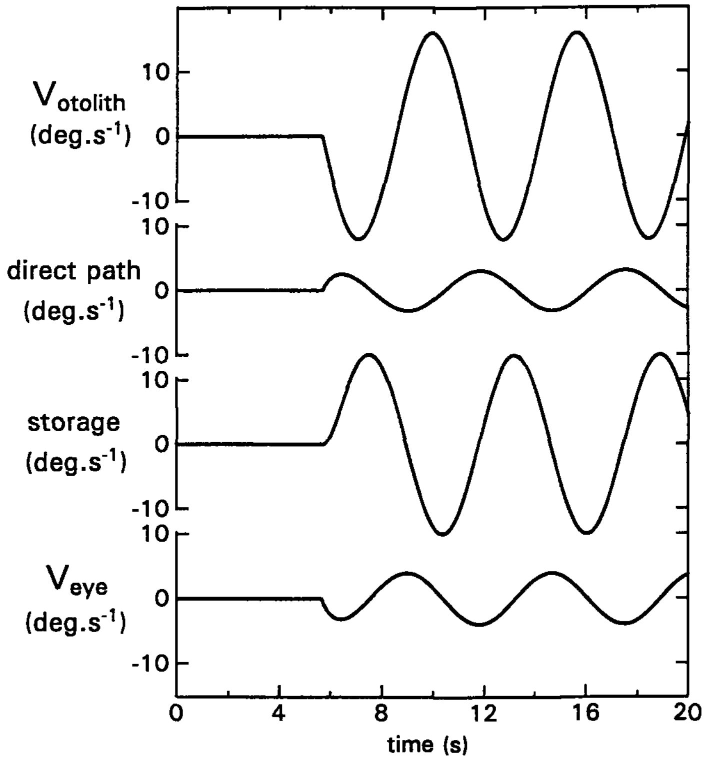

Fig. 6.4 Model calculations for *sinusoidal specific force* input: The otolith-induced velocity signal $V_{otolith}$, the direct path, the storage path, and the sinusoidal component of the output V_{eye}. The observed phase lead of V_{eye} with respect to $V_{otolith}$ is 58 deg. The weighting factors in this simulation are $g_1=0.8$ and $g_2=3.8$.

In the simulations so far, the surround velocity input was zero. For a complete simulation of our sled experiment, we should extend the inputs with a step in surround velocity before the sled movement starts. Results are plotted in Fig. 6.5.

Fig. 6.5 illustrates that the response of V_{eye} to the step in $V_{surround}$ is damped. (This is also derived from the transfer function in Appendix B6.) The sinusoidal modulation of V_{eye} induced by the sled (already shown in Fig. 6.4) is superimposed on the response of V_{eye} to the step input of $V_{surround}$.

***In conclusion:** Given the sled frequency, the phase lead induced by the model may reach values up to 85 deg, by increasing g_2. With OK stimulation at 80 deg $\cdot$ s^{-1}, and current values $g_1=0.8$ and $h=0.1$, we find $g_2=3.8$. The phase leads, observed with OK stimulation at 40 deg $\cdot$ s^{-1} and at 60 deg $\cdot$ s^{-1}, cannot be explained completely by the model.*

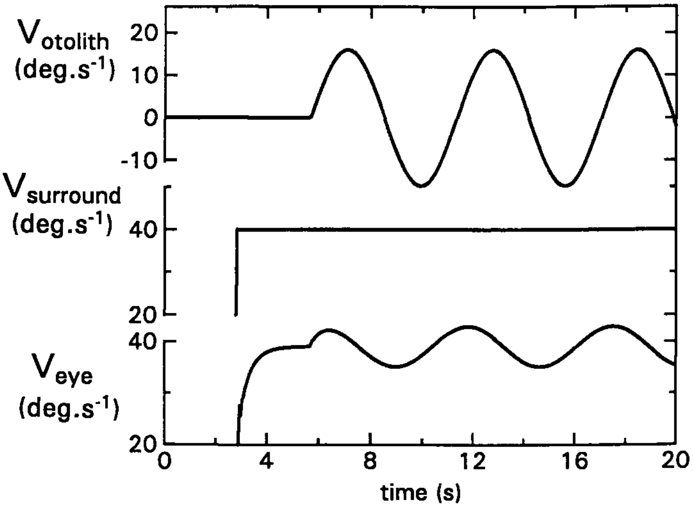

Fig. 6.5 Model calculations for inputs of sinusoidal specific force and a *step in surround velocity*. In the linear-model approach, the constant surround velocity does not influence the sinusoidal component of V_{eye}.

6.2.5 Otolithic and visual pathways in the parabolic flight experiment

In parabolic flight, the inputs to the integrated model in Fig. 6.1 are G force and surround velocity. The G force is generated by the flight profile, and it has been argued in Chapter 4 that the angular velocity input may be neglected. In order to test the general validity of the integrated model, we make predictions of the responses in parabolic flight, based on the *same* model structure and parameters as derived from the sled experiment. Thus $g_1=0.8$, $g_2=3.8$ and $h=0.1$. More specifically, we try to understand why the modulation of V_{eye} observed in parabolic flight is as low as 3 deg $\cdot$ s^{-1} amplitude per g unit.

In order to clarify the predictions of our model in parabolic flight, the moduli of the transfer functions are calculated (see Appendices B3 and B6). The results are presented in Table 6.2.

Table 6.2 Comparison between model predictions on the sled (sinusoidal stimulus with frequency $\omega_{sled}=1.1$ rad $\cdot$ s^{-1}) and in parabolic flight.

	Modulus $H_{storage,otolith}$	Modulus $H_{storage,surround}$
Sled	0.249	0.97
Parabolic flight	0.025	0.97

The modulus of $H_{storage,surround}$ is the same on the sled and in parabolas, because the input frequency of surround velocity is zero in both cases.

The difference between the responses on the sled and in parabolic flight is expressed by the difference in the modulus of $H_{storage,otolith}$. This modulus is a factor 10 larger on the sled, due to the frequency-dependent part in the transfer function $H_{storage,otolith}$. It means that lower-frequency components of $V_{otolith}$ are more suppressed than higher-frequency components, by the velocity storage activity. As a consequence, our model predicts that the relative contribution of $V_{otolith}$ to eye velocity is about a factor 10 smaller in parabolas, than on the sled. This prediction is quite consistent with the experimental data in Table 6.1: Modulation amplitude, in $deg \cdot s^{-1}$ per g unit, was in flight 3 $deg \cdot s^{-1}$, and on the sled about 15 $deg \cdot s^{-1}$ (thus in flight a factor 5 smaller).

This comparison between model predictions on the sled and in flight should be considered with caution, because on the sled we induced horizontal eye movements, and in flight vertical eye movements.

In conclusion: *The model, constructed on the basis of the sled experiment, is qualitatively also consistent with the experimental finding in parabolic flight of only 3* $deg \cdot s^{-1}$ *per g OKN-SCV modulation amplitude.*

6.3 Discussion

6.3.1 Centrifuge: influence of head position during hypergravity

The most likely explanation for the sustained SCV-down nystagmus in response to $+G_z$ is a direct action of the G force on the otolith organ. Because the otolith hair cells are sensitive to the "shear force", some dependence of head position relative to the G vector might be expected.

We have positioned 6 subjects in the *supine* position in the centrifuge gondola, and thus applied the G vector along the x-axis of the subject, with amplitude $G_x=3g$. In 4 out of these 6 subjects we observed the sustained SCV-down nystagmus (Marcus et al., 1989).

McGrath (1990) replicated our finding of a sustained SCV-down nystagmus in responses to sustained $G_z=3g$ in a centrifuge. McGrath et al. (1992) also investigated the effect of head position by measuring the nystagmus response during $G=3g$ with the head *pitched-forward*. Forward pitch of the head reduced the SCV-down nystagmus to zero in 4 out of 6 subjects, and reversed its direction in the 2 other subjects. Returning the head to upright position restored the vertical SCV-down nystagmus.

Combining our findings and those of McGrath et al. (1991), the following mechanism seems likely when we take the orientation of the utricles in the head into account. We presume that the utricle, which is about 30 deg tilted backward in the upright head, is responsible for the induction of the SCV-down nystagmus. With the head in a supine position, there still is a considerable shear force on the utricular maculae, and thus the SCV-down is present. However, with the head pitched-forward, the utricular shear will reduce and finally change direction.

However, it is puzzling what the functional meaning of an SCV-down nystagmus might be, when the head is in a supine position with respect to the G vector.

In conclusion: *The dependence of nystagmus on head position confirms a direct otolithic effect, but the underlying mechanism needs further clarification.*

6.3.2 Sled: alternative model concepts

Potential effect of perceived object velocity

It was reported by Pavard and Berthoz (1977), and by Berthoz and Droulez (1982), that linear acceleration can modify drastically the perceived velocity of a visual scene. This is also predicted by the model of Wertheim (1990). Some of our subjects indeed reported perceived changes in pattern velocity during acceleration. The question might be raised whether during acceleration this percept is primary and changes in eye velocity are a consequence of this percept, or whether the changes in eye velocity are the primary phenomenon.

In a pilot-study with two subjects, we asked them to mark the time (with a hand-held button), during which the pattern velocity seemed to be decreased. Simultaneously we measured and analyzed their SCV responses. We found that perceived pattern velocity was *decreased*, at the moments when the SCV was *increased* (and thus retinal slip reduced). Similar results were reported by Buizza et al. (1980). In other trials in this pilot-study, the subjects were asked to fixate on a stationary point while the pattern was moving. In this condition, with constant retinal-image velocity, the subjects did perceive *no changes* in pattern velocity during sled motion.

Thus, it seems that the SCV response is not a consequence of perceived target velocity, but a reflex to visual and vestibular inputs.

The "pattern centre" hypothesis

Our model does not explain all values found for the phase of SCV-modulation, that we observed on the sled. Given the sled frequency, the storage network can induce a maximum phase lead of 85 deg with respect to the -175 deg phase of the otolith-induced velocity signal $V_{otolith}$, whereas the phases of modulation, observed at 40 deg · s^{-1} (phase = -69 deg) and at 60 deg · s^{-1} (phase = -83 deg), were leading more than 85 deg with respect to the -175 deg value. We therefore mention an alternative hypothesis.

The "pattern centre" hypothesis, proposed by Collewijn (1985), may be applicable. In this view, patterns of retinal slip are stored in the nervous system. The stored pattern could later interact with eye movements when a similar type of motion returns, and induce additional phase shifts in the resulting eye velocity. We consider this hypothesis here because the sled motion is highly predictable in our experiment, and a pattern storage may indeed occur. Retrieval of the stored pattern might result in anticipation, and thus in an additional phase lead.

> ***In conclusion:*** *There are no indications that perceived object velocity played a primary role in our sled experiment. The "pattern centre" hypothesis, however, may explain part of the phase shifts reported. Yet, our model strongly suggests that SCV modulation is primarily due to the vestibulo-ocular reflex.*

6.3.3 Cross-coupling in velocity storage

Our modelling so far has been based on a linear-systems approach, implicating that there are no mutual interactions. However, we should be aware that this is a simplification, and make some references related to non-linear interactions.

Benson (1974) has reviewed the conditions, where canal-induced nystagmus is modified by otolith influence, e.g. when the direction of the subject's head is changing with respect to the G vector. A similar interaction was reported by Lafortune et al. (1991): Static tilt in roll produced suppression of horizontal optokinetic after-nystagmus. Effects of G-force were determined by DiZio and Lackner (1992) in parabolic flight: The decay rate of the velocity storage integrator is affected by the magnitude of the G vector: decay is faster in G=0g relative to G=1g.

Another otolith effect is the so-called cross-coupling. If a monkey is in a static tilted position with regard to gravity, while it views movement of the visual surround around its yaw axis, the OKAN has a vertical component, although the preceding OKN was only in the monkey's horizontal plane. The direction of this oblique after-nystagmus is understood on the basis of the following concept: Velocity storage acts as a gyroscopic mechanism that tends to keep the horizontal eye rotation axis aligned with the spatial-vertical, rather than with the subject-vertical (Raphan and Cohen, 1988). It means that optokinetic following is re-oriented parallel to the earth's surface. This transfer of the response to a different plane is denoted as "cross-coupling", because in mathematical terms it is expressed by cross-products. With head tilt in roll, cross-coupling is from horizontal to vertical eye velocity; with tilt in pitch, cross-coupling is from horizontal to roll eye velocity (Raphan and Sturm, 1991; Angelaki et al., 1991; Dai et al., 1991). It is not certain whether cross-coupling in man is as strong as in monkey (Lafortune et al., 1991).

In cross-coupling, the transfer of response occurs only from the horizontal plane, thus from nystagmus initiated by horizontal angular acceleration or OK stimulation. *A vertical nystagmus always stays vertical with respect to the subject.*

In our experiments in the centrifuge and in parabolic flight, we observed only vertical eye movement responses to the $+G_z$ vector. There was no tilt of the G vector with respect to the subject. In our experiment on the sled, we observed only horizontal eye movement responses to the G_y vector. Further research is needed to determine any role of cross-coupling in our model.

In conclusion: *There is no indication that cross-coupling played a role in our experimental results.*

6.4 Practical implications

In this section we interpret the meaning of our model in several motion environments. We start with a physiological condition like walking, and indicate the functional significance of the otolith-ocular pathway. Subsequently, we discuss the consequences of the same reflex in sustained hypergravity.

6.4.1 Physiological interpretation of the model

The new element in our model is the otolithic contribution to eye velocity, linked with velocity storage. In order to get some feeling for what this means in terms of human physiology, we indicate here what the model predicts during natural head movements with simultaneous visual input of a stable world.

During walking, the head makes a vertical oscillation and apparently gaze is stabilized. Both the otolithic and the visual pathways are activated and contribute to this gaze stabilization. The inputs of specific force and surround velocity then have the same frequency. The predicted frequency responses of the otolithic and visual contributions are plotted in Fig. 6.6.

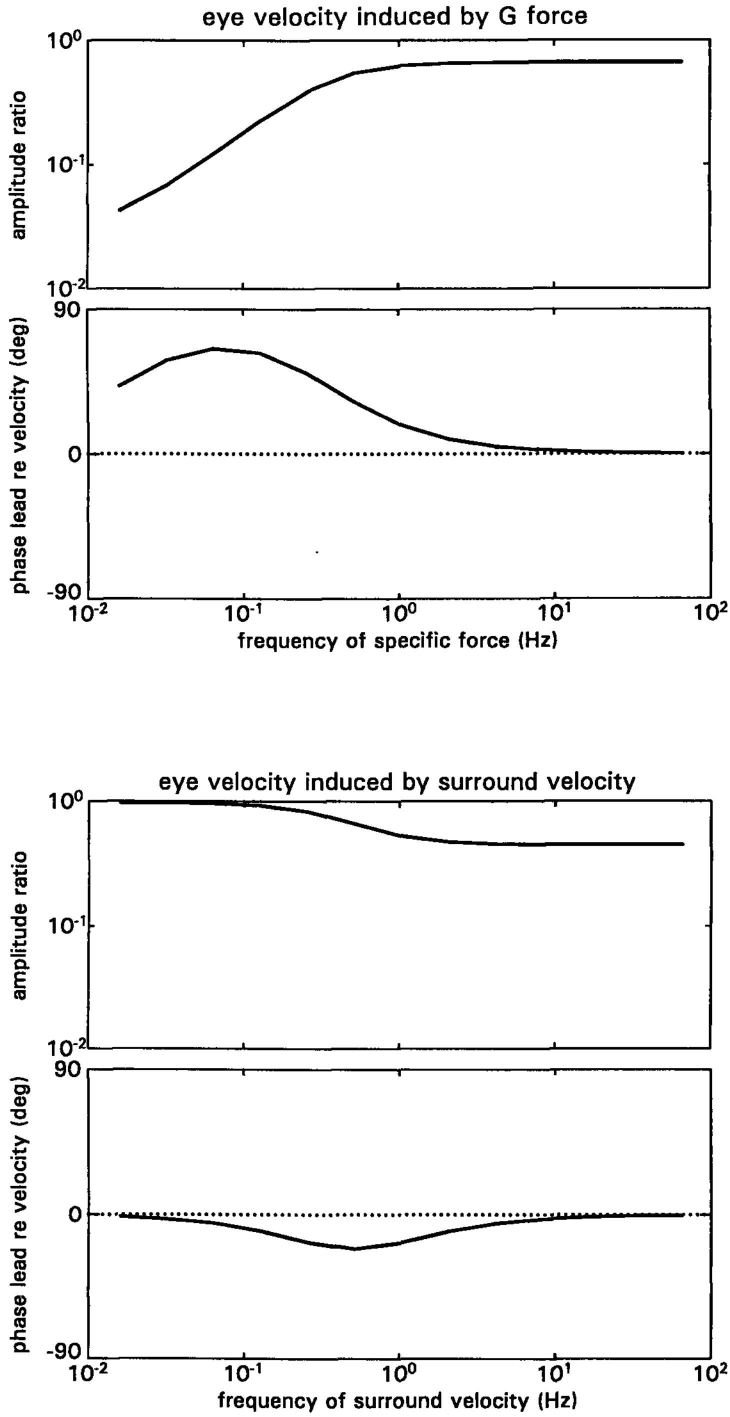

Fig. 6.6 Frequency characteristics of the contributions of G force (upper panel) and surround velocity (lower panel) to eye velocity. These model predictions (with $g_2 = 3.8$) are valid if the velocity storage network is activated, and thus if there is input of surround velocity.

In our linear-model approach, the otolithic and visual-induced eye velocity signals are added. The upper and lower panels of Fig. 6.6 show that both contributions are mutually complementary. In the otolithic contribution, the amplitude ratio increases over frequency, thus compensating for the decrease over frequency for the visual contribution. Similarly, the phase *lead* of the otolith contribution compensates for the phase *lag* of the visual contribution. The result is an optimized eye velocity that keeps the gaze stable with respect to the world, while the head is moving. Thus there is synergy between the otolithic and visual pathways for vertical eye movements during natural head movements (similar to the synergy between semicircular canals and visual pathways; Robinson, 1977).

The relevance of the otolithic contribution becomes manifest when the otolithic function is disturbed in acute peripheral vestibular disorders. The model predictions in Fig. 6.6 show that without otolithic contribution, the compensatory eye velocity becomes insufficient for frequencies above about 1Hz. These patients see the world oscillating, while they are walking (oscillopsia).

***In conclusion:** During walking, the model predicts synergistic action of the otolithic and visual pathways for stabilizing the gaze.*

6.4.2 Oculomotor search in $+G_z$ hypergravity

The same otolith-ocular path, that is useful during walking, will also be activated during sustained hypergravity. Such an implication was demonstrated in a study on oculomotor search during $G_z=3g$ (Wientjes and Marcus, 1991). An experiment had been designed in order to determine whether exposure to a sustained $G_z=3g$ load influences performance in a task involving both visual search and memory search aspects. During $G_z=3g$, easy and difficult versions of a memory comparison task were performed with and without visual search that involved eye movements. Subjects had to rapidly identify a target letter on a screen. Between target presentations the subject fixated a dot in the middle of the monitor; the target position on the monitor was displaced either in the horizontal or in the vertical direction, thus requiring visual search in one of these directions. The results showed that task performance was influenced by $+G_z$ load in one aspect only: During $G_z=3g$ the reaction time was prolonged during *visual search in the vertical direction*, but not during search in the horizontal direction. See Fig. 6.7.

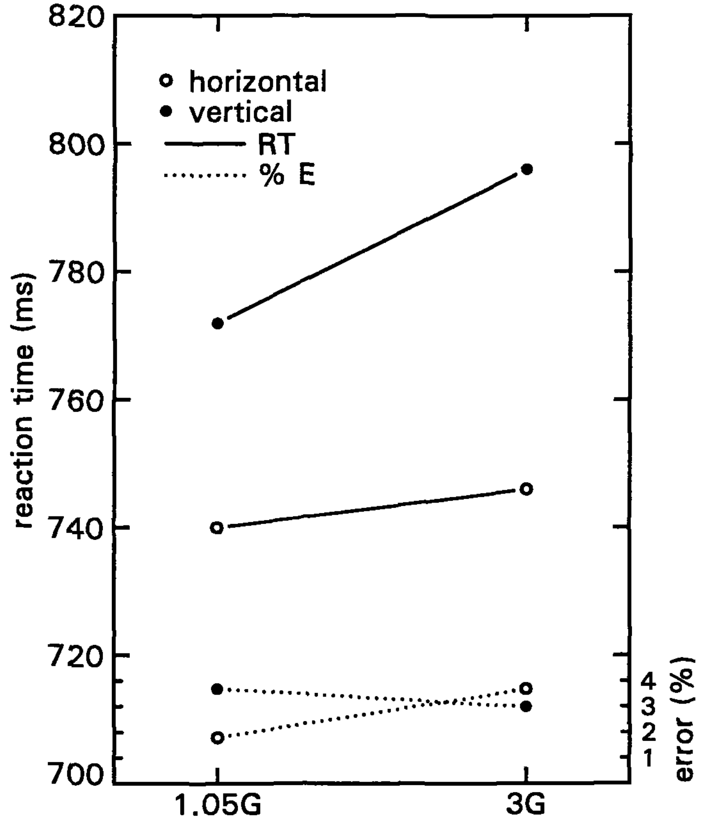

Fig. 6.7 A potential manifestation of the G_z-induced vertical nystagmus on an *oculomotor search task* (Wientjes and Marcus, 1991). During G_z=3g hypergravity, the reaction time is prolonged when vertical eye movements are required for identifying the target. The reaction time is not prolonged when horizontal eye movements are involved.

It seems probable that the vertical vestibular nystagmus, provoked during $+G_z$, interacted with the vertical visual search. Related observations on head-eye coordination during increased $+G_z$ have been reported by Cohen (1970,I; 1970,II).

The above effects were assessed under *sustained* $+G_z$ conditions, while our model predicts that the *transient* effects during G-onset and G-offset are much larger. In terms of our model, the velocity storage integrator is "not fast enough to compensate" for rapid changes in the otolith-induced eye velocity signal, initiated by G-transients.

This could have implications for the visual scanning of instruments in high performance aircraft, in which high G-onset and G-offset rates are frequently encountered. A possible solution would be to arrange the visual information on the instrument panel (or head-up display) by preference in a horizontal orientation. By this arrangement on the display, the number of vertical eye movements that have to be made by the pilot while scanning the display, could be reduced.

***In conclusion:** During increased $+G_z$ force, the reaction time in an oculomotor search task is prolonged when vertical eye movements are involved.*

6.5 Conclusions and recommendations

6.5.1 Conclusions

Experimental results are expressed in the linear VOR (LVOR) in darkness, and in the Slow-Component eye Velocity (SCV) of OptoKinetic Nystagmus (OKN).

A direct otolith-ocular pathway is activated by G forces, and contributes to the SCV. This otolith path is linked with the velocity storage model of Raphan and Cohen. Our integrated model accounts for most of the experimental findings in the centrifuge, on the sled, and in parabolic flight:

1 In the centrifuge, a sustained SCV-down nystagmus is induced in response to increased $+G_z$ force.
2 On the sled, the phase (related to sled velocity) of LVOR-SCV modulation in darkness is -190 deg, and thus about compensatory to sled velocity. This is described by the frequency-response of the tonic otolith cells.
3 With OK stimulation on the sled, the phase lag of OKN-SCV modulation is reduced. This reduction in phase lag is partially explained by the velocity storage mechanism in the visual feedback.
4 In parabolic flight, the observed small OKN-SCV modulation amplitude is consistent with the model, that was constructed on the basis of the sled results.
5 A practical implication is demonstrated by a decrement in vertical oculomotor search performance during increased $+G_z$ force.

6.5.2 Recommendations

We are aware that our model is a simplification. We have assumed that horizontal and vertical eye movement responses are characterized by the same model parameters, but these may be different. Also, our linear model approach is only a starting point for a more complete description of vestibulo-visual interactions in man. From our experiments, several specific questions emerged for future research.

Eye velocity responses to G forces

In the centrifuge, the effect of head position on the G-induced nystagmus may be investigated in more detail. In a future experimental design, the head position in pitch should be varied forward and backward within the *same* subject, thus extending our findings and those of McGrath et al. (1992).

On the sled, the SCV modulation during AI tracking might serve as a technique to quantify the role of proximity cues for the amplitude of modulation. Alternative models, like the pattern centre hypothesis, should be considered. Perhaps some form of pattern retrieval may induce the phase leads (with OK stimulation at 40 $\mathrm{deg} \cdot s^{-1}$ and 60 $\mathrm{deg} \cdot s^{-1}$), that are still unexplained by our model. With non-predictable motion stimuli, the effects of anticipation could be tested.

Non-linear model elements

We have assumed that retinal processing of an OK stimulus is a linear process, but it is almost certainly non-linear. For example, at larger OK stimulus velocities, the perceived pattern tends to "blur", which sometimes leads to a sudden decrease in OKN response. In our data, this results in a lower mean OKN-SCV. Also, retinal processing induces a delay time, and thus larger phase lags than predicted by our model (Fig. 6.6, lower panel) will occur in the visual contribution to eye velocity. In future research, more details of this retinal processing should be taken into account.

Oculomotor search performance during $+G_z$

With regard to the effects of the otolith-ocular reflex in the cockpit of high performance aircraft, the following suggestions may serve as incentives to future research.

Our model indicates that proper choices with respect to the visual environment may help the aviator to minimize unwanted otolith-ocular responses to high $+G_z$ forces:

1 Presenting the visual information in a *horizontal arrangement*, rather than vertical. Thus vertical eye movements are minimized during instrument scanning.

2 *Reducing the proximity cues of visual information*, e.g. by presenting it optically at infinity. This reduction in proximity cues may reduce the amplitude of the otolith-ocular response to G forces.

3 Presenting a stationary reference in the *peripheral visual field*. We have seen in our model that the peripheral pathway (weighted by g_2 in our model) is important for suppression of the G-induced eye velocity response. The model shows that a larger value of the weighting factor g_2 will lead to a rapid decrease in the amplitude of the otolith-induced eye velocity (see Appendix

B3, eq. 5a). Interpreting g_2 as weighting peripheral vision, this means that peripheral vision may be important in the suppression of G-induced eye velocity response. We think of a wide-angle artificial horizon. A similar suggestion was made by Kuipers et al. (1990).

These potential effects of the visual environment are still to be assessed in simulated and in real flight, before any firm conclusions can be drawn.

References

Angelaki, D.E., Anderson, J.H. & Blakley, B.W. (1991). Changes in the dynamics of the vertical vestibulo-ocular reflex due to linear acceleration in the frontal plane of the cat. *Exp. Brain Res.* 86, 27-39.

Baarsma, E.A. & Collewijn H. (1975). Eye movements due to linear acceleration in the rabbit. *J. Physiol. (London)* 245, 227-247.

Baloh, R.W., Honrubia, V., Yee, R.D. & Jacobson, K. (1986). Vertical visual-vestibular interaction in normal human subjects. *Exp. Brain Res.* 64, 400-406.

Baloh, R.W., Beykirch, K., Honrubia, V. & Yee, R.D. (1988). The otolith-ocular reflex in man. *Abstracts of 11th Meeting of the Association for Research in Otolaryngology*. Clearwater Beach, Florida.

Baloh, R.W., Beykirch, K., Honrubia, V. & Yee, R.D. (1988). Eye movements induced by linear acceleration on a parallel swing. *J. Neurophysiol.* 60, 2000-2013.

Baloh, R.W. & Demer, J. (1991). Gravity and the vertical vestibulo-ocular reflex. *Exp. Brain Res.* 83, 427-433.

Barnes, G.R. (1982). A procedure for the analysis of nystagmus and other eye movements. *Aviat. Space Environ. Med.* 53, 676-682.

Benson, A.J. (1974). Modification of the response to angular accelerations by linear accelerations. In H.H. Kornhuber (Ed.), *Handbook of sensory physiology VI, The vestibular system part 2* (pp. 295-305). New York: Springer-Verlag.

Benson, A.J., Spencer, M.B. & Stott, J.R.R. (1986). Thresholds for the detection of the direction of whole-body, linear movement in the horizontal plane. *Aviat. Space Environ. Med.* 57, 1088-1096.

Benson, A.J. (1988). Spatial disorientation-general aspects. In J. Ernsting & P.F. King (Eds), *Aviation Medicine, Chapter 20.* London: Butterworths.

Berthoz, A. & Droulez, J. (1982). Linear self motion perception. In A.H. Wertheim, W.A. Wagenaar & H.W. Leibowitz (Eds), *Tutorials on motion perception* (pp. 157-198). New York: Plenum Press.

Berthoz, A. & Israel, I. (1988). Linear displacement measured by the otoliths can be memorized and reproduced by the saccadic system of man. *J. Physiology* 406, 22P.

Bles, W. & Kapteyn, T.S. (1973). Separate recording of the movements of the human eyes during parallel swing tests. *Acta Otolaryngol.* 75, 6-9.

Bles, W., Van der Heijde, G.L., Kotaka, S. & Reulen, J.P.H. (1985). Some modelling aspects of nystagmus due to somatosensory-visual-vestibular interactions in stepping around. In Igarashi & Black (Eds), *Vestibular and visual control on posture and locomotor equilibrium* (pp. 38-42). 7th Int. Symp. Int. Soc. Posturography, Houston, Texas. Basel: Karger.

Bles, W. & De Graaf, J.E. (1991). Ocular rotation and perception of the horizontal under static tilt conditions in patients without labyrinthine function. *Acta Otolaryngol.* 111, 456-462.

Bos, J.E. & Kistemaker, N. (1991). *Interactive computerprograms for data-acquisition and processing.* Amsterdam: Dep. Medical Physics, Free University.

Boumans, L.J.J.M. (1982). *The human vestibulo-ocular reflex, effects of adaptation* (pp. 98-101), PhD Thesis. Rotterdam: Erasmus University.

Brodal, A. (1981). *Neurological anatomy in relation to clinical medicine.* 3rd edition. New York: Oxford University Press.

Buizza, A., Leger, A., Droulez, J., Berthoz, A. & Schmid, R. (1980). Influence of otolithic stimulation by horizontal linear acceleration on optokinetic nystagmus and visual motion perception. *Exp. Brain Res.* 39, 165-176.

Buizza A., Schmid, R. & Droulez, J. (1981). Influence of linear acceleration on oculomotor control. In Fuchs & Becker (Eds), *Progress in oculomotor research* (pp. 517-524). Amsterdam: Elsevier North Holland, Inc.

Buizza, A. & Schmid, R. (1982). Visual-vestibular interaction in the control of eye movement: mathematical modeling and computer simulation. *Biol. Cybern.* 43, 209-223.

Clemens, A. & Gallé, H. (1976). *The sacculus of rana esculenta*, PhD Thesis. Utrecht: State University.

Clement, G., Vieville, T., Lestienne, F. & Berthoz, A. (1986). Modifications of gain asymmetry and beating field of vertical optokinetic nystagmus in microgravity. *Neurosci. Lett.* 63, 271-274.

Clement, G., Andre-Deshays, C. & Lathan, C.E. (1989). Effects of gravito-inertial force variations on vertical gaze direction during oculomotor reflexes and visual fixation. *Aviat. Space Environ. Med.* 60, 1194-1198.

Clement, G. & Lathan, C.E. (1991). Effects of static tilt about the roll axis on horizontal and vertical optokinetic nystagmus and optokinetic after-nystagmus in humans. *Exp. Brain Res.* 84, 335-341.

Cohen, B., Matsuo V. & Raphan, T. (1977). Quantitative analysis of the velocity characteristics of optokinetic nystagmus and optokinetic afternystagmus. *J. Physiol.* 270, 321-344.

Cohen, M.M. (1970,I). Sensory-motor adaptation and after-effects of exposure to increased gravitational forces. *Aviat. Space Environ. Med.* 41, 318-322.

Cohen, M.M. (1970,II). Hand-eye coordination in altered gravitational fields. *Aviat. Space Environ. Med.* 41, 647-649.

Collewijn, H., Curio, G. & Gruesser, O.J. (1981). Interaction of the vestibulo-ocular reflex and sigma-optokinetic nystagmus in man. In Fuchs & Becker (Eds), *Progress in oculomotor research* (pp. 567-576). Amsterdam: Elsevier North Holland, Inc.

Collewijn, H. (1985). Integration of adaptive changes of the optokinetic reflex, pursuit and the vestibulo-ocular reflex. In A. Berthoz & G. Melvill Jones (Eds), *Adaptive mechanisms in gaze control* (pp. 51-69). Amsterdam: Elsevier Science Publishers.

Collewijn, H. (1986). Fysiologie van oogbewegingen. In: *Neuro-ophthalmologie II, Oogbewegingsstoornissen.* Leiden: Boerhaave cursus, Leiden University.

Collins, W.E. (1974). Arousal and vestibular habituation. In H.H. Kornhuber (Ed.), *Handbook of Sensory Physiology. The Vestibular System, vol. VI, part 2.* New York: Springer-Verlag.

Committee on Hearing, Bioacoustics, and Biomechanics (C.H.A.B.A.), Working group on evaluation of tests for vestibular function (1992). Evaluation of tests for vestibular function. *Aviat. Space Environ. Med.* 63, Supplement p. A4-A23.

Curthoys, I.S. (1987). Eye movements produced by utricular and saccular stimulation. *Aviat. Space Environ. Med.* 58, A192-A197.

Dai, M., Raphan, T. & Cohen, B. (1991). Spatial orientation of the vestibular system: dependence of optokinetic after-nystagmus on gravity. *J. Neurophysiol.* 66, 1422-1439.

De Graaf, J.E. (1990). *Influence of eye movements on visual perception.* Thesis, Utrecht: State University.

De Jong, H.A.A. & Oosterveld, W.J. (1987). Rotation test in the weightless phase of parabolic flight. *Aviat. Space Environ. Med.* 58 (9, Suppl.), A253-A256.

Diamond, S.G. & Markham, C.H. (1983). Ocular counterrolling as an indicator of vestibular otolith function. *Neurology* 33, 1460-1469.

DiZio, P., Lackner, J.R. & Evanoff, J.N. (1987). The influence of gravito-inertial force level on oculomotor and perceptual responses to Coriolis, cross coupling stimulation. *Aviat. Space Environ. Med.* 58 (9, Suppl.), A218-A223.

DiZio, P. & Lackner, J.R. (1992). Influence of gravitoinertial force level on vestibular and visual velocity storage in yaw and pitch. *Vision Res.* 32, 111-120.

Fernandez, C. & Goldberg, J.M. (1976,I). Physiology of peripheral neurons innervating otolith organs of the squirrel monkey. I. Response to static tilts and to long-duration centrifugal force. *J. Neurophysiol.* 39, 970-985.

Fernandez, C. & Goldberg, J.M. (1976,II). Physiology of peripheral neurons innervating otolith organs of the squirrel monkey. II. Direction selectivity and force-response relations. *J. Neurophysiol.* 39, 985-995.

Fernandez, C. & Goldberg, J.M. (1976,III). Physiology of peripheral neurons innervating otolith organs of the squirrel monkey. III. Response dynamics. *J. Neurophysiol.* 39, 996-1008.

Fluur, E. (1970). The interaction between the utricle and the saccule. *Acta Otolaryngol. (Stockholm)* 69, 17-24.

Fluur, E. & Mellstrom, A. (1970a). Utricular stimulation and oculomotor reactions. *Laryngoscope (St. Louis)* 80, 1701-1712.

Fluur, E. & Mellstrom, A. (1970b). Saccular stimulation and oculomotor reactions. *Laryngoscope (St. Louis)* 80, 1713-1721.

Fluur, E. & Mellstrom, A. (1971). The otolith organs and their influence on oculomotor movements. *Experimental Neurology* 30, 139-147.

Fukushima, K. & Fukushima J. (1991). Otolith-visual interaction in the control of eye movement produced by sinusoidal vertical linear acceleration in alert cats. *Exp. Brain Res.* 85, 36-44.

Fulgham, D.D. & Gillingham, K.K. (1989). Inflight assessment of motion sensation thresholds and disorienting maneuvers. AsMA Annual Meeting, paper nr. 44, Washington, May 1989. Abstract in: *Aviat. Space Environ. Med.* 60, 484.

Gernandt B.E. (1970). Nystagmus evoked by utricular stimulation. *Experimental Neurology* 27, 90-100.

Gillingham, K.K. & Wolfe, J.W. (1986). *Spatial orientation in flight.* Report TR-85-31, Brooks Air Force Base, TX: USAF School of Aerospace Medicine.

Gizzi, M.S., Rudolph, S.H., Cohen, B. & Raphan, T. (1991). Gravitational influences on human optokinetic nystagmus. *Investigative Ophthalmology & Visual Science* 32(4), 895.

Goldberg, J.M. (1991). The vestibular end organs: morphological and physiological diversity of afferents. *Current Opinion in Neurobiology* 1, 229-235.

Grant, W. & Best, W. (1987). Otolith-organ mechanics: lumped parameter model and dynamic response. *Aviat. Space Environ. Med.* 58, 970-976.

Grant, J.W. & Cotton J.R. (1991). A model for otolith dynamic response with a visco-elastic gel layer. *J. Vestib. Res.* 1, 139-151.

Guedry, F.E. (1974). Psychophysics of vestibular sensation. In H.H. Kornhuber (Ed.), *Handbook of Sensory Physiology VI, The vestibular system part 2.* New York: Springer-Verlag.

Hardy, M. (1934). Observations on the innervation of the macula sacculi in man. *Anat. Rec.* 59, 403-78.

Hixson, W.C., Niven, J.I. & Correia, M.J. (1966). *Kinematics nomenclature for physiological accelerations: with special reference to vestibular applications.* Monograph 14, Pensacola, FL: Naval Aerospace Medical Institute.

Hosman, R.J.A.W. & Van der Vaart, J.C. (1978). *Vestibular models and thresholds of motion perception. Results of tests in a flight simulator.* Report LR-265, Delft: University of Technology.

Igarashi, M., Takahashi, M., Kubo, T., Alford, B.R. & Wright, W.K. (1980). Effect of off-vertical tilt and macular ablation on postrotatory nystagmus in the squirrel monkey. *Acta Otolaryngol.* 90, 93-99.

Jongkees, L.B.W. & Phillipszoon, A.T. (1962). Nystagmus provoked by linear accelerations. *Acta Physiol. Pharmacol Neerl.* 10, 238-247.

Kelly, J.P. (1981). Vestibular system. In E.R. Kandel & J.H. Schwartz (Eds), *Principles of neural science* (pp. 406-418). New York: Elsevier.

Kostelijk, T. (1982). *The Raphan-Cohen model.* Amsterdam: Dep. of Medical Physics, Free University.

Kuipers, A., Kappers, A., Van Holten, C.R., Van Bergen, J.H.W. & Oosterveld, W.J. (1990). Spatial disorientation incidents in the RNLAF F-16 and F-5 aircraft and suggestions for prevention. *AGARD Conference Proceedings* No. 478.

Lafortune, S.H., Ireland, D.J. & Jell, R.M. (1991). Suppression of optokinetic velocity storage in humans by static tilt in roll. *J. Vestib. Res.* 1, 347-355.

Lansberg, M.P., Guedry, F.E. & Graybiel, A. (1965). The effect of changing the resultant linear acceleration relative to the subject on nystagmus generated by angular acceleration. *Aerospace Medicine* 36, 456-460.

Malcolm, R. & Melvill Jones, G. (1970). A quantitative study of vestibular adaptation in humans. *Acta Otolaryngol. (Stockholm)* 70, 126-135.

Marcus, J.T., Bles, W. & Van Holten, C.R. (1989). Influence of gravitoinertial force on vestibular nystagmus in man, observed in a centrifuge. *Advances in Space Research* 9(11), 213-222.

Marcus, J.T. & Van Holten, C.R. (1990). Vestibulo-ocular responses in man to $+G_z$ hypergravity. *Aviat. Space Environ. Med.* 61, 631-635.

Matsuo, V. & Cohen, B. (1984). Vertical optokinetic nystagmus and vestibular nystagmus in the monkey: up-down asymmetry and effects of gravity. *Exp. Brain Res.* 53, 197-216.

Mayne, R. (1974). A systems concept of the vestibular organs. In H.H. Kornhuber (Ed.), *Handbook of Sensory Physiology VI, The vestibular system part 2* (pp. 493-580). New York: Springer-Verlag.

McGrath, B.J. (1990). *Human vestibular response during 3Gz centrifuge stimulation,* MSc Thesis: Cambridge, MA: MIT.

McGrath, B.J., Rupert, A.H., Ries, J.E. & Guedry, F.E. (1992). The effect of head position on L_z nystagmus during $3G_z$ centrifuge stimulation. *Aviat. Space Environ. Med.* 63, 443.

Meerman Automation (1988). *Tutsim, a program for engineering design and optimation, by simulation of continuous dynamic systems, Version 6.55.* Neede (NL): Meerman Automation.

Murasugi, C.M. & Howard, I.P. (1989). Up-down asymmetry in human vertical optokinetic nystagmus and afternystagmus: contributions of the central and peripheral retinae. *Exp. Brain Res.* 77, 183-192.

Niven, J.I., Whiteside, T.C.D. & Graybiel, L.A. (1963). *The elevator illusion.* Report No 89, Pensacola, FL: Bureau of Medicine and Surgery, US Naval Aviation Medical Center.

Niven, S.I., Hixson, C.E. & Correia, M.J. (1966). Elicitation of horizontal nystagmus by periodical acceleration. *Acta Otolaryngol.* 62, 429-441.

Norusis, M.J. (1990). SPSS/PC+ Advanced Statistics 4.0, p. B63-B108. Chicago: SPSS Inc.

Oosterveld, W.J. (1970). The parallel swing. *Arch. Oto-laryng.* 91, 154.

Paige, G.D. & Tomko, D.L. (1991). Eye movement responses to linear head motion in the squirrel monkey. II. Visual-vestibular interactions and kinematic considerations. *J. Neurophysiol.* 65, 1183-1196.

Pavard, B. & Berthoz, A. (1977). Linear acceleration modifies the perceived velocity of a moving visual scene. *Perception* 6, 529-540.

Ranalli, P.J. & Sharpe, J.A. (1988). The vertical vestibulo-ocular reflex. In H.O. Barber & J.A. Sharpe (Eds), *Vestibular disorders* (pp. 159-1880. Chicago, IL: Year Book Medical Publishers.

Raphan, Th., Cohen, B. & Matsuo, V. (1977). A velocity-storage mechanism responsible for optokinetic nystagmus (OKN), optokinetic afternystagmus (OKAN) and vestibular nystagmus. In Baker & Berthoz (Eds), *Control of gaze by brain stem neurons, Developments in Neuroscience, Vol. 1.* Amsterdam, NL: Elsevier/North-Holland Biomedical Press.

Raphan, T., Matsuo, V. & Cohen, B. (1979). Velocity storage in the vestibulo-ocular reflex arc. *Exp. Brain Res.* 35, 229-248.

Raphan, T. & Cohen, B. (1988). Organizational principles of velocity storage in three dimensions: the effect of gravity on cross-coupling of optokinetic after-nystagmus. *Ann NY Acad Sci* 545, 74-92.

Raphan, T. & Schnabolk C. (1988). Modelling slow phase velocity generation during off-vertical axis rotation. In: Representation of three-dimensional space in the vestibular, oculomotor, and visual systems. *Ann NY Acad Sci* 545, 29-50.

Raphan, T. & Sturm, D. (1991). Modeling spatiotemporal organization of velocity storage in the vestibulo-ocular reflex by optokinetic studies. *J. Neurophysiol.* 66, 1410-1421.

Robinson, D.A. (1977). Linear addition of optokinetic and vestibular signals in the vestibular nucleus. *Exp. Brain Res.* 30, 447-450.

Schwarz, U., Busettini, C. & Miles, F.A. (1989). Ocular responses to linear motion are inversely proportional to viewing distance. *Science* 245, 1394-1396.

Schwarz, U. & Miles, F.A. (1991). Ocular responses to translation and their dependence on viewing distance. I. Motion of the observer. *J. Neurophysiol.* 66, 851-863.

Shelhamer, M.J. (1990). *Linear acceleration and horizontal eye movements in man*, PhD Thesis. Cambridge, MA: MIT.

Shelhamer, M.J. & Young, L.R. (1991). Linear acceleration and horizontal eye movements in man. *Acta Otolaryngol. (Stockh) Suppl.* 481, 277-281.

Skalar Medical (1991). *Data analysis software "blik".* Delft: Skalar Medical BV.

Van den Berg, A.V. & Collewijn, H. (1988). Directional asymmetries of human optokinetic nystagmus. *Exp. Brain Res.* 70, 597-604.

Van Die, G.C. (1983). *Stimulus-respons relaties van de optokinetische nystagmus van de mens*, PhD Thesis. Rotterdam: Erasmus University.

Waespe, W. & Henn, V. (1977). Neuronal activity in the vestibular nuclei of the alert monkey during vestibular and optokinetic stimulation. *Exp. Brain Res.* 27, 523-538.

Wertheim, A.H. (1990). Visual, vestibular, and oculomotor interactions in the perception of object motion during egomotion. In R. Warren & A. Wertheim (Eds), *Perception and control of self-motion.* Hillsdale, NJ: Lawrence Erlbaum.

Whiteside, T.C.D., Graybiel, L.A. & Niven, J.I. (1965). Visual illusions of movement. *Brain* 88, 193-210.

Wientjes, C.J.E. & Marcus, J.T. (1991). *Situational awareness and vestibular stimulation (II): Influence of* $+G_z$ *load upon visual and memory search.* Report 1991 A-22, Soesterberg: TNO Institute for Perception.

Winer, B.J. (1962). *Statistical principles in experimental design* (pp. 80-85), New York: McGraw-Hill.

Winer, B.J., Brown, D.R. & Michels, K.M. (1991). *Statistical principles in experimental design*, 3rd edition (pp. 172-182), New York: McGraw-Hill.

Xerri, C., Barthelemy, J., Harlay, F., Borel, L. & Lacour, M. (1987). Neuronal coding of linear motion in the vestibular nuclei of the alert cat. *Exp. Brain Res.* 65, 569-581.

Yasui, S. & Young, L.R. (1975). Perceived visual motion as effective stimulus to pursuit eye movement system. *Science* 190, 906-908.

Young, L.R. (1967). *Effects of linear acceleration on vestibular nystagmus.* Proc. 3rd symposium on the role of the vestibular organs in space exploration. Report SP-152, Pensacola, FL: NASA.

Young, L.R. & Meiry, J.L. (1967). *A revised dynamic otolith model.* Proc. 3rd Symposium on the role of the vestibular organs in space exploration. Report SP-152, Pensacola, FL: NASA.

Young, L.R. & Meiry, J.L. (1968). A revised dynamic otolith model. *Aerospace Medicine* 39, 606-608.

Zee, D.S. (1988). New concepts of vestibular nystagmus. In H.O. Barber & J.A. Sharpe (Eds), *Vestibular disorders* (pp. 189-200). Chicago, IL: Year Book Medical Publishers.

Summary

Vestibulo-ocular responses in man to gravito-inertial forces

J.T. Marcus

Gravito-inertial (G) forces are sensed by the otolithic system, which transmits the information of sensed forces to nerve centres that control eye movements. This thesis starts with the new observation of a sustained vertical nystagmus with a downward slow-component, induced by otolithic stimulation during a G force of 3g in a centrifuge. Our line of investigation was directed by the following questions:

1 What is the relation between the G force input, and the otolith-induced eye velocity response? We identify this relation in different force environments: the centrifuge, parabolic flight, and a linear acceleration track. The dependent variables are the eye movements of purely vestibular origin, and the otolith-induced modulation of optokinetic nystagmus.
2 Can we describe the otolith-induced eye velocity responses in the various experimental conditions in one model?

The current literature was reviewed in Chapter 1, with regard to otolith physiology and otolith-ocular reflexes. The otolithic system was approached in two different ways: basic physiology and black box analysis. Evidence for otolith-induced eye movements was provided. Current models predict that otolith responses have a dynamic range up to at least 5g.

A comparative description of our experimental conditions was given in Chapter 2, showing how these conditions are complementing each other with regard to the motion stimulus. In the centrifuge $G=3g$, but the gravito-inertial force is necessarily coupled with initial angular acceleration during force onset. In parabolic flight there is no confounding angular acceleration stimulating the semicircular canals, but the G profile has a lower amplitude. On the linear track the G profile is even lower. However, the sinusoidal acceleration on the track yields both amplitude and phase of the response, which is basic information for the construction of our model.

In the **centrifuge** experiment (Chapter 3), we have resolved the problem of confounding semicircular canal stimulation by measuring responses with the subjects facing forward, and facing backward. Thus the canals were stimulated in opposite directions, while the otolith stimulus was the same. The pure otolith responses were obtained by adding the "forward" and "backward" responses, under the assumption of linear superposition. No sustained response was measured during G=2g.

In **parabolic flight** (Chapter 4) we stimulated only the otolithic system, and not the semicircular canals, because the angular acceleration was minimized. However, the G-level did not exceed G=1.8g, and at this level an otolith-induced nystagmus in darkness was not expected. Therefore we applied vertical optokinetic stimulation throughout the parabolic manoeuvre, and measured the otolith effect as expressed in the G-induced modulation of optokinetic eye velocity. Otolith-induced modulation was found indeed, but the amplitude was much smaller than expected from current literature, based mainly on experiments in which linear acceleration tracks are used. This was our incentive to investigate the otolith-induced modulation of eye velocity in more detail using a linear track.

On the **linear track** (Chapter 5) we applied a sinusoidal acceleration along the subject's lateral axis, and measured the modulation of eye velocity in darkness, as well as with optokinetic stimulation. In darkness, the observed phase of modulation was consistent with an eye velocity compensatory to subject velocity. With optokinetic stimulation, the amplitude of otolith-induced modulation was strongly dependent on the optokinetic stimulus settings. The phase of modulation was leading with respect to the phase of modulation in darkness. Since the otolith stimulus was identical in all conditions, the visual pathways were held responsible for this phase lead.

In an integrated model (Chapter 6) we tried to explain both the vestibular and optokinetic contributions to eye velocity, using the current concept of velocity storage. This concept implies that angular velocity information is integrated or "stored" in the vestibular nuclei. We extended this model by including a direct otolith pathway involved in eye velocity control. This pathway was suggested by the results of the centrifuge experiment. By systems analysis, we showed that the otolith contribution to eye velocity is modified by the parameters of velocity storage, whenever there also is visual input. The extended model largely explained the phase lead of eye velocity observed on the linear track. The same model also explained the relatively low vestibular modulation of optokinetically induced eye velocity observed in parabolic flight.

In physiological conditions like walking, the model shows that the otolith pathway functions in synergy with the visual system to stabilize the gaze. During hypergravity, however, the same otolith pathway may interfere with vertical oculomotor search. This model prediction was verified in an additional centrifuge experiment.

Samenvatting

Vestibulo-oculaire responsies bij de mens geïnduceerd door traagheidskrachten en de zwaartekracht

J.T. Marcus

De resultante van een traagheidskracht en de zwaartekracht, de "G-kracht", wordt gedetecteerd door het otolietensysteem. Dit systeem geeft de informatie vervolgens door aan zenuwcentra die de oogbewegingen sturen. Het onderzoek van dit proefschrift vond zijn oorsprong in de waarneming van een blijvende verticale nystagmus met een langzame slag naar beneden, geïnduceerd door otoliet-stimulatie met een G-kracht van 3g in een centrifuge. Na deze waarneming werd onze onderzoekslijn bepaald door de volgende vragen:

1 Wat is de relatie tussen de G-kracht, en de otoliet-geïnduceerde oogsnelheids-responsie? Wij onderzochten deze relatie in verschillende G-condities: in de centrifuge, in paraboolvlucht, en op een lineaire versnellingsbaan. De afhankelijke variabelen zijn de oogbewegingen van zuiver vestibulaire oorsprong, en de otoliet-geïnduceerde modulatie van de optokinetische nystagmus.

2 Kunnen wij de otoliet-geïnduceerde oogsnelheids-responsies in de diverse experimentele condities beschrijven met één model?

In hoofdstuk 1 werd een overzicht gegeven van de bestaande literatuur over de fysiologie van de otolieten en de otoliet-oculaire reflexen. De functie van de otolieten werd benaderd vanuit twee verschillende invalshoeken: de basale fysiologie en een systeem-analytische methode. Voor het bestaan van otoliet-geïnduceerde oogbewegingen werd bewijsmateriaal geleverd. De bestaande modellen voorspellen dat de otolietresponsies een dynamisch bereik hebben over een stimulusbereik tot tenminste 5g.

Een vergelijkende beschrijving van onze experimentele condities werd gegeven in hoofdstuk 2, waarmee werd aangetoond hoe deze condities elkaar onderling aanvullen met betrekking tot de bewegingsstimulus. In de centrifuge bedraagt de G-waarde 3g, maar er is noodzakelijkerwijs een hoekversnelling gekoppeld aan de opbouw-fase van de G-kracht. Deze hoekversnelling leidt tot responsies van de halfcirkelvormige kanalen, die interfereren met de otolietresponsies. In paraboolvlucht is er geen hoekversnelling, maar het G-profiel heeft een lagere amplitude. Op de lineaire versnellingsbaan is het G-profiel nog lager; de sinusoïdale versnelling op deze baan levert echter een responsie op met zowel amplitude als fase, welke fundamentele informatie verschaffen voor de opbouw van ons model.

In het **centrifuge** experiment (hoofdstuk 3) hebben wij het probleem van de interfererende kanalen-stimulatie opgelost, door responsies te meten bij dezelfde proefpersonen in twee verschillende condities: vooruit (in de draairichting) kijkend, en achteruit kijkend. In deze beide condities werden de halfcirkelvormige kanalen gestimuleerd in tegengestelde richtingen, terwijl de otolietstimulatie in beide condities dezelfde was. De pure otoliet-responsie werd verkregen door de "vooruit" en "achteruit" responsies op te tellen, daarbij aannemend dat otoliet- en kanaalresponsies lineair gesuperponeerd zijn. Terwijl bij een G-kracht van 3g nog wel een blijvende nystagmus-responsie werd gemeten, werd bij 2g géén blijvende responsie meer gemeten.

In **paraboolvlucht** (hoofdstuk 4) stimuleerden wij alleen het otolieten systeem, en niet de halfcirkelvormige kanalen, omdat de hoekversnelling tot een minimum was teruggebracht. De waarde van de G-kracht was echter niet hoger dan 1.8g, en op basis van het voorgaande experiment werd bij dit niveau een otoliet-geïnduceerde nystagmus in duisternis niet verwacht. Derhalve werd verticale optokinetische stimulatie toegepast tijdens de complete parabolische manoeuvre, en het otoliet-effect werd bepaald door de modulatie te meten die door het G-profiel werd geïnduceerd in de snelheid van de optokinetisch opgewekte oogbeweging. Deze modulatie werd inderdaad gevonden, maar de amplitude ervan was aanzienlijk geringer dan verwacht op grond van de bestaande literatuur, die vooral gebaseerd is op metingen op lineaire versnellingsbanen. Dit vormde voor ons de aanzet om de otoliet-geïnduceerde modulatie van de oogsnelheid in meer detail te onderzoeken, gebruikmakend van een lineaire versnellingsbaan.

Op de **lineaire versnellingsbaan** (hoofdstuk 5) hebben wij een sinusvormige versnelling toegepast in de zij-richting (links-rechts) van de proefpersoon. De modulatie van de oogsnelheid werd gemeten zowel in duisternis, als met gelijktijdige optokinetische stimulatie. In duisternis was de fase van de modulatie consistent met een oogsnelheid die compensatoir is voor de snelheid van de proefpersoon. Met optokinetische stimulatie was de amplitude van de otoliet-geïnduceerde modulatie sterk afhankelijk van de condities van optokinetische stimulatie. De fase van de modulatie had een voorsprong ten opzichte van de fase van de modulatie gevonden in duisternis. Omdat de otoliet-stimulatie identiek was in alle condities, werd het visuele systeem verantwoordelijk gehouden voor deze fase-voorsprong.

In een geïntegreerd model (hoofdstuk 6) hebben wij getracht om zowel de vestibulaire als de optokinetische bijdragen aan de oogsnelheid te verklaren, uitgaande van het bestaande concept van "velocity storage". Dit concept houdt in dat hoeksnelheidsinformatie wordt geïntegreerd of "opgeslagen" in de vestibulaire zenuwkernen. Wij hebben dit model uitgebreid met een directe sturing van de oogsnelheid vanaf de otolieten. Het bestaan van een dergelijke sturing werd gesuggereerd door de resultaten van het centrifuge experiment. Met behulp van systeemanalyse werd aangetoond dat de bijdrage van de otolieten aan de oogsnelheid wordt gemodificeerd door het velocity storage mechanisme, steeds wanneer er gelijktijdige visuele stimulatie is. Dit uitgebreide model verklaarde grotendeels de fase-voorsprong van de oogsnelheid, die bij gelijktijdige visuele stimulatie was waargenomen op de lineaire versnellingsbaan. Hetzelfde model verklaarde ook de relatief lage vestibulaire modulatie van de visueel opgewekte oogbeweging, die was gemeten in paraboolvlucht.

vergroot

In fysiologische condities zoals lopen, geeft het model aan dat de verbinding tussen de otolieten en de sturing van de ogen functioneel is. Er ontstaat synergie met het visuele systeem, in de zin dat de blikrichting van de ogen wordt gestabiliseerd. Tijdens verhoogde G-krachten kan echter dezelfde otolietensturing interfereren met een visuele zoektaak waarbij verticale oogbewegingen moeten worden gemaakt. Deze predictie van het model werd geverifieerd in een toegevoegd centrifuge experiment.

Appendix A

Frequency response of tonic otolith cells

The transfer function $H_{tonic}(s)$ of the tonic otolith cells has been derived in the introductory chapter:

$$H_{tonic}(s) = \frac{1}{(1+T_1 \cdot s) \cdot (1+T_2 \cdot s)}$$

with $T_1 = 10$ sec and $T_2 = 0.0002$ sec.
For sinusoidal input, and in steady state, s may be replaced by the complex frequency $j\omega$. The frequency response is then given by:

$$\text{Amplitude ratio } (\omega) = \frac{1}{\sqrt{1+(T_1 \cdot \omega)^2} \cdot \sqrt{1+(T_2 \cdot \omega)^2}}$$

$$\text{Phase } (\omega) = -\arctan(T_1 \cdot \omega) - \arctan(T_2 \cdot \omega)$$

At the sled frequency, $\omega_{sled} = 1.1 \text{ rad} \cdot \text{sec}^{-1}$, the phase (referred to specific force G) is -85 deg. The tonic otolith cells are then responding about in phase with sled velocity, rather than with specific force. Because the otolith-ocular response is compensatory, it means that the phase of the otolith-ocular velocity signal $V_{otolith}$ is -175 deg, referred to sled velocity.

In our sled experiment, the averaged phase of eye velocity in darkness (-190 deg) was not significantly different from -175 deg. In darkness, we consider the observed V_{eye} as being identical to $V_{otolith}$. Thus, the model of the tonic otolith cells adequately describes the phase of the otolith-induced velocity signal.

***In conclusion:** In our model description of the sled experiment, we assume that the phase of $V_{otolith}$, referred to sled velocity, is -175 deg.*

Appendix B

Calculation of otolith output

Outline of the calculation procedure

The aim of this appendix is to calculate the velocity signal induced by the otoliths, to be indicated as $V_{otolith}$. In the extended velocity storage model, the contribution of $V_{otolith}$ to the observed eye velocity V_{eye} is modified by the velocity storage network. This means that $V_{otolith}$ cannot be directly derived from V_{eye} when there is optokinetic stimulation. The parameters in the velocity storage network must then be determined first.

We are able to perform these calculations on the basis of the observed modulation of V_{eye} on the sled. We assume that the *phase* of $V_{otolith}$ is determined by the tonic otolith-cell model (Appendix A), and thus amounts to -175 deg (referred to sled velocity). The *amplitude* of $V_{otolith}$ is not yet known from the otolith cell model, because the gain factor due to "proximity cues" is unknown. We calculate the g_2 weighting factor of the velocity storage circuit, and subsequently deduce the amplitude of $V_{otolith}$.

Finally, we also calculate the transfer function from surround velocity $V_{surround}$ to V_{eye}. The model is now completely determined on the basis of the sled experiment. This will allow us to check whether the same model structure and parameters, as determined on the sled, are also consistent with our findings in parabolic flight.

B1 Definition of symbols and notations in the model

Symbol	*Unit*	*Definition*
G	g	specific force
ω	$\mathrm{rad \cdot sec^{-1}}$	angular frequency (= 2π times frequency)
ω_{sled}	$\mathrm{rad \cdot sec^{-1}}$	angular frequency of sled movement
V_{eye}	$\mathrm{deg \cdot sec^{-1}}$	slow-component eye velocity response
g_1		gain factor of the direct visual pathway
g_2	$\mathrm{sec^{-1}}$	gain factor of the velocity storage pathway
h	$\mathrm{sec^{-1}}$	feedback factor of velocity storage integrator
s		Laplace variable
H_{storage}		transfer function of the combination of the direct and storage pathways
V_{otolith}	$\mathrm{deg \cdot sec^{-1}}$	velocity signal induced by otoliths
$V_{\mathrm{eye,otolith}}$	$\mathrm{deg \cdot sec^{-1}}$	contribution of V_{otolith} to V_{eye}
$H_{\mathrm{storage,otolith}}$		transfer function from V_{otolith} to $V_{\mathrm{eye,otolith}}$
$K_{\mathrm{storage,otolith}}$		constant gain element in $H_{\mathrm{storage,otolith}}$
$T_{\mathrm{d,o}}$	sec	differentiating time constant in $H_{\mathrm{storage,otolith}}$
$T_{\mathrm{i,o}}$	sec	integrating time constant in $H_{\mathrm{storage,otolith}}$
ϕ_{Veye}	deg	phase of modulation of $V_{\mathrm{eye,otolith}}$ referred to the phase of modulation of V_{otolith}
V_{surround}	$\mathrm{deg \cdot sec^{-1}}$	surround velocity (= OK stimulus velocity)
$V_{\mathrm{eye,surround}}$	$\mathrm{deg \cdot sec^{-1}}$	contribution of V_{surround} to V_{eye}
$H_{\mathrm{storage,surround}}$		transfer function from V_{surround} to $V_{\mathrm{eye,surround}}$
$K_{\mathrm{storage,surround}}$		constant gain element in $H_{\mathrm{storage,surround}}$
$T_{\mathrm{d,s}}$	sec	differentiating time constant in $H_{\mathrm{storage,surround}}$
$T_{\mathrm{i,s}}$	sec	integrating time constant in $H_{\mathrm{storage,surround}}$

B2 Rewriting the extended model as a control system

In Fig. A, upper part, the velocity storage model is shown extended with a direct otolith path. The output eye velocity V_{eye} will be written as a superposition of contributions of the otolith-induced velocity signal $V_{otolith}$, and the surround velocity $V_{surround}$. We begin with rewriting the transfer function $H_{storage}$ of the direct and indirect visual pathways as follows:

$$H_{storage} = \frac{g_2}{h + s} + g_1$$

$$H_{storage} = \frac{g_2 + g_1 \cdot (h+s)}{h + s} \qquad (1)$$

The final summation in the model (Fig. A, middle part) can now be written as:

$$V_{eye} = V_{otolith} + H_{storage} \cdot (V_{surround} - V_{eye})$$

Solving of V_{eye} yields:

$$(1 + H_{storage}) \cdot V_{eye} = V_{otolith} + H_{storage} \cdot V_{surround}$$

$$V_{eye} = \frac{1}{1 + H_{storage}} \cdot V_{otolith} + \frac{H_{storage}}{1 + H_{storage}} \cdot V_{surround} \qquad (2)$$

The lower part of Fig. A is the graphical presentation of equation (2). Applying the notations for transfer functions, as defined in section B1, yields:

$$H_{storage,otolith} = \frac{1}{1 + H_{storage}} \qquad (3)$$

$$H_{storage,surround} = \frac{H_{storage}}{1 + H_{storage}} \qquad (4)$$

B3 Expression of the transfer function $H_{storage,otolith}$ in g_1, g_2 and h

The transfer function $H_{storage,otolith}(s)$ has been defined by:

$$V_{eye,otolith} = H_{storage,otolith} \cdot V_{otolith}$$

The calculation of this transfer function proceeds as follows: Substitute eq. (1) into eq. (3), and write $H_{storage,otolith}$ in terms of time constants:

$$H_{storage,otolith} = K_{storage,otolith} \cdot \frac{(1 + T_{d,o} \cdot s)}{(1 + T_{i,o} \cdot s)} \qquad (5)$$

$$K_{storage,otolith} = \frac{h}{h + g_2 + h \cdot g_1} \qquad (5a)$$

$$T_{d,o} = \frac{1}{h}$$

$$T_{i,o} = \frac{1 + g_1}{h + g_2 + h \cdot g_1}$$

The expression (5a) for $K_{storage,otolith}$ shows that this factor can be reduced more effectively by increasing g_2, than by increasing g_1 (h is about 0.1). This is referenced in the "practical application" section of chapter 6, where $V_{eye,otolith}$ is regarded as a "disturbing signal".

For the calculation of responses to a sinusoidal input, s can be replaced by the complex frequency jω (disregarding here the transient response after onset of the sinusoidal input). The frequency response can then be derived from equation (5). We recall that ϕ_{Veye} is defined as the phase of modulation of $V_{eye,otolith}$ referred to the phase of modulation of $V_{otolith}$; thus ϕ_{Veye} is the phase shift induced by $H_{storage,otolith}$.

$$\text{Amplitude ratio } (\omega) = K_{storage,otolith} \cdot \frac{\sqrt{1 + (T_{d,o} \cdot \omega)^2}}{\sqrt{1 + (T_{i,o} \cdot \omega)^2}} \qquad (6)$$

$$\phi_{Veye}(\omega) = \arctan(T_{d,o} \cdot \omega) - \arctan(T_{i,o} \cdot \omega) \qquad (7)$$

B4 Calculation of g_2 from the observed phase of eye velocity modulation

The calculation of parameters in the velocity storage model proceeds as follows. Equation (7) helps us to determine the factor g_2, based on the observed value of ϕ_{Veye}. We start with the following assumptions:

(a) The phase of modulation of $V_{otolith}$ is -175 deg (this has been derived in Appendix A).

(b) The parameters h and g_1 in velocity storage are chosen as fixed: $h = 0.1$ and $g_1 = 0.8$ (estimated, from Kostelijk, 1982).

Substitution of the expressions for $T_{d,o}$ and $T_{i,o}$ in (7) yields:

$$\phi_{Veye} = \arctan(\omega/h) - \arctan\left[\frac{\omega \cdot (g_1+1)}{h + g_2 + g_1 \cdot h}\right]$$

This expression shows that the maximum value of ϕ_{Veye} on the sled, that can be predicted by the model, is smaller than $\arctan(\omega_{sled}/h) = 85$ deg (h, g_1 and g_2 are positive numbers). We rewrite the above expression so that g_2 is an expression of ω_{sled}, h, g_1 and ϕ_{Veye}:

$$\tan[\arctan(\omega/h) - \phi_{Veye}] = \frac{\omega \cdot (g_1 + 1)}{h + g_2 + g_1 \cdot h}$$

$$g_2 = \frac{\omega \cdot (g_1 + 1)}{\tan[\arctan(\omega/h) - \phi_{Veye}]} - h - g_1 \cdot h \qquad (8)$$

By equation (8), g_2 is calculated from the value of $\omega_{sled} = 1.1 \text{ rad} \cdot \text{sec}^{-1}$, the assumed values of h and g_1, and the observed value of ϕ_{Veye}.

For the binocular OK stimulus with 80 deg $\cdot$ s^{-1}, the observed phase of modulation of V_{eye} referred to sled velocity is -117 deg. Thus, ϕ_{Veye} (which is the phase of modulation referred to $V_{otolith}$) is -117 deg-(-175 deg)=+58 deg. Equation (8) then yields $g_2=3.8$.

Effect of fixed-parameter values

About the choices of the fixed parameters h and g_1 we can make some remarks. We should check whether the functioning of the model is critically dependent on the exact values of these parameters.

The parameter h determines the frequency characteristic of velocity storage: The velocity storage circuit can be regarded as a low-pass filter with lower corner frequency $\omega_{corner} = h \text{ rad} \cdot \text{sec}^{-1}$. As long as ω_{sled} is much larger than ω_{corner}, the phase shift by this low-pass filter is asymptotically approaching -90 deg, and the precise value of h is not critical in the range between 0.01 and 0.2. See Table A. This range of the value of h is quite reasonable, when we remind that h^{-1} is the time constant of velocity storage, which in man may be estimated between 5 and 20 sec (Kostelijk, 1982).

The relatively low sensitivity of g_2 for changes in the choice of h is illustrated by evaluating equation (8) for fixed values of $\phi_{Veye}=58$ deg, $g_1=0.8$ and $\omega_{sled}=1.1$. Table A shows matching pairs of h and g_2.

Table A The sensitivity of g_2 for changes in the preset value of h ($g_1=0.8$).

h	g_2
0.01	3.2
0.05	3.4
0.1	3.8
0.2	4.6

With regard to the choice of g_1, eq. 8 shows that for each value of g_1 there is a matching value of g_2. Table B shows some matching pairs.

Table B The sensitivity of g_2 for changes in the preset value of g_1 ($h=0.1$).

g_1	g_2
0.6	3.3
0.8	3.8
1.0	4.2
2.0	6.3

We conclude that the functioning of the model is not critically dependent upon the chosen parameter values of h and g_1.

B5 Calculation of $V_{otolith}$

We recall the equation:

$$V_{eye,otolith} = H_{storage,otolith} \cdot V_{otolith}$$

The transfer function $H_{storage,otolith}$ has been given by equation 5. The model parameters are: $h = 0.1$; $g_1 = 0.8$; $g_2 = 3.8$.

We are now at the point where $V_{eye,otolith}$ and $H_{storage,otolith}$ have been completely determined. This means that $V_{otolith}$ can be calculated. The amplitude ratio of $H_{storage,otolith}$, as given by equation (6), is equal to 0.25. The experimental modulation amplitude $V_{eye,otolith}$ is 3.4 $deg \cdot sec^{-1}$. It follows that the amplitude of $V_{otolith}$ is 13.6 $deg \cdot sec^{-1}$.

B6 Expression of the transfer function $H_{storage,surround}$ in g_1, g_2 and h

$H_{storage,surround}$ is defined as the transfer function from $V_{surround}$ to $V_{eye,surround}$. This transfer function is applied for the model prediction of $V_{eye,surround}$ in parabolic flight.

Substitution of equation (1) in equation (4) yields:

$$H_{storage,surround} = K_{storage,surround} \cdot \frac{(1 + T_{d,s} \cdot s)}{(1 + T_{i,s} \cdot s)} \tag{9}$$

$$K_{storage,surround} = \frac{g_2 + h \cdot g_1}{h + g_2 + h \cdot g_1} \tag{9a}$$

$$T_{d,s} = \frac{g_1}{g_2 + g_1 \cdot h}$$

$$T_{i,s} = \frac{1 + g_1}{h + g_2 + h \cdot g_1}$$

When the surround velocity is constant (as in our parabolic flight experiment), the modulus of the transfer function is only determined by the constant gain element $K_{storage,surround}$ in equation (9). This gain element has the value of 0.97.

When the surround velocity is sinusoidal, the formulas for the frequency response are the same as equations (6) and (7), with the substitution of $K_{storage,surround}$, $T_{d,s}$ and $T_{i,s}$ in these equations. Because $T_{d,s}$ is smaller than $T_{i,s}$, the phase of the response $V_{eye,surround}$ lags behind the phase of the input $V_{surround}$.

B7 Listing of parameter values, based on the sled experiment

h = 0.1 $\sec^{-1}$ (preset value)
g_1 = 0.8 (preset value)
g_2 = 3.8 $\sec^{-1}$

$K_{\text{storage,otolith}}$ = 0.025
$T_{d,o}$ = 10.0 sec
$T_{i,o}$ = 0.45 sec

$K_{\text{storage,surround}}$ = 0.97
$T_{d,s}$ = 0.21 sec
$T_{i,s}$ = 0.45 sec

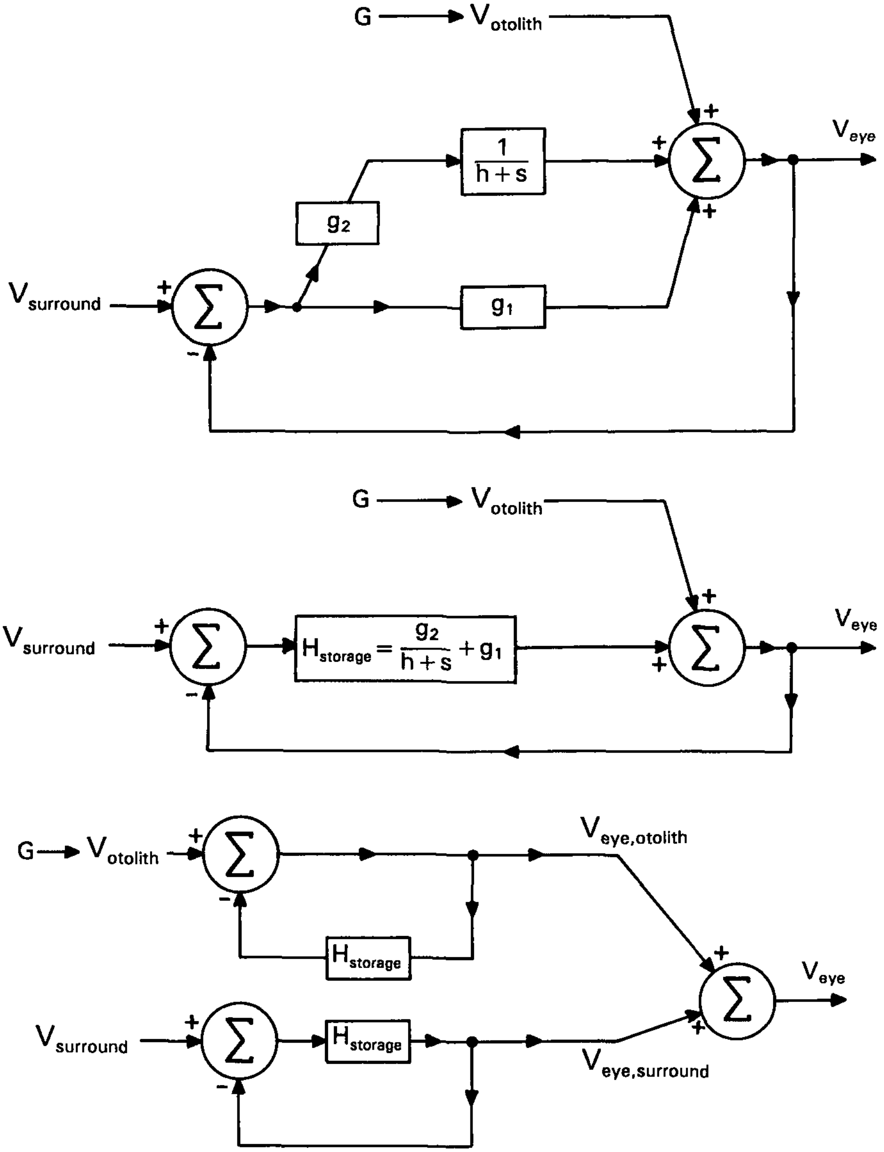

Fig. A Different presentations of the *same* model: velocity storage, extended with a direct otolith path. The upper diagram shows the velocity storage circuit presented by $1/(h+s)$. In the middle diagram, the direct and indirect pathways have been written as one transfer function $H_{storage}$. In the lower diagram, the otolith path and the visual path have been separated completely; it shows more explicitely that velocity storage modifies the contribution of the otolith-induced velocity $V_{otolith}$ to V_{eye}, when there is optokinetic input simultaneous with the G input.

Appendix C

Cupula dynamics

Semicircular canal model: a structure similar to the otolith model derived in the introductory chapter, but with a differentiator inserted after the angular velocity input. See Fig. B.

$$\ddot{\theta}_c = \ddot{\theta}_h - \frac{B}{I}\,\dot{\theta}_c - \frac{K}{I}\,\theta_c$$

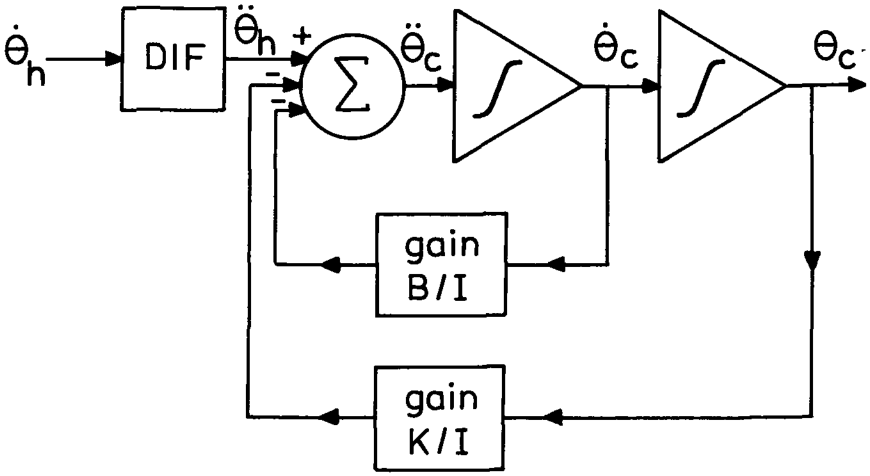

Fig. B Approximate model for the cupula-endolymph system (Boumans, 1982), applied in the model. Input is angular velocity of the head, output is cupula deflection. Feedback terms in the second-order system are the damping torque B/I and elastic torque K/I.

θ_h = angular displacement of the head; θ_c = angular displacement of the cupula; I = moment of inertia of the endolymph; B = damping torque, determined by the viscosity of the endolymph; K = elastic torque, determined by the stiffness of the cupula. Estimated numerical values are (Boumans, 1982): B/I = 100 [sec^{-1}]; K/I = 5 [sec^{-2}].

Curriculum Vitae

J. Tim Marcus werd geboren op 10 september 1954 in Amsterdam. Hij behaalde het diploma Gymnasium-B aan het Pius X Lyceum te Amsterdam.

Aan de Vrije Universiteit te Amsterdam voltooide hij de natuurkunde studie, en behaalde hij ook het doctoraalexamen geneeskunde. Bij de vakgroep Medische Fysica ontwikkelde hij een infrarood-systeem voor de meting van oogbewegingen en pupilreacties, en verrichtte daarmee klinisch onderzoek bij patiënten met neuritis optica. Bij dezelfde vakgroep was hij student-assistent. Tevens werkte hij aan de analyse van klinische MRI-beelden in het Academisch Ziekenhuis Utrecht. Zijn literatuurstudie en colloquium handelden over de medische toepassingen van NMR-spectroscopie.

Tijdens zijn studie was hij mede-oprichter en bestuurslid van de Amsterdamse Studentenvereniging voor Internationale Betrekkingen. Hij vervulde zijn militaire dienstplicht bij een geneeskundige compagnie.

Sinds 1986 werkt hij bij het TNO Instituut voor Zintuigfysiologie te Soesterberg. Binnen het programma Evenwicht en Oriëntatie verrichtte hij onderzoek naar de effecten van traagheidskrachten op het vestibulaire systeem van de mens. Hij was onder meer verantwoordelijk voor experimenten in een centrifuge, en in parabolische vluchten met een laboratoriumvliegtuig. Daarnaast onderzocht hij de mogelijke rol van desoriëntatie bij het ontstaan van luchtvaartongevallen.